General average balance equations and buoyancy closure for a mixture of a continuous fluid and rigid particles

Thomas Pähtz,[1,*] Yulan Chen,[1] Rui Zhu,[1,†] Katharina Tholen,[2] and Zhiguo He[1]

[1] *Institute of Port, Coastal and Offshore Engineering, Ocean College, Zhejiang University, 316021 Zhoushan, China*

[2] *Institute for Theoretical Physics, Leipzig University, Brüderstraße 16, 04103 Leipzig, Germany*

(Dated: February 17, 2025)

The equations of motion of a continuous fluid and rigid, non-Brownian particles that interact through contacts are averaged to derive average balance equations. The averaging procedure is generic, requiring only linearity and commutation with the space and time derivatives. No assumptions about the fluid's rheology and the particles' shapes and compositions are made. We obtain mathematically exact micromechanical expressions for the fluid phase, solid phase, and mixture fields of interest. We demonstrate for a specific example, numerical simulations of sediment transport, based on Direct Numerical Simulations and the Discrete Element Method, that they can be conveniently extracted from such particle-resolved simulations without the need of approximations. In contrast, fields extracted using previous formalisms based on first-order Taylor expansions in the ratio between the particle size and the macroscopic flow scale are in clear disagreement with the exact ones due to a lack of scale separation. This study therefore lays the groundwork for numerically studying the rheology of particulate two-phase flows in systems without scale separation. We also use the simulations to test existing buoyancy closures, that is, decompositions of the fluid-solid interaction force density into a generalized-drag force density and a generalized-buoyancy force density. We find that only one existing closure is consistent with the simulation data and existing experiments. However, it leads to a contradictory fluid momentum balance for certain stationary fluid-particle systems. We resolve this contradiction through a physically-motivated improvement. The improved closure essentially low-pass-filters buoyancy effects of the original closure.

arXiv:2308.09661v5 [physics.flu-dyn] 14 Feb 2025

I. INTRODUCTION

Systems of rigid, non-Brownian particles dispersed in a continuous fluid are often modeled using balance equations for the fluid phase that involve some form of averaging of the local, instantaneous flow due to the large computational cost of resolving the flow at the sub-particle scale [1–3]. The associated information loss makes it necessary to complement the averaged equations with closure relations accounting for the effects of fluid-solid interactions and turbulence. In addition, especially when the density of particles is high and particle-particle contacts frequent, average fluid-like balance equations are also commonly used to model the motion of the actually discrete particle phase, complemented by further closure relations as individual particles are no longer resolved [2–9]. The unclosed average one-fluid or two-fluid balance equations, containing all the undetermined fields that require closure, are here termed the *closure problem*. This study derives mathematically exact micromechanical expressions for the fields of the closure problem, but not closures for these fields (except a closure for buoyancy), and shows how they can be extracted, without approximation in a computationally cheap manner, from particle-resolved Computational Fluid Dynamics-Discrete Element Method (CFD-DEM) numerical simulations, even in systems without separation between the particle scale R and the macroscopic-flow scale L.

The classical approach to derive the closure problem for particulate two-phase flows is to start from the nonaveraged continuum equations of fluid motion and combine them with rigid-body dynamics [10–13]. Alternatively, the solid phase can also be treated as a continuum, where the stresses arising from internal interactions in the particle interiors are *a posteriori* linked to rigid body properties [14–17]. Both approaches are mathematically equivalent [18, 19]. Where these studies differ is in the procedure used to average the equations of motion and the considered rheology of the fluid and shapes and compositions of the particles. On the one hand, sphere-symmetrical volume averaging has been applied to identical homogeneous spheres dispersed in an incompressible Newtonian fluid [10–13]. However, this procedure has the disadvantage that it smooths out, by construction, potential spatial gradients in the macroscopic flow [16]. For example, the macroscopic behavior of sediment transport, a particulate two-phase flow of vital importance in geophysical settings, can change very rapidly over a fraction of R in the direction normal to the sediment bed due to a

* 0012136@zju.edu.cn

† zhurui@zju.edu.cn

typically sudden transition from a densely packed bed to a potentially very dilute transport layer [20–22], and in the directions tangential to the bed due to bed inhomogeneities such as bedforms [23]. In other words, spatial averaging is, by construction, only applicable to systems in which R is sufficiently smaller than the characteristic distance over which the macroscopic flow varies in the averaged direction(s). A similar constraint also limits the applicability of time averaging procedures [16]. Ensemble averaging, on the other hand, does not share this weakness and can, in principle, be applied to systems in which R/L is arbitrarily large [16]. However, the existing micromechanical expressions for the fields of the closure problem derived from ensemble averaging, like those derived from existing formalisms based on volume averaging, involve Taylor expansions in R/L [16–18]. This implies that potentially many higher-order terms have to be considered to accurately determine these fields for high-gradient particulate two-phase flows from particle-resolved CFD-DEM simulations. This not only enhances mathematical complexity but can also lead to computational-resolution problems due to the associated higher-order derivatives that need to be numerically evaluated. Furthermore, it is generally unknown in advance how many orders of the Taylor expansions have to be considered to capture the salient features of the macroscopic-flow dynamics.

In this study, we resolve these problems through deriving, for arbitrary averaging procedures, fluid rheologies, and particle shapes and compositions, exact micromechanical expressions for the fields of the closure problem, whose numerical extraction from particle-resolved CFD-DEM simulations is as simple and computationally costly as that of first-order-approximated expressions. As an example, we calculate the fluid and solid phase stresses from a simulation of steady, homogeneous sediment transport, using a coupled Direct Numerical Simulation (DNS)-DEM method. These calculations demonstrate that it is not only convenient but also necessary to calculate exact micromechanical expressions for systems without scale separation, since first-order approximations in R/L clearly fail.

One of the first steps that is usually taken in an attempt to close the closure problem is to decompose fluid-solid interactions into two contributions: one arising from and another one independent of the relative motion between the fluid and solid phases [12]. In the case of the momentum balances, the former and latter contributions are here termed *generalized drag* (including drag, lift, lubrication, etc) and *generalized buoyancy*, respectively, and the associated closure is referred to as *buoyancy closure*. It has been a matter of debate whether the buoyancy closure should be based on the fluid weight [12], mixture weight [24], average interfacial pressure [25, 26], effective fluid pressure (i.e., the total pressure from all possible normal-stress contributions in the average fluid momentum balance) [12], fluid-phase-averaged fluid stress tensor [27, 28], effective fluid stress tensor [11–13], or effective fluid stress tensor without Reynolds stress contributions [5]. This ambiguity in choosing the buoyancy closure can be problematic since in statistically unidirectional systems, the generalized-drag force tends to be small and the generalized-buoyancy force dominating in the directions perpendicular to the flow direction due to locally absent relative fluid-solid average translational motion. For example, for steady, bed-tangentially homogeneous sediment transport, at any given elevation above the sediment bed, the bed-normal component of the (actual) drag force on upward-moving particles tends to exactly cancel that on downward-moving particles on average [20], while the bed-normal components of other generalized-drag forces, such as lift and lubrication forces, are often negligible. Hence, knowing the one true buoyancy closure that captures the actual physics may lead to a better understanding of such systems.

In this study, we show that the buoyancy closure based on the effective fluid stress tensor, originally proposed by Anderson and Jackson [11], is the only existing one consistent with our DNS-DEM simulations and existing experiments [29, 30]. Furthermore, we show that, in a mathematically exact context, almost all existing buoyancy closures lead to a contradictory fluid momentum balance for a homogeneous particle bed immersed in a resting fluid that exhibits density gradients. We propose an improvement of the buoyancy closure by Anderson and Jackson [11] that resolves this contradiction. Then using granular kinetic theory [7–9] and standard closures for drag-based fluids-solid interactions [31], we compare how the original and improved buoyancy closures affect the stability characteristics of a homogeneous fluidized bed.

The improved buoyancy closure derived in this study is discussed from another angle in a companion paper [32]. It shows additional validations with DNS-DEM simulations and demonstrates why this closure can be interpreted as a generalization of Archimedes' principle from stationary to dynamic systems.

The remaining paper is organized as follows. After introducing our mathematical notation (§II), we derive the closure problem without any approximation under very general circumstances (§III). Then, we extract the derived exact micromechanical expressions for the fluid and solid phase stresses from a DNS-DEM simulation of steady, bed-tangentially homogeneous sediment transport, and we show that stresses extracted using previous formalisms based on a first-order Taylor expansion in R/L are in clear disagreement with the exact ones (§IV). Finally, we test existing buoyancy closures with our simulation data, demonstrate that they lead to a contradiction, propose a physically-motivated, non-contradictory closure, and carry out a linear-stability analysis for a homogeneous fluidized bed (§V).

Symbol(s)	Mathematical or physical meaning
X_∞	Indicator function of entire fluid-particle system ($\boldsymbol{x} \in \mathcal{V}_\infty$)
X_f	Indicator function of fluid phase ($\boldsymbol{x} \in \mathcal{V}_\mathrm{f}$)
X_s	Indicator function of solid phase ($\boldsymbol{x} \in \mathcal{V}_\mathrm{s}$)
X^p	Indicator function of an individual particle p ($\boldsymbol{x} \in \mathcal{V}^p$)
$\boldsymbol{n}^p$	Outward unit normal vector on surface $\mathcal{S}^p$ of an individual particle p
ρ, $\boldsymbol{u}$	Local mass density and velocity fields, defined for all $\boldsymbol{x} \in \mathcal{V}_\infty$
$\mathrm{D}_t A \equiv \dot{A} \equiv \partial_t A + \boldsymbol{u} \cdot \boldsymbol{\nabla} A$	Material derivative of A
V^p, M^p, S^p	Volume, mass, surface area of an individual particle p
$V^p \underline{A}_{\mathcal{V}^p}$	Integral of A over volume of an individual particle p
$M^p \underline{A}_{\mathcal{M}^p}$	Integral of ρA over volume of an individual particle p
$S^p \underline{A}_{\mathcal{S}^p}$	Integral of A over surface of an individual particle p
$\underline{\rho}_{\mathcal{V}^p} = M^p / V^p$	Average mass density of an individual particle p
$\underline{A}_\mathcal{V} \equiv \sum_p \underline{A}_{\mathcal{V}^p} X^p$	Field associated with $\underline{A}_{\mathcal{V}^p}$
$\underline{A}_\mathcal{M} \equiv \sum_p \underline{A}_{\mathcal{M}^p} X^p$	Field associated with $\underline{A}_{\mathcal{M}^p}$
$\rho_* \equiv \rho X_\mathrm{f} + \underline{\rho}_\mathcal{V}$	Mass density field without particle-rotational degrees of freedom
$A_\uparrow \equiv A X_\mathrm{f} + \underline{A}_\mathcal{M}$	Field A without particle-rotational degrees of freedom
$\boldsymbol{x}^p \equiv \underline{\boldsymbol{x}}_{\mathcal{M}^p}$	Center of mass of an individual particle p
$\boldsymbol{r}^p \equiv \boldsymbol{x} - \boldsymbol{x}^p$	Coordinate relative to center of mass of an individual particle p
$\boldsymbol{r}^{pq} \equiv \boldsymbol{x}^q - \boldsymbol{x}^p$	Distance vector between centers of mass of individual particles p and q
$\boldsymbol{r}_\mathrm{c}^{pq} \equiv \boldsymbol{x}_\mathrm{c}^{pq} - \boldsymbol{x}^p$	Vector connecting $\boldsymbol{x}^p$ and contact point $\boldsymbol{x}_\mathrm{c}^{pq}$
$\boldsymbol{v}_\uparrow^p \equiv \underline{\boldsymbol{u}}_{\mathcal{M}^p}$	Center of mass velocity of an individual particle p
$\boldsymbol{\omega}^p$	Angular velocity of an individual particle p
$\boldsymbol{v}_\circlearrowleft^p = \boldsymbol{\omega}^p \times \boldsymbol{r}^p$	Rotational velocity of an individual particle p
$\delta_\mathcal{S}^p \equiv -\boldsymbol{n}^p \cdot \boldsymbol{\nabla} X^p$	Delta distribution picking out surface points of an individual particle p
$\delta_{\boldsymbol{x}}^p$	Delta distribution centered at $\boldsymbol{x}^p$
$\delta_{\mathrm{L}\boldsymbol{x}}^p[\boldsymbol{y}]$	Delta line connecting $\boldsymbol{x}^p$ and $\boldsymbol{y}$
$\delta_{\mathrm{L}\boldsymbol{x}}^{pq} = \delta_{\mathrm{L}\boldsymbol{x}}^{qp}$	Delta line connecting $\boldsymbol{x}^p$ and $\boldsymbol{x}^q$
$\delta_{\mathrm{cL}\boldsymbol{x}}^{pq}$	Delta line connecting $\boldsymbol{x}^p$ and contact point $\boldsymbol{x}_\mathrm{c}^{pq}$
$\langle A \rangle$	Mixture average of A, based on a generic averaging procedure $\langle\cdot\rangle$
$\beta_\mathrm{f} \equiv \langle X_\mathrm{f} \rangle$	Fluid volume fraction
$\beta_\mathrm{s} \equiv \langle X_\mathrm{s} \rangle$	Solid volume fraction
$c_\mathrm{g} \equiv \langle \sum_p V^p \delta_{\boldsymbol{x}}^p \rangle$	Grain concentration
$\langle A \rangle^\mathrm{f} \equiv \langle X_\mathrm{f} A \rangle / \beta_\mathrm{f}$	Fluid phase average of A
$\langle A \rangle^\mathrm{s} \equiv \langle X_\mathrm{s} A \rangle / \beta_\mathrm{s}$	Solid phase average of A
$\langle A \rangle^\mathrm{g} \equiv \left\langle \sum_p \underline{A}_{\mathcal{V}^p} V^p \delta_{\boldsymbol{x}}^p \right\rangle / c_\mathrm{g}$	Grain phase average of A
$\langle A \rangle_w^{(\cdot)} \equiv \langle wA \rangle^{(\cdot)} / \langle w \rangle^{(\cdot)}$	Weighted mixture, fluid phase, solid phase, grain phase averages
$A \overset{\mathrm{R}}{=} B$	$A = B$ if the Reynolds rule Eq. (40) is satisfied
$A \overset{\circ}{=} B$	$A = B$ if all particles are spheres of a constant radius R with sphere-symmetrical interiors
$A \overset{\mathrm{R},\circ}{=} B$	$A = B$ if both of the above requirements are satisfied
$\boldsymbol{A} \overset{(\cdot)}{\simeq} \boldsymbol{B}$	$\boldsymbol{A} \overset{(\cdot)}{=} \boldsymbol{B}$ but for a divergence-free term, equivalent to $\boldsymbol{\nabla} \cdot \boldsymbol{A} \overset{(\cdot)}{=} \boldsymbol{\nabla} \cdot \boldsymbol{B}$
$\cdot'$, $[\cdot]_\mathrm{s}'$	Fluctuation operators defined by Eqs. (45) and (46)

TABLE I. Summary of the notations introduced in §II. The symbol '$(\cdot)$' stands for a placeholder (it can be empty).

II. NOTATIONS, DEFINITIONS, AND IMPORTANT MATHEMATICAL IDENTITIES

The notations and definition introduced below are summarized in Table I to guide the reader.

A. Fluid-particle system

The entire fluid-particle system shall be contained in a three-dimensional fixed domain $\mathcal{V}_\infty \subset \mathcal{R}^3$. The subsets $\mathcal{V}_\mathrm{f}[t]$ and $\mathcal{V}_\mathrm{s}[t]$, with $\mathcal{V}_\infty = \mathcal{V}_\mathrm{f}[t] \cup \mathcal{V}_\mathrm{s}[t]$, shall contain those of the points $\boldsymbol{x} \in \mathcal{V}_\infty$ that are occupied by the fluid and solid phases, respectively, at time t. The solid phase is further subdivided into the subsets $\mathcal{V}^p[t]$ with surfaces $\mathcal{S}^p[t] = \partial\mathcal{V}^p[t]$, where $p = 1 \ldots N$ numbers the particles consecutively. Hence, the indicator functions corresponding

to these domains satisfy

$$X_\infty[\boldsymbol{x}] = X_\mathrm{f}[\boldsymbol{x},t] + X_\mathrm{s}[\boldsymbol{x},t] = X_\mathrm{f}[\boldsymbol{x},t] + \sum\nolimits_p X^p[\boldsymbol{x},t], \tag{1}$$

where X_∞, X_f, X_s, and X^p are defined as being equal to 1 in the interiors and equal to 0 outside of $\mathcal{V}_\infty$, $\mathcal{V}_\mathrm{f}$, $\mathcal{V}_\mathrm{s}$, and $\mathcal{V}^p$, respectively.

The fields $\rho[\boldsymbol{x},t]$ and $\boldsymbol{u}[\boldsymbol{x},t]$ shall denote the mass density and velocity fields, defined within both the fluid and solid phases. There is no restriction on the particle shape and composition. For example, particles are allowed to have density inhomogeneities and can also be hollow in their interiors. Since we do not consider phase change or mass transfer across the fluid-solid interface, the normal component of $\boldsymbol{u}$ is continuous and therefore [25]

$$\dot{X}_\mathrm{f}[\boldsymbol{x},t] = 0, \qquad \dot{X}_\mathrm{s}[\boldsymbol{x},t] = 0, \qquad \dot{X}^p[\boldsymbol{x},t] = 0, \tag{2}$$

where the overdot denotes the material derivative, i.e., $\mathrm{D}_t \equiv \partial_t + u_i[\boldsymbol{x},t]\partial_i$.

B. Particle properties

1. Individual-particle volume and surface integrals

Properties of an individual particle p may refer to locations within p or the particle as a whole, that is, integrated over $\mathcal{V}^p$ or $\mathcal{S}^p$. Since such integrals will often emerge in the analysis, we introduce the following mathematical abbreviations to ease the notation:

$$\underline{A}_{\mathcal{V}^p}[t] \equiv \frac{1}{V^p}\int_{\mathcal{V}^p[t]} A[\boldsymbol{x},t]\mathrm{d}V_x, \qquad \underline{A}_{\mathcal{V}}[\boldsymbol{x},t] \equiv \sum\nolimits_p \underline{A}_{\mathcal{V}^p}[t]X^p[\boldsymbol{x},t], \tag{3}$$

$$\underline{A}_{\mathcal{M}^p}[t] \equiv \frac{1}{M^p}\int_{\mathcal{V}^p[t]} (\rho A)[\boldsymbol{x},t]\mathrm{d}V_x, \qquad \underline{A}_{\mathcal{M}}[\boldsymbol{x},t] \equiv \sum\nolimits_p \underline{A}_{\mathcal{M}^p}[t]X^p[\boldsymbol{x},t], \tag{4}$$

$$\underline{A}_{\mathcal{S}^p}[t] \equiv \frac{1}{S^p}\int_{\mathcal{S}^p[t]} A[\boldsymbol{x},t]\mathrm{d}S_x, \tag{5}$$

with V^p, $M^p = V^p\underline{\rho}_{\mathcal{V}^p}$, and S^p the volume, mass, and surface area, respectively, of the particle p. For the definitions in the first two or the third above lines to make sense, A must be well-defined for $\boldsymbol{x} \in \mathcal{V}^p$ or $\boldsymbol{x} \in \mathcal{S}^p$, respectively, for all particles p. Due to the conservation of individual-particle volume (property of rigid bodies) and mass, the following identities are direct consequences of the Reynolds transport theorem:

$$\mathrm{D}_t\underline{A[\boldsymbol{x},t]}_{\mathcal{M}^p}[t] = \underline{(\mathrm{D}_t A)[\boldsymbol{x},t]}_{\mathcal{M}^p}[t], \qquad X^p\mathrm{D}_t\rho = 0, \qquad \mathrm{D}_t\underline{A[\boldsymbol{x},t]}_{\mathcal{V}^p}[t] = \underline{(\mathrm{D}_t A)[\boldsymbol{x},t]}_{\mathcal{V}^p}[t]. \tag{6}$$

2. Rotational velocity, angular velocity, and associated fields

Based on Eq. (3), the velocity field within an individual particle p, $(X^p\boldsymbol{u})[\boldsymbol{x},t]$, can be expressed as

$$(X^p\boldsymbol{u})[\boldsymbol{x},t] = X^p[\boldsymbol{x},t]\left(\boldsymbol{v}^p_\uparrow[t] + \boldsymbol{v}^p_\circlearrowleft[\boldsymbol{x},t]\right), \tag{7}$$

where $\boldsymbol{v}^p_\uparrow[t] \equiv \underline{\boldsymbol{u}}_{\mathcal{M}^p}[t]$ is its center-of-mass velocity and $\boldsymbol{v}^p_\circlearrowleft[\boldsymbol{x},t] \equiv \boldsymbol{\omega}^p[t] \times \boldsymbol{r}^p[\boldsymbol{x},t]$ its rotational velocity, with $\boldsymbol{\omega}^p[t]$ its angular velocity and $\boldsymbol{r}^p[\boldsymbol{x},t] \equiv \boldsymbol{x} - \boldsymbol{x}^p[t]$ its coordinate relative to its center of mass $\boldsymbol{x}^p[t] \equiv \underline{\boldsymbol{x}}_{\mathcal{M}^p}[t]$.

Given the mass density field $\rho[\boldsymbol{x},t]$ and an arbitrary field $A[\boldsymbol{x},t]$ well-defined for $\boldsymbol{x} \in \mathcal{V}_\infty$, we define the corresponding fields ρ_* and $A_\uparrow$ devoid of the particle-rotational degrees of freedom:

$$\rho_*[\boldsymbol{x},t] \equiv (\rho X_\mathrm{f})[\boldsymbol{x},t] + \underline{\rho}_{\mathcal{V}}[\boldsymbol{x},t], \qquad A_\uparrow[\boldsymbol{x},t] \equiv (AX_\mathrm{f})[\boldsymbol{x},t] + \underline{A}_{\mathcal{M}}[\boldsymbol{x},t]. \tag{8}$$

3. Particle-associated generalized functions

Here, we introduce mathematical abbreviations for special generalized functions used multiple times throughout the remaining paper, all of which are based on the multivariate delta distribution $\delta[\boldsymbol{x}]$. For example, the indicator

function $X^p[\boldsymbol{x},t]$ of an individual particle p and its gradient can be expressed, respectively, as (readily confirmed through application on a test function [25])

$$X^p[\boldsymbol{x},t]=\int_{\mathcal{V}^p[t]}\delta[\boldsymbol{x}-\boldsymbol{y}]\mathrm{d}V_y, \tag{9}$$

$$\boldsymbol{\nabla}X^p[\boldsymbol{x},t]=\int_{\mathcal{V}^p[t]}\boldsymbol{\nabla}_{\boldsymbol{x}}\delta[\boldsymbol{x}-\boldsymbol{y}]\mathrm{d}V_y=-\int_{\mathcal{S}^p[t]}\delta[\boldsymbol{x}-\boldsymbol{y}]\boldsymbol{n}^p[\boldsymbol{y},t]\mathrm{d}S_y, \tag{10}$$

where $\boldsymbol{n}^p[\boldsymbol{x},t]$ is the unit normal vector pointing outward of the particle p. For Eq. (10) and the following expressions to make sense, $\boldsymbol{n}^p[\boldsymbol{x},t]$ only needs to be well-defined for $\boldsymbol{x}\in\mathcal{S}^p[t]$. Motivated by the above relations, we define the delta distribution $\delta^p_{\mathcal{S}}[\boldsymbol{x},t]$ that picks out the surface points $\mathcal{S}^p[t]$:

$$\delta^p_{\mathcal{S}}[\boldsymbol{x},t]\equiv-\boldsymbol{n}^p[\boldsymbol{x},t]\cdot\boldsymbol{\nabla}X^p[\boldsymbol{x},t]=\int_{\mathcal{S}^p[t]}\delta[\boldsymbol{x}-\boldsymbol{y}]\mathrm{d}S_y, \tag{11}$$

$$\Rightarrow\boldsymbol{\nabla}X^p[\boldsymbol{x},t]=-\delta^p_{\mathcal{S}}[\boldsymbol{x},t]\boldsymbol{n}^p[\boldsymbol{x},t]. \tag{12}$$

Furthermore, the multivariate delta distribution at the center of mass $\boldsymbol{x}^p[t]$ of the particle p shall be denoted as

$$\delta^p_{\boldsymbol{x}}[t]\equiv\delta[\boldsymbol{x}-\boldsymbol{x}^p[t]]. \tag{13}$$

We also introduce two 'delta lines' connecting $\boldsymbol{x}^p[t]$ with (i) an arbitrary point $\boldsymbol{y}$ and (ii) the center of mass $\boldsymbol{x}^q[t]$ of another particle q, respectively, as

$$\delta^p_{\mathrm{L}\boldsymbol{x}}[\boldsymbol{y},t]\equiv\int_0^1\delta[\boldsymbol{x}-\boldsymbol{x}^p[t]-\lambda(\boldsymbol{y}-\boldsymbol{x}^p[t])]\mathrm{d}\lambda, \tag{14}$$

$$\delta^{pq}_{\mathrm{L}\boldsymbol{x}}[t]\equiv\delta^p_{\mathrm{L}\boldsymbol{x}}[\boldsymbol{x}^q[t],t]=\int_0^1\delta[\boldsymbol{x}-\boldsymbol{x}^p[t]-\lambda\boldsymbol{r}^{pq}[t]]\mathrm{d}\lambda, \tag{15}$$

with $\boldsymbol{r}^{pq}[t]\equiv\boldsymbol{x}^q[t]-\boldsymbol{x}^p[t]$. Note that $\delta^{pq}_{\mathrm{L}\boldsymbol{x}}[t]=\delta^{qp}_{\mathrm{L}\boldsymbol{x}}[t]$ and $\delta^{pp}_{\mathrm{L}\boldsymbol{x}}[t]=\delta^p_{\boldsymbol{x}}[t]$. For the case that the particles p and q are contacting each other at the point $\boldsymbol{x}^{pq}_{\mathrm{c}}[t]=\boldsymbol{x}^{qp}_{\mathrm{c}}[t]$, we also define the delta line connecting $\boldsymbol{x}^p[t]$ with $\boldsymbol{x}^{pq}_{\mathrm{c}}[t]$ as

$$\delta^{pq}_{\mathrm{cL}\boldsymbol{x}}[t]\equiv\delta^p_{\mathrm{L}\boldsymbol{x}}[\boldsymbol{x}^{pq}_{\mathrm{c}}[t],t]=\int_0^1\delta[\boldsymbol{x}-\boldsymbol{x}^p[t]-\lambda\boldsymbol{r}^{pq}_{\mathrm{c}}[t]]\mathrm{d}\lambda, \tag{16}$$

with $\boldsymbol{r}^{pq}_{\mathrm{c}}[t]\equiv\boldsymbol{x}^{pq}_{\mathrm{c}}[t]-\boldsymbol{x}^p[t]$. Note that $\boldsymbol{r}^{pq}[t]=\boldsymbol{r}^{pq}_{\mathrm{c}}[t]-\boldsymbol{r}^{qp}_{\mathrm{c}}[t]$. Given an arbitrary direction vector $\boldsymbol{r}$, delta lines are linked to delta points via

$$\delta^p_{\boldsymbol{x}-\boldsymbol{r}}[t]-\delta^p_{\boldsymbol{x}}[t]=\int_0^1\frac{\partial}{\partial\lambda}\delta\left[\boldsymbol{x}-\boldsymbol{x}^p[t]-\lambda\boldsymbol{r}\right]\mathrm{d}\lambda=-\boldsymbol{\nabla}_{\boldsymbol{x}}\cdot\boldsymbol{r}\delta^p_{\mathrm{L}\boldsymbol{x}}[\boldsymbol{x}^p[t]+\boldsymbol{r},t]. \tag{17}$$

It follows from special cases of Eq. (17) that

$$\delta^q_{\boldsymbol{x}}[t]-\delta^p_{\boldsymbol{x}}[t]=-\boldsymbol{\nabla}_{\boldsymbol{x}}\cdot\boldsymbol{r}^{pq}[t]\delta^{pq}_{\mathrm{L}\boldsymbol{x}}[t]=-\boldsymbol{\nabla}_{\boldsymbol{x}}\cdot\left(\boldsymbol{r}^{pq}_{\mathrm{c}}[t]\delta^{pq}_{\mathrm{cL}\boldsymbol{x}}[t]-\boldsymbol{r}^{qp}_{\mathrm{c}}[t]\delta^{qp}_{\mathrm{cL}\boldsymbol{x}}[t]\right). \tag{18}$$

In particular, if two sphere-symmetrical particles are in contact, the equality on the right-hand holds also for the terms inside the divergences since the line connecting $\boldsymbol{x}^p[t]$ with $\boldsymbol{x}^q[t]$ passes through $\boldsymbol{x}^{pq}_{\mathrm{c}}[t]$.

An alternative approach is to express $\delta^p_{\boldsymbol{x}-\boldsymbol{r}}[t]-\delta^p_{\boldsymbol{x}}[t]$ through an infinite Taylor expansion:

$$\delta^p_{\boldsymbol{x}-\boldsymbol{r}}[t]-\delta^p_{\boldsymbol{x}}[t]=\sum_{k=1}^{\infty}\frac{(-1)^k}{k!}\boldsymbol{\nabla}^{(k)}_{\boldsymbol{x}}\odot\boldsymbol{r}^{(k)}\delta^p_{\boldsymbol{x}}[t], \tag{19}$$

where $\cdot^{(k)}$ denotes the k-th power with respect to the dyadic product (e.g., $\boldsymbol{r}^{(3)}=\boldsymbol{rrr}$) and $\odot$ operates as follows: $\boldsymbol{A}^{(1)}\odot\boldsymbol{B}^{(1)}=\boldsymbol{A}\cdot\boldsymbol{B}$, $\boldsymbol{A}^{(2)}\odot\boldsymbol{B}^{(2)}=\boldsymbol{AA}:\boldsymbol{BB}$, and so forth. This expansion, cut off at the desired order (usually the first or second), is essentially the route taken in previous studies [e.g., 10, 14]. However, in that case, the resulting analysis will be valid only for a sufficiently small value of R/L. In contrast, as we will see, the expressions resulting from Eq. (17), used to derive the closure problem in this study, can be evaluated directly, without a Taylor-expansion-like approximation, both analytically and numerically, rendering it superior in terms of both accuracy and convenience. Note that the first-order expansion in Eq. (19) can be formally obtained from Eq. (17) through replacing $\delta^p_{\mathrm{L}\boldsymbol{x}}[\boldsymbol{x}^p[t]+\boldsymbol{r},t]$ by $\delta^p_{\boldsymbol{x}}[t]$.

4. Important mathematical identities for an individual particle

Using the above definitions, mathematical abbreviations, and the expansion Eq. (17), a stringent relationship between the field $(AX^p)[\boldsymbol{x},t]$ on the one hand and the fields $\underline{A}_{\mathcal{V}^p}[t]V^p\delta^p_{\boldsymbol{x}}$ and $\underline{A}_{\mathcal{V}^p}[t]X^p[\boldsymbol{x},t]$ on the other hand can be derived for an individual particle p:

$$\begin{aligned}
(AX^p)\,[\boldsymbol{x},t] &= \int_{\mathcal{R}^3} (AX^p)\,[\boldsymbol{x}^p[t]+\boldsymbol{r},t]\,\delta^p_{\boldsymbol{x}-\boldsymbol{r}}[t]\mathrm{d}^3r \\
&= \delta^p_{\boldsymbol{x}}[t]\int_{\mathcal{R}^3} (AX^p)\,[\boldsymbol{x}^p[t]+\boldsymbol{r},t]\,\mathrm{d}^3r - \boldsymbol{\nabla}\cdot\int_{\mathcal{R}^3}\boldsymbol{r}(AX^p)\,[\boldsymbol{x}^p[t]+\boldsymbol{r},t]\,\delta^p_{\mathrm{L}\boldsymbol{x}}[\boldsymbol{x}^p[t]+\boldsymbol{r},t]\mathrm{d}^3r \\
\boldsymbol{x}^p+\boldsymbol{r}\to\boldsymbol{y}\Rightarrow &= \delta^p_{\boldsymbol{x}}[t]\int_{\mathcal{R}^3} (AX^p)\,[\boldsymbol{y},t]\,\mathrm{d}^3y - \boldsymbol{\nabla}\cdot\int_{\mathcal{R}^3}(\boldsymbol{r}^pAX^p)[\boldsymbol{y},t]\delta^p_{\mathrm{L}\boldsymbol{x}}[\boldsymbol{y},t]\mathrm{d}^3y \\
&= \delta^p_{\boldsymbol{x}}[t]\int_{\mathcal{V}^p[t]} A\,[\boldsymbol{y},t]\,\mathrm{d}V_y - \boldsymbol{\nabla}\cdot\int_{\mathcal{V}^p[t]}(\boldsymbol{r}^pA)\,[\boldsymbol{y},t]\,\delta^p_{\mathrm{L}\boldsymbol{x}}[\boldsymbol{y},t]\mathrm{d}V_y.
\end{aligned} \tag{20}$$

Henceforth, we drop showing the explicit dependencies on $\boldsymbol{x}$ and/or t except when necessary for clarity. Then, Eq. (20) can be written in the compact forms

$$AX^p = \underline{A}_{\mathcal{V}^p}V^p\delta^p_{\boldsymbol{x}} - \boldsymbol{\nabla}\cdot V^p\underline{\boldsymbol{r}^pA\delta^p_{\mathrm{L}\boldsymbol{x}}}_{\mathcal{V}^p}, \tag{21}$$

$$AX^p = \underline{A}_{\mathcal{V}^p}X^p - \boldsymbol{\nabla}\cdot V^p\underline{\boldsymbol{r}^p\,(A-\underline{A}_{\mathcal{V}^p})\,\delta^p_{\mathrm{L}\boldsymbol{x}}}_{\mathcal{V}^p}, \tag{22}$$

where Eq. (21) for $A=1$ was used to substitute $\delta^p_{\boldsymbol{x}}$ in Eq. (21), resulting in Eq. (22). A calculation for $A\delta^p_{\mathcal{S}}$ completely analogous to Eq. (20) leads to

$$A\delta^p_{\mathcal{S}} = \underline{A}_{\mathcal{S}^p}S^p\delta^p_{\boldsymbol{x}} - \boldsymbol{\nabla}\cdot S^p\underline{\boldsymbol{r}^pA\delta^p_{\mathrm{L}\boldsymbol{x}}}_{\mathcal{S}^p}, \tag{23}$$

$$A\delta^p_{\mathcal{S}} = \underline{A}_{\mathcal{S}^p}\delta^p_{\mathcal{S}} - \boldsymbol{\nabla}\cdot S^p\underline{\boldsymbol{r}^p\,(A-\underline{A}_{\mathcal{S}^p})\,\delta^p_{\mathrm{L}\boldsymbol{x}}}_{\mathcal{S}^p}. \tag{24}$$

Replacing $A\to An^p_i$ in Eq. (23) and then using Eq. (12) on its left-hand side yields

$$A\partial_iX^p = -S^p\underline{An^p_i}_{\mathcal{S}^p}\delta^p_{\boldsymbol{x}} + \boldsymbol{\nabla}\cdot S^p\underline{\boldsymbol{r}^pAn^p_i\delta^p_{\mathrm{L}\boldsymbol{x}}}_{\mathcal{S}^p}, \tag{25}$$

$$A\partial_iX^p = -\frac{S^p}{V^p}\underline{An^p_i}_{\mathcal{S}^p}X^p + \boldsymbol{\nabla}\cdot S^p\left(\underline{\boldsymbol{r}^pAn^p_i\delta^p_{\mathrm{L}\boldsymbol{x}}}_{\mathcal{S}^p} - \underline{\boldsymbol{r}^p\delta^p_{\mathrm{L}\boldsymbol{x}}}_{\mathcal{V}^p}\underline{An^p_i}_{\mathcal{S}^p}\right), \tag{26}$$

where Eq. (21) for $A=1$ was again used to substitute $\delta^p_{\boldsymbol{x}}$ in Eq. (25), resulting in Eq. (26). Furthermore, using $S^p\underline{An^p_i}_{\mathcal{S}^p} = V^p\underline{\partial_iA}_{\mathcal{V}^p}$ (Gauss's theorem), it follows from Eqs. (21) and (25) that

$$\partial_iAX^p = A\partial_iX^p + X^p\partial_iA = \boldsymbol{\nabla}\cdot S^p\underline{\boldsymbol{r}^pAn^p_i\delta^p_{\mathrm{L}\boldsymbol{x}}}_{\mathcal{S}^p} - \boldsymbol{\nabla}\cdot V^p\underline{\boldsymbol{r}^p(\partial_iA)\delta^p_{\mathrm{L}\boldsymbol{x}}}_{\mathcal{V}^p}. \tag{27}$$

The identities Eqs. (21)-(26) represent important manners in which surface fluxes such as stresses (the second terms on their right-hand sides) can mathematically emerge in our formalism. At the level of an individual particle p, they occur in the form of generalized functions due to the conversion of pointwise quantities ($A[\boldsymbol{x},t]$) into quantities averaged over its volume ($\underline{A}_{\mathcal{V}^p}[t]$) or surface ($\underline{A}_{\mathcal{S}^p}[t]$). Macroscopic averaging, which will be introduced in §II C, will then smooth out the associated discontinuities and singularities but not in itself generate new surface fluxes, with the exception of surface fluxes associated with the macroscopic fluid and particle fluctuation motions (e.g., Reynolds stresses).

The generalized functions involved in Eqs. (21)-(27) may appear complicated. However, they can be straightforwardly analytically evaluated without approximation, even for general particle shapes (Appendix A). In the case that the particle's center of mass $\boldsymbol{x}^p$ and the set of lines connecting $\boldsymbol{x}^p$ with all surface points $\boldsymbol{x}\in\mathcal{S}^p$ lie completely within $\mathcal{V}^p$ (true for most relevant particle shapes), implying that there is exactly one surface point in any given direction $\hat{\boldsymbol{r}}^p\equiv\boldsymbol{r}^p/|\boldsymbol{r}^p|$ from $\boldsymbol{x}^p$, the expressions become rather simple. For example, the flux terms on the right-hand sides of Eqs. (21) and (25), which will often appear in the forms $S^p\underline{(\boldsymbol{r}^p)^{(k)}An^p_i\delta^p_{\mathrm{L}\boldsymbol{x}}}_{\mathcal{S}^p}$ and $V^p\underline{(\boldsymbol{r}^p)^{(k)}A\delta^p_{\mathrm{L}\boldsymbol{x}}}_{\mathcal{V}^p}$, with $k>0$ an integer, become

$$S^p\underline{(\boldsymbol{r}^p)^{(k)}An^p_i\delta^p_{\mathrm{L}\boldsymbol{x}}}_{\mathcal{S}^p} = \frac{L^{1+k}_{\hat{\boldsymbol{r}}^p}(\boldsymbol{r}^p)^{(k)}}{|\boldsymbol{r}^p|^{2+k}}X^p\,(An^p_i)\,[\boldsymbol{x}^p+L_{\hat{\boldsymbol{r}}^p}\hat{\boldsymbol{r}}^p]\,, \tag{28}$$

$$V^p\underline{(\boldsymbol{r}^p)^{(k)}A\delta^p_{\mathrm{L}\boldsymbol{x}}}_{\mathcal{V}^p} = (\boldsymbol{r}^p)^{(k)}X^p\int_{|\boldsymbol{r}^p|/L_{\hat{\boldsymbol{r}}^p}}^1\frac{A[\boldsymbol{x}^p+\boldsymbol{r}^p/\lambda]}{\lambda^{3+k}}\mathrm{d}\lambda, \tag{29}$$

where $L_{\hat{\boldsymbol{r}}^p}$ denotes the distance between $\boldsymbol{x}^p$ and $\mathcal{S}^p$ in the direction $\hat{\boldsymbol{r}}^p$ (for a sphere of radius R_p, $L_{\hat{\boldsymbol{r}}^p} = R_p$). In particular, setting $A = 1$ in Eq. (29), we obtain

$$V^p \underline{(\boldsymbol{r}^p)^{(k)} \delta^p_{\mathrm{L}\boldsymbol{x}}}_{\mathcal{V}^p} = \frac{(\boldsymbol{r}^p)^{(k)}}{2+k} X^p \left(\left(\frac{L_{\hat{\boldsymbol{r}}^p}}{|\boldsymbol{r}^p|} \right)^{2+k} - 1 \right). \tag{30}$$

Hence, the generalized functions involved in Eqs. (21)-(27) are typically nothing more than weighted indicator functions.

C. Macroscopic averaging

1. *Generic averaging procedure*

The operator $\langle\cdot\rangle$ shall define a generic averaging procedure with the properties

$$\langle cA_1 + A_2 \rangle = c\langle A_1 \rangle + \langle A_2 \rangle, \qquad \langle \partial_i A \rangle = \partial_i \langle A \rangle, \qquad \langle \partial_t A \rangle = \partial_t \langle A \rangle, \qquad \langle A X_\infty \rangle = \langle A \rangle, \tag{31}$$

where the A-s are fields well-defined for $\boldsymbol{x} \in \mathcal{V}_\infty$ and c a constant. The first three properties, linearity and commutation with the spatial and temporal derivatives, are satisfied for most standard averaging procedures, such as the ensemble and sphere-symmetrical spatiotemporal averages employed in previous studies:

$$\langle A[\boldsymbol{x}, t] \rangle \equiv \int A[\boldsymbol{x}, t, \mathcal{F}] \mathrm{d}\mathcal{P}, \tag{32}$$

$$\langle A[\boldsymbol{x}, t] \rangle \equiv \int_{\mathcal{R}^4} A[\boldsymbol{x} - \boldsymbol{r}, t - \tau] k[|\boldsymbol{r}|, \tau] \mathrm{d}^3 r \mathrm{d}\tau. \tag{33}$$

Here $\mathcal{F}$ is an abstract infinite-dimensional flow state of the ensemble of flows, $\mathrm{d}\mathcal{P}$ its corresponding probability measure, and $k[|\boldsymbol{r}|, \tau]$ denotes a sphere-symmetrical kernel that integrates to unity. The formal description of the ensemble average in Eq. (32) was discussed in detail by Zhang *et al.* [27], who also demonstrated its consistency with the formalism used to obtain the closure problem in the studies by Prosperetti and coworkers based on a time-evolving probability density of particle configurations [16]. The fourth property in Eq. (31) ensures that the averaging procedure only operates within $\mathcal{V}_\infty$. It implies trivially that terms involving $\partial_i X_\infty$ (nonzero only at the boundary of $\mathcal{V}_\infty$) do not contribute to the average:

$$\langle A \partial_i X_\infty \rangle = \langle \partial_i A X_\infty - X_\infty \partial_i A \rangle = \partial_i \langle A X_\infty \rangle - \langle \partial_i A \rangle = \partial_i \langle A \rangle - \partial_i \langle A \rangle = 0. \tag{34}$$

This property is generally not satisfied for sphere-symmetrical spatial averages, except if $\mathcal{V}_\infty = \mathcal{R}^3$ or if $k[|\boldsymbol{r}|, \tau]$ has a compact support (i.e., $k[|\boldsymbol{r}|, \tau] = 0$ for $|\boldsymbol{r}| > \zeta$). In the latter case, the eventually derived expressions for the fields of the closure problem will be mathematically exact for all points $\boldsymbol{x}$ that are separated from the boundary of $\mathcal{V}_\infty$ by a distance larger than ζ.

For statistically steady systems or systems that are statistically homogeneous in a given direction s (the latter requires that the extent of $\mathcal{V}_\infty$ in the s-direction is infinite), such as bed-tangentially homogeneous sediment transport, it is physically meaningful to average the system over all times t or the entire s-direction, respectively:

$$\langle A[\boldsymbol{x}, t] \rangle \equiv \lim_{T \to \infty} \frac{1}{T} \int_0^T A[\boldsymbol{x}, t] \mathrm{d}t, \tag{35}$$

$$\langle A[\boldsymbol{x}, t] \rangle \equiv \lim_{L \to \infty} \frac{1}{L} \int_0^L A[\boldsymbol{x}, t] \mathrm{d}s. \tag{36}$$

These averages satisfy all the properties in Eq. (31) and, if the ergodic hypothesis is true, are equivalent to the ensemble average.

Finally, we note that also the identity operation satisfies all the properties in Eq. (31). In that case, many of the eventually derived expressions for the fields of the closure problem will still be mathematically exact at the level of generalized functions (indicator functions and delta distributions), but not physically meaningful, since they will exhibit numerous discontinuities and singularities. In other words, the averaging procedure should, in the context of actual physical systems, also ensure smoothing out discontinuities and singularities. Due to their infinite scale, this property is satisfied by Eqs. (32), (35), and (36). It is also satisfied by Eq. (33) if $k[|\boldsymbol{r}|, \tau]$ decays with $|\boldsymbol{r}|$ and/or τ sufficiently slowly.

2. Phase averages

The fluid phase, solid phase, and grain phase averages (for clarity, we avoid the term "particle phase" used in previous studies) of a field A are defined, respectively, as

$$\langle A\rangle^{\mathrm{f}} \equiv \langle AX_{\mathrm{f}}\rangle/\beta_{\mathrm{f}}, \qquad \langle A\rangle^{\mathrm{s}} \equiv \langle AX_{\mathrm{s}}\rangle/\beta_{\mathrm{s}}, \qquad \langle A\rangle^{\mathrm{g}} \equiv \langle \sum\nolimits_p \underline{A}_{\mathcal{V}^p} V^p \delta^p_{\boldsymbol{x}}\rangle/c_{\mathrm{g}}, \tag{37}$$

where $\beta_{\mathrm{f}} \equiv \langle X_{\mathrm{f}}\rangle$ and $\beta_{\mathrm{s}} \equiv \langle X_{\mathrm{s}}\rangle = 1-\beta_{\mathrm{f}}$ are the fluid and solid volume fractions, respectively, and $c_{\mathrm{g}} \equiv \left\langle \sum_p V^p \delta^p_{\boldsymbol{x}} \right\rangle$ the grain concentration (based on the grain number density). For the above definitions to make sense, A must be well-defined for $\boldsymbol{x} \in \mathcal{V}_{\mathrm{f}}$ ($\langle\cdot\rangle^{\mathrm{f}}$) or $\boldsymbol{x} \in \mathcal{V}_{\mathrm{s}}$ ($\langle\cdot\rangle^{\mathrm{s,g}}$). The mixture average of A, defined as $\langle A\rangle$, is related to the fluid phase and solid phase averages through

$$\langle A\rangle = \beta_{\mathrm{f}}\langle A\rangle^{\mathrm{f}} + \beta_{\mathrm{s}}\langle A\rangle^{\mathrm{s}}. \tag{38}$$

While the volume-weighted averages above are suited for quantities conveying information per unit volume or surface area, such as stresses, the mass-weighted phase averages defined below are suited for quantities conveying information per unit mass:

$$\langle A\rangle^{\mathrm{f}}_{\rho} \equiv \langle \rho A\rangle^{\mathrm{f}}/\langle\rho\rangle^{\mathrm{f}}, \qquad \langle A\rangle^{\mathrm{s}}_{\rho} \equiv \langle \rho A\rangle^{\mathrm{s}}/\langle\rho\rangle^{\mathrm{s}}, \qquad \langle A\rangle^{\mathrm{g}}_{\rho} \equiv \langle \rho A\rangle^{\mathrm{g}}/\langle\rho\rangle^{\mathrm{g}}, \qquad \langle A\rangle_{\rho} \equiv \langle \rho A\rangle/\langle\rho\rangle, \tag{39}$$

where the subscript w in expressions of the type $\langle\rangle^{(\cdot)}_w$, with '$(\cdot)$' a placeholder, shall indicate a weighting by w.

3. Averages satisfying the Reynolds rule

Certain averages, such as Eqs. (32), (35), and (36), satisfy the Reynolds rule

$$\langle\langle A_1\rangle A_2\rangle \overset{\mathrm{R}}{=} \langle A_1\rangle\langle A_2\rangle \tag{40}$$

in addition to the rules in Eq. (31). Here and henceforth, the symbol '$\overset{\mathrm{R}}{=}$' shall indicate equalities that require the Reynolds rule to be true. Furthermore, Eq. (33) also satisfies Eq. (40), at least approximately, if the characteristic radius of its kernel $k[|\boldsymbol{r}|,\tau]$ is much smaller than the macroscopic-flow length scale L. The Reynolds rule immediately implies $\langle A_2\rangle\langle A_1/\langle A_2\rangle\rangle \overset{\mathrm{R}}{=} \langle A_1\rangle$ and therefore

$$\langle A_1/\langle A_2\rangle\rangle \overset{\mathrm{R}}{=} \langle A_1\rangle/\langle A_2\rangle, \tag{41}$$

$$\Rightarrow \langle\langle A_1\rangle^{(\cdot)} A_2\rangle^{(\cdot)} \overset{\mathrm{R}}{=} \langle A_1\rangle^{(\cdot)}\langle A_2\rangle^{(\cdot)}. \tag{42}$$

Further consequences of Eq. (40) are

$$\langle A_1\partial\langle A_2\rangle\rangle = \langle A_1\langle\partial A_2\rangle\rangle \overset{\mathrm{R}}{=} \langle A_1\rangle\partial\langle A_2\rangle, \tag{43}$$

$$\begin{aligned}\beta_{\mathrm{f,s}}\langle\partial\langle A\rangle^{\mathrm{f,s}}\rangle^{\mathrm{f,s}} &= \langle X_{\mathrm{f,s}}\partial\langle A\rangle^{\mathrm{f,s}}\rangle = \langle\partial X_{\mathrm{f,s}}\langle A\rangle^{\mathrm{f,s}}\rangle - \langle\langle A\rangle^{\mathrm{f,s}}\partial X_{\mathrm{f,s}}\rangle \\ &\overset{\mathrm{R}}{=} \partial\langle X_{\mathrm{f,s}}\langle A\rangle^{\mathrm{f,s}}\rangle - \langle A\rangle^{\mathrm{f,s}}\langle\partial X_{\mathrm{f,s}}\rangle = \partial\beta_{\mathrm{f,s}}\langle A\rangle^{\mathrm{f,s}} - \langle A\rangle^{\mathrm{f,s}}\partial\beta_{\mathrm{f,s}} = \beta_{\mathrm{f,s}}\partial\langle A\rangle^{\mathrm{f,s}}.\end{aligned} \tag{44}$$

It means that, if the Reynolds rule is satisfied, regardless of the kind of averages involved (mixture or phase), averaged quantities and derivatives thereof inside of another average can be taken out of the latter, like constants. This property will turn out useful in many of the coming calculations.

4. Fluctuation operators

To simplify some of the coming calculations (especially in regard to the buoyancy closure), we define the fluctuation operators $\cdot'$ and $[\cdot]'_{\mathrm{s}}$ acting on macroscopically-averaged tensor fields $\boldsymbol{A}$, respectively, as

$$\boldsymbol{A}' \equiv \boldsymbol{\nabla}\cdot\left\langle \sum\nolimits_p V^p \underline{\boldsymbol{r}^p\left(\boldsymbol{A}-\underline{\boldsymbol{A}}_{\mathcal{V}^p}\right)\delta^p_{\mathrm{L}\boldsymbol{x}}}_{\mathcal{V}^p} \right\rangle = \beta_{\mathrm{s}}\left\langle \underline{\boldsymbol{A}}_{\mathcal{V}} - \boldsymbol{A}\right\rangle^{\mathrm{s}} \overset{\mathrm{R}}{=} \beta_{\mathrm{s}}\left\langle \underline{\boldsymbol{A}}_{\mathcal{V}}\right\rangle^{\mathrm{s}} - \beta_{\mathrm{s}}\boldsymbol{A}, \tag{45}$$

$$[\boldsymbol{A}]'_{\mathrm{s}} \equiv \left\langle \sum\nolimits_p V^p \underline{\boldsymbol{r}^p\left(\boldsymbol{\nabla}\cdot\boldsymbol{A}-\boldsymbol{\nabla}\cdot\underline{\boldsymbol{A}}_{\mathcal{V}^p}\right)\delta^p_{\mathrm{L}\boldsymbol{x}}}_{\mathcal{V}^p} \right\rangle, \tag{46}$$

where we used Eq. (22) in Eq. (45). One can immediately see that they are related through

$$\boldsymbol{\nabla}\cdot[\boldsymbol{A}]'_{\mathrm{s}}=(\boldsymbol{\nabla}\cdot\boldsymbol{A})'. \tag{47}$$

Henceforth, the symbol '$\overset{\circ}{=}$' shall indicate equalities for the case of spheres of a constant radius R with sphere-symmetrical interiors, while the symbol '$\overset{\mathrm{R},\circ}{=}$' is used when in addition the Reynolds rule is satisfied. The latter case is interesting because it allows expanding $\boldsymbol{A}'$ in an infinite series of derivatives of $\boldsymbol{A}$ (Appendix B), which will become useful later. In the fifth order of R/L, it reads (Eq. (B14))

$$\boldsymbol{A}'\overset{\mathrm{R},\circ}{=}\frac{R^2}{5}\boldsymbol{\nabla}\cdot\beta_{\mathrm{s}}\boldsymbol{\nabla}\boldsymbol{A}-\frac{R^4}{175}\Delta\boldsymbol{\nabla}\cdot\beta_{\mathrm{s}}\boldsymbol{\nabla}\boldsymbol{A}+\frac{R^4}{350}\Delta\beta_{\mathrm{s}}\Delta\boldsymbol{A}+\frac{9R^4}{350}\boldsymbol{\nabla}\boldsymbol{\nabla}:\beta_{\mathrm{s}}\boldsymbol{\nabla}\boldsymbol{\nabla}\boldsymbol{A}-\frac{R^4}{175}\boldsymbol{\nabla}\cdot\beta_{\mathrm{s}}\boldsymbol{\nabla}\Delta\boldsymbol{A}+O(R^6/L^6), \tag{48}$$

where $\Delta=\boldsymbol{\nabla}\cdot\boldsymbol{\nabla}$ denotes the Laplace operator. Using Eq. (47), Eq. (48) implies

$$[\boldsymbol{A}]'_{\mathrm{s}}\overset{\mathrm{R},\circ}{\simeq}\frac{R^2}{5}\beta_{\mathrm{s}}\boldsymbol{\nabla}\boldsymbol{\nabla}\cdot\boldsymbol{A}-\frac{R^4}{175}\Delta\beta_{\mathrm{s}}\boldsymbol{\nabla}\boldsymbol{\nabla}\cdot\boldsymbol{A}+\frac{R^4}{350}\boldsymbol{\nabla}\beta_{\mathrm{s}}\Delta\boldsymbol{\nabla}\cdot\boldsymbol{A}+\frac{9R^4}{350}\boldsymbol{\nabla}\cdot\beta_{\mathrm{s}}\boldsymbol{\nabla}\boldsymbol{\nabla}\boldsymbol{\nabla}\cdot\boldsymbol{A}-\frac{R^4}{175}\beta_{\mathrm{s}}\boldsymbol{\nabla}\Delta\boldsymbol{\nabla}\cdot\boldsymbol{A}+O(R^6/L^6). \tag{49}$$

Here and henceforth, the symbol '$\simeq$' shall indicate equality but for a divergence-free term: $\boldsymbol{A}\simeq\boldsymbol{B}\Leftrightarrow\boldsymbol{\nabla}\cdot\boldsymbol{A}=\boldsymbol{\nabla}\cdot\boldsymbol{B}$.

III. DERIVATION OF AVERAGE BALANCE EQUATIONS

Previous studies deriving the closure problem usually focused on the local, instantaneous mass and momentum balances:

$$\partial_t\rho+\boldsymbol{\nabla}\cdot\rho\boldsymbol{u}=0, \tag{50}$$

$$\partial_t\rho\boldsymbol{u}+\boldsymbol{\nabla}\cdot\rho\boldsymbol{u}\boldsymbol{u}=\boldsymbol{\nabla}\cdot\boldsymbol{\sigma}+\rho\boldsymbol{g}, \tag{51}$$

where $\boldsymbol{g}$ is the body force per unit mass and $\boldsymbol{\sigma}$ the stress tensor. The task was to macroscopically average these equations over the fluid ($\langle\cdot\rangle^{\mathrm{f}}$), solid ($\langle\cdot\rangle^{\mathrm{s}}$), or mixture ($\langle\cdot\rangle$) phases and transform the averaged equations into forms structurally equivalent to Eqs. (50) and (51). The main mathematical challenge that thereby arises is to express the emerging term $\beta_{\mathrm{f}}\langle\boldsymbol{\nabla}\cdot\boldsymbol{\sigma}\rangle^{\mathrm{f}}$ or $\beta_{\mathrm{s}}\langle\boldsymbol{\nabla}\cdot\boldsymbol{\sigma}\rangle^{\mathrm{s}}$ as a divergence of an effective stress, $\boldsymbol{\nabla}\cdot\boldsymbol{\sigma}^{\mathbf{f}}$ or $\boldsymbol{\nabla}\cdot\boldsymbol{\sigma}^{\mathbf{s}}$, minus or plus a fluid-solid interaction force density $\boldsymbol{f}$.

In what follows, we average not only the mass and momentum balances but generic balance equations. To do so, we first transform the nonaveraged balance equations into suitable forms based on generalized functions, using the identities derived in §II B 4, that allow straightforward application of the averaging rules Eq. (31). In the case of solid phase balance equations, for which local, instantaneous surface fluxes such as $\boldsymbol{\sigma}$ arise from internal interactions in the particle interiors and are usually unknown, we take a detour via rigid-body dynamics and *a posteriori* express emerging terms as effective solid phase surface fluxes.

A. Generic fluid phase balance equation

A generic nonaveraged local balance equation of an infinitesimal continuous-fluid property, $\mathrm{d}\Psi=\rho\psi\mathrm{d}V$, shall be satisfied for all points $\boldsymbol{x}\in\mathcal{V}_{\mathrm{f}}[t]$ [33]:

$$X_{\mathrm{f}}\left(\partial_t\rho\psi+\boldsymbol{\nabla}\cdot\rho\boldsymbol{u}\psi\right)=X_{\mathrm{f}}\left(-\boldsymbol{\nabla}\cdot\boldsymbol{J}_{\boldsymbol{\Psi}}+\rho\dot{\psi}_{\mathrm{b}}+D_{\Psi}\right), \tag{52}$$

where $\boldsymbol{J}_{\boldsymbol{\Psi}}$ is the surface flux of Ψ, and $\rho\dot{\psi}_{\mathrm{b}}$ and D_{Ψ} are the body sources and internal sources, respectively, of Ψ (the term 'sources' shall also include negative sources, that is, sinks). For example, the cases $(\psi,\boldsymbol{J}_{\boldsymbol{\Psi}},D_{\Psi})=(1,0,0)$ and $(\psi,\boldsymbol{J}_{\boldsymbol{\Psi}},D_{\Psi})=(\boldsymbol{u},-\boldsymbol{\sigma},0)$ represent Eqs. (50) and (51), respectively; see Table II. Note that internal sources from pairwise interactions between fluid constituents in the interior of an infinitesimal volume $\mathrm{d}V$ that cancel out upon summation, such as interaction forces, can be treated as surface flux divergences and shall therefore be included in $-\boldsymbol{\nabla}\cdot\boldsymbol{J}_{\boldsymbol{\Psi}}$, while D_{Ψ} shall include all other internal sources, such as viscous heat dissipation from frictional interactions (Table II).

Using Eqs. (1) and (2), and the chain rule of differentiation, Eq. (52) can be transformed to

$$\partial_t\rho\psi X_{\mathrm{f}}+\boldsymbol{\nabla}\cdot\rho\boldsymbol{u}\psi X_{\mathrm{f}}=-\boldsymbol{\nabla}\cdot\boldsymbol{J}_{\boldsymbol{\Psi}}X_{\mathrm{f}}+\boldsymbol{J}^{\mathrm{T}}_{\boldsymbol{\Psi}}\cdot\boldsymbol{\nabla}X_{\infty}-\sum\nolimits_p\boldsymbol{J}^{\mathrm{T}}_{\boldsymbol{\Psi}}\cdot\boldsymbol{\nabla}X^p+\left(\rho\dot{\psi}_{\mathrm{b}}+D_{\Psi}\right)X_{\mathrm{f}}. \tag{53}$$

Balance of	ψ	$\boldsymbol{J}_{\Psi}$	$\dot{\psi}_{\mathrm{b}}$	D_{Ψ}
Mass	1	0	0	0
Momentum	$\boldsymbol{u}$	$-\boldsymbol{\sigma}$	$\boldsymbol{g}$	0
Angular momentum	$\boldsymbol{x}\times\boldsymbol{u}$	$\boldsymbol{\sigma}\times\boldsymbol{x}$	$\boldsymbol{x}\times\boldsymbol{g}$	0
Mechanical energy	$\boldsymbol{u}^2/2$	$-\boldsymbol{\sigma}\cdot\boldsymbol{u}$	$\boldsymbol{g}\cdot\boldsymbol{u}$	$-\boldsymbol{\sigma}:\boldsymbol{\nabla}\boldsymbol{u}$

TABLE II. Typical examples for the terms ψ, $\boldsymbol{J}_{\Psi}$, $\dot{\psi}_{\mathrm{b}}$, and D_{Ψ}, appearing in Eq. (52), after Ishii and Hibiki [33]. Here $\boldsymbol{\sigma}$ is the stress tensor, and $\boldsymbol{g}$ the body (e.g., gravitational) acceleration. Note that, with the above definitions of $\boldsymbol{J}_{\Psi}$ and $\dot{\psi}_{\mathrm{b}}$, the angular momentum balance simplifies to $\sigma_{ij}=\sigma_{ji}$ [33].

We now use Eq. (26) for $A=(\boldsymbol{J}_{\Psi}^{\mathrm{T}})_i$ to calculate $\boldsymbol{J}_{\Psi}^{\mathrm{T}}\cdot\boldsymbol{\nabla}X^p$ in Eq. (53):

$$\boldsymbol{J}_{\Psi}^{\mathrm{T}}\cdot\boldsymbol{\nabla}X^p=-\frac{S^p}{V^p}\underline{\boldsymbol{n}^p\cdot\boldsymbol{J}_{\Psi}}_{\mathcal{S}^p}X^p+\boldsymbol{\nabla}\cdot S^p\left(\underline{\boldsymbol{r}^p\boldsymbol{n}^p\cdot\boldsymbol{J}_{\Psi}\delta^p_{\mathrm{L}\boldsymbol{x}}}_{\mathcal{S}^p}-\underline{\boldsymbol{r}^p\delta^p_{\mathrm{L}\boldsymbol{x}}}_{\mathcal{V}^p}\underline{\boldsymbol{n}^p\cdot\boldsymbol{J}_{\Psi}}_{\mathcal{S}^p}\right). \tag{54}$$

The thereby arising term $-S^p\underline{\boldsymbol{n}^p\cdot\boldsymbol{J}_{\Psi}}_{\mathcal{S}^p}$ can be identified as the temporal change of the particle property $\Psi^p\equiv V^p\underline{\rho\psi}_{\mathcal{V}^p}$, which is the total amount of Ψ contained in an individual particle p, due to the transfer of Ψ from the fluid into the particle p, denoted as $\dot{\Psi}^p_{\mathrm{f}}$:

$$-S^p\underline{\boldsymbol{n}^p\cdot\boldsymbol{J}_{\Psi}}_{\mathcal{S}^p}=-\int_{\mathcal{S}^p}(\boldsymbol{n}^p\cdot\boldsymbol{J}_{\Psi})\,\mathrm{d}S=\dot{\Psi}^p_{\mathrm{f}}=V^p\underline{\rho\dot{\psi}_{\mathrm{f}}}_{\mathcal{V}^p}, \tag{55}$$

where we used Eq. (6). Then, summing Eq. (55) divided by V^p over all particles and averaging ($\langle\cdot\rangle$), using the definitions in Eq. (8), yields

$$\begin{aligned}-\left\langle\sum\nolimits_p\frac{S^p}{V^p}\underline{\boldsymbol{n}^p\cdot\boldsymbol{J}_{\Psi}}_{\mathcal{S}^p}X^p\right\rangle&=\left\langle\sum\nolimits_p\underline{\rho\dot{\psi}_{\mathrm{f}}}_{\mathcal{V}^p}X^p\right\rangle=\left\langle\sum\nolimits_p\underline{\rho}_{\mathcal{V}^p}\underline{\dot{\psi}_{\mathrm{f}}}_{\mathcal{M}^p}X^p\right\rangle=\left\langle\sum\nolimits_p\sum\nolimits_q\underline{\rho}_{\mathcal{V}^q}X^q\underline{\dot{\psi}_{\mathrm{f}}}_{\mathcal{M}^p}X^p\right\rangle\\&=\left\langle\underline{\rho}_{\mathcal{V}}\underline{\dot{\psi}_{\mathrm{f}}}_{\mathcal{M}}\right\rangle=\left\langle X_{\mathrm{s}}\rho_*\dot{\psi}_{\uparrow\mathrm{f}}\right\rangle=\beta_{\mathrm{s}}\left\langle\rho_*\dot{\psi}_{\uparrow\mathrm{f}}\right\rangle^{\mathrm{s}},\end{aligned} \tag{56}$$

which is our preferred notation to denote the fluid-solid interaction term in the average balance equations below. In fact, summing Eq. (54) over all particles, inserting it into Eq. (53), and averaging ($\langle\cdot\rangle$), using Eq. (56) and the definitions and rules of §II B and §II C, yields

$$\partial_t\beta_{\mathrm{f}}\langle\rho\psi\rangle^{\mathrm{f}}+\boldsymbol{\nabla}\cdot\beta_{\mathrm{f}}\langle\rho\boldsymbol{u}\psi\rangle^{\mathrm{f}}=-\boldsymbol{\nabla}\cdot\left(\boldsymbol{J}^{\mathbf{f}}_{\Psi}-\boldsymbol{J}^{\mathbf{f}}_{\Psi\mathbf{Re}}\right)+\beta_{\mathrm{f}}\langle\rho\dot{\psi}_{\mathrm{b}}\rangle^{\mathrm{f}}+\beta_{\mathrm{f}}\langle D_{\Psi}\rangle^{\mathrm{f}}-\beta_{\mathrm{s}}\langle\rho_*\dot{\psi}_{\uparrow\mathrm{f}}\rangle^{\mathrm{s}}, \tag{57}$$

$$\partial_t\beta_{\mathrm{f}}\langle\rho\rangle^{\mathrm{f}}\langle\psi\rangle^{\mathrm{f}}_{\rho}+\boldsymbol{\nabla}\cdot\beta_{\mathrm{f}}\langle\rho\rangle^{\mathrm{f}}\langle\boldsymbol{u}\rangle^{\mathrm{f}}_{\rho}\langle\psi\rangle^{\mathrm{f}}_{\rho}=-\boldsymbol{\nabla}\cdot\boldsymbol{J}^{\mathbf{f}}_{\Psi}+\beta_{\mathrm{f}}\langle\rho\rangle^{\mathrm{f}}\langle\dot{\psi}_{\mathrm{b}}\rangle^{\mathrm{f}}_{\rho}+\beta_{\mathrm{f}}\langle D_{\Psi}\rangle^{\mathrm{f}}-\beta_{\mathrm{s}}\langle\rho_*\rangle^{\mathrm{s}}\langle\dot{\psi}_{\uparrow\mathrm{f}}\rangle^{\mathrm{s}}_{\rho_*}, \tag{58}$$

where $\boldsymbol{J}^{\mathbf{f}}_{\Psi}$ is the effective fluid phase surface flux of Ψ. It is defined through the equivalent $\boldsymbol{J}^{\tilde{\mathbf{f}}}_{\Psi}$ to distinguish it from the final form $\boldsymbol{J}^{\mathbf{f}}_{\Psi}$ derived afterward ($\boldsymbol{\nabla}\cdot\boldsymbol{J}^{\tilde{\mathbf{f}}}_{\Psi}=\boldsymbol{\nabla}\cdot\boldsymbol{J}^{\mathbf{f}}_{\Psi}$):

$$\boldsymbol{J}^{\mathbf{f}}_{\Psi}\simeq\boldsymbol{J}^{\tilde{\mathbf{f}}}_{\Psi}\equiv\beta_{\mathrm{f}}\langle\boldsymbol{J}_{\Psi}\rangle^{\mathrm{f}}+\boldsymbol{J}^{\mathbf{f}}_{\Psi\mathbf{Re}}+\boldsymbol{J}^{\tilde{\mathbf{f}}}_{\Psi\mathbf{s}}, \tag{59}$$

$$\boldsymbol{J}^{\mathbf{f}}_{\Psi\mathbf{Re}}\equiv\beta_{\mathrm{f}}\langle\rho\rangle^{\mathrm{f}}\left(\langle\boldsymbol{u}\psi\rangle^{\mathrm{f}}_{\rho}-\langle\boldsymbol{u}\rangle^{\mathrm{f}}_{\rho}\langle\psi\rangle^{\mathrm{f}}_{\rho}\right)\overset{\mathrm{R}}{=}\beta_{\mathrm{f}}\langle\rho\rangle^{\mathrm{f}}\left\langle\left(\boldsymbol{u}-\langle\boldsymbol{u}\rangle^{\mathrm{f}}_{\rho}\right)\left(\psi-\langle\psi\rangle^{\mathrm{f}}_{\rho}\right)\right\rangle^{\mathrm{f}}_{\rho}, \tag{60}$$

$$\boldsymbol{J}^{\tilde{\mathbf{f}}}_{\Psi\mathbf{s}}\equiv\left\langle\sum\nolimits_p S^p\left(\underline{\boldsymbol{r}^p\boldsymbol{n}^p\cdot\boldsymbol{J}_{\Psi}\delta^p_{\mathrm{L}\boldsymbol{x}}}_{\mathcal{S}^p}-\underline{\boldsymbol{r}^p\delta^p_{\mathrm{L}\boldsymbol{x}}}_{\mathcal{V}^p}\underline{\boldsymbol{n}^p\cdot\boldsymbol{J}_{\Psi}}_{\mathcal{S}^p}\right)\right\rangle. \tag{61}$$

It consists of three components: one from the local, instantaneous flow ($\beta_{\mathrm{f}}\langle\boldsymbol{J}_{\Psi}\rangle^{\mathrm{f}}$), one from the (turbulent) fluid fluctuation motion ($\boldsymbol{J}^{\mathbf{f}}_{\Psi\mathbf{Re}}$), and one from the presence of particles ($\boldsymbol{J}^{\tilde{\mathbf{f}}}_{\Psi\mathbf{s}}$).

Equations (59)-(61) represent a form equivalent to that derived in a previous exact analysis for the momentum balance ($\boldsymbol{J}_{\Psi}=-\boldsymbol{\sigma}$) and sphere-symmetrical volume averaging [19]. However, this form obscures physical insights and can be transformed into a more insightful form via

$$\beta_{\mathrm{f}}\langle\boldsymbol{J}_{\Psi}\rangle^{\mathrm{f}}=\langle\boldsymbol{J}_{\Psi}\rangle^{\mathrm{f}}-\beta_{\mathrm{s}}\langle\boldsymbol{J}_{\Psi}\rangle^{\mathrm{f}}=\langle\boldsymbol{J}_{\Psi}\rangle^{\mathrm{f}}-\beta_{\mathrm{s}}\left\langle\langle\boldsymbol{J}_{\Psi}\rangle^{\mathrm{f}}\right\rangle^{\mathrm{s}}+\beta_{\mathrm{s}}\left(\left\langle\langle\boldsymbol{J}_{\Psi}\rangle^{\mathrm{f}}\right\rangle^{\mathrm{s}}-\langle\boldsymbol{J}_{\Psi}\rangle^{\mathrm{f}}\right) \tag{62}$$

and applying Eq. (27) to calculate

$$\begin{aligned}
&\boldsymbol{\nabla}\cdot\beta_\mathrm{s}\left\langle\langle\boldsymbol{J}_{\boldsymbol{\Psi}}\rangle^\mathrm{f}\right\rangle^\mathrm{s}=\boldsymbol{\nabla}\cdot\left\langle X_\mathrm{s}\langle\boldsymbol{J}_{\boldsymbol{\Psi}}\rangle^\mathrm{f}\right\rangle=\left\langle\boldsymbol{\nabla}\cdot X_\mathrm{s}\langle\boldsymbol{J}_{\boldsymbol{\Psi}}\rangle^\mathrm{f}\right\rangle=\left\langle\sum\nolimits_p\boldsymbol{\nabla}\cdot X^p\langle\boldsymbol{J}_{\boldsymbol{\Psi}}\rangle^\mathrm{f}\right\rangle\\
&=\boldsymbol{\nabla}\cdot\left\langle\sum\nolimits_p S^p\underline{\boldsymbol{r}^p\boldsymbol{n}^p\cdot\langle\boldsymbol{J}_{\boldsymbol{\Psi}}\rangle^\mathrm{f}\delta^p_{\mathrm{L}\boldsymbol{x}}}_{\mathcal{S}^p}\right\rangle-\boldsymbol{\nabla}\cdot\left\langle\sum\nolimits_p V^p\underline{\boldsymbol{r}^p\left(\boldsymbol{\nabla}\cdot\langle\boldsymbol{J}_{\boldsymbol{\Psi}}\rangle^\mathrm{f}\right)\delta^p_{\mathrm{L}\boldsymbol{x}}}_{\mathcal{V}^p}\right\rangle\\
&=\boldsymbol{\nabla}\cdot\left\langle\sum\nolimits_p S^p\left(\underline{\boldsymbol{r}^p\boldsymbol{n}^p\cdot\langle\boldsymbol{J}_{\boldsymbol{\Psi}}\rangle^\mathrm{f}\delta^p_{\mathrm{L}\boldsymbol{x}}}_{\mathcal{S}^p}-\underline{\boldsymbol{r}^p\delta^p_{\mathrm{L}\boldsymbol{x}}}_{\mathcal{V}^p}\underline{\boldsymbol{n}^p\cdot\langle\boldsymbol{J}_{\boldsymbol{\Psi}}\rangle^\mathrm{f}}_{\mathcal{S}^p}\right)\right\rangle-\boldsymbol{\nabla}\cdot\left\langle\sum\nolimits_p V^p\underline{\boldsymbol{r}^p\left(\boldsymbol{\nabla}\cdot\langle\boldsymbol{J}_{\boldsymbol{\Psi}}\rangle^\mathrm{f}-\underline{\boldsymbol{\nabla}\cdot\langle\boldsymbol{J}_{\boldsymbol{\Psi}}\rangle^\mathrm{f}}_{\mathcal{V}^p}\right)\delta^p_{\mathrm{L}\boldsymbol{x}}}_{\mathcal{V}^p}\right\rangle\\
&=\boldsymbol{\nabla}\cdot\left\langle\sum\nolimits_p S^p\left(\underline{\boldsymbol{r}^p\boldsymbol{n}^p\cdot\langle\boldsymbol{J}_{\boldsymbol{\Psi}}\rangle^\mathrm{f}\delta^p_{\mathrm{L}\boldsymbol{x}}}_{\mathcal{S}^p}-\underline{\boldsymbol{r}^p\delta^p_{\mathrm{L}\boldsymbol{x}}}_{\mathcal{V}^p}\underline{\boldsymbol{n}^p\cdot\langle\boldsymbol{J}_{\boldsymbol{\Psi}}\rangle^\mathrm{f}}_{\mathcal{S}^p}\right)\right\rangle-\boldsymbol{\nabla}\cdot\left[\langle\boldsymbol{J}_{\boldsymbol{\Psi}}\rangle^\mathrm{f}\right]'_\mathrm{s},
\end{aligned}\tag{63}$$

where we used $S^p\underline{\boldsymbol{n}^p\cdot\langle\boldsymbol{J}_{\boldsymbol{\Psi}}\rangle^\mathrm{f}}_{\mathcal{S}^p}=V^p\underline{\boldsymbol{\nabla}\cdot\langle\boldsymbol{J}_{\boldsymbol{\Psi}}\rangle^\mathrm{f}}_{\mathcal{V}^p}$ (Gauss's theorem) and Eq. (46). Hence, we obtain

$$\boldsymbol{J}^{\tilde{\mathbf{f}}}_{\boldsymbol{\Psi}}\simeq\boldsymbol{J}^{\mathbf{f}}_{\boldsymbol{\Psi}}\equiv\langle\boldsymbol{J}_{\boldsymbol{\Psi}}\rangle^\mathrm{f}+\boldsymbol{J}^{\mathbf{f}}_{\boldsymbol{\Psi}\mathbf{Re}}+\boldsymbol{J}^{\mathbf{f}}_{\boldsymbol{\Psi}\mathbf{s}}+\left[\langle\boldsymbol{J}_{\boldsymbol{\Psi}}\rangle^\mathrm{f}\right]'_\mathrm{s},\tag{64}$$

$$\begin{aligned}
\boldsymbol{J}^{\mathbf{f}}_{\boldsymbol{\Psi}\mathbf{s}}&\equiv\left\langle\sum\nolimits_p S^p\left(\underline{\boldsymbol{r}^p\boldsymbol{n}^p\cdot\left(\boldsymbol{J}_{\boldsymbol{\Psi}}-\langle\boldsymbol{J}_{\boldsymbol{\Psi}}\rangle^\mathrm{f}\right)\delta^p_{\mathrm{L}\boldsymbol{x}}}_{\mathcal{S}^p}-\underline{\boldsymbol{r}^p\delta^p_{\mathrm{L}\boldsymbol{x}}}_{\mathcal{V}^p}\underline{\boldsymbol{n}^p\cdot\left(\boldsymbol{J}_{\boldsymbol{\Psi}}-\langle\boldsymbol{J}_{\boldsymbol{\Psi}}\rangle^\mathrm{f}\right)}_{\mathcal{S}^p}\right)\right\rangle+\beta_\mathrm{s}\left(\left\langle\langle\boldsymbol{J}_{\boldsymbol{\Psi}}\rangle^\mathrm{f}\right\rangle^\mathrm{s}-\langle\boldsymbol{J}_{\boldsymbol{\Psi}}\rangle^\mathrm{f}\right)\\
&\overset{\mathrm{R}}{=}\left\langle\sum\nolimits_p S^p\left(\underline{\boldsymbol{r}^p\boldsymbol{n}^p\cdot\left(\boldsymbol{J}_{\boldsymbol{\Psi}}-\langle\boldsymbol{J}_{\boldsymbol{\Psi}}\rangle^\mathrm{f}\right)\delta^p_{\mathrm{L}\boldsymbol{x}}}_{\mathcal{S}^p}-\underline{\boldsymbol{r}^p\delta^p_{\mathrm{L}\boldsymbol{x}}}_{\mathcal{V}^p}\underline{\boldsymbol{n}^p\cdot\left(\boldsymbol{J}_{\boldsymbol{\Psi}}-\langle\boldsymbol{J}_{\boldsymbol{\Psi}}\rangle^\mathrm{f}\right)}_{\mathcal{S}^p}\right)\right\rangle.
\end{aligned}\tag{65}$$

The chief advantage of $\boldsymbol{J}^{\mathbf{f}}_{\boldsymbol{\Psi}}$ over $\boldsymbol{J}^{\tilde{\mathbf{f}}}_{\boldsymbol{\Psi}}$ is that its particle contributions are expressed in terms of fluctuations: $\boldsymbol{J}^{\mathbf{f}}_{\boldsymbol{\Psi}\mathbf{s}}$ results from fluctuations of $\boldsymbol{J}_{\boldsymbol{\Psi}}$ relative to the fluid phase average $\langle\boldsymbol{J}_{\boldsymbol{\Psi}}\rangle^\mathrm{f}$ and $\left[\langle\boldsymbol{J}_{\boldsymbol{\Psi}}\rangle^\mathrm{f}\right]'_\mathrm{s}$ from fluctuations of $\boldsymbol{\nabla}\cdot\langle\boldsymbol{J}_{\boldsymbol{\Psi}}\rangle^\mathrm{f}$ within the particle interiors. In particular, for completely stationary fluid-particle systems, $\boldsymbol{J}^{\mathbf{f}}_{\boldsymbol{\Psi}\mathbf{s}}$, in contrast to $\boldsymbol{J}^{\tilde{\mathbf{f}}}_{\boldsymbol{\Psi}\mathbf{s}}$, vanishes for averaging procedures that satisfy $\langle\boldsymbol{J}_{\boldsymbol{\Psi}}\rangle^\mathrm{f}=\boldsymbol{J}_{\boldsymbol{\Psi}}$ (e.g., ensemble averaging).

B. Generic solid phase balance equation

To derive the local average solid phase balance equation of $\rho\psi\mathrm{d}V$, we could carry out an analysis analogous to that for the fluid phase above. However, the resulting expressions would be of little use, since nonaveraged quantities such as $\boldsymbol{J}_{\boldsymbol{\Psi}}$ would have to be evaluated in the particle interiors, where they are unknown. It means, in order to evaluate these expressions, one would have to link them to the rigid-body properties of individual particles and their interactions. To avoid redundancy, we instead directly derive a generic balance equation for an individual particle, link the terms therein to the different kind of interactions, followed by summing over all particles and macroscopic averaging. We start with the mass balance of an individual particle p, $X^p(\partial_t\rho+\boldsymbol{\nabla}\cdot\rho\boldsymbol{u})=0$, multiply it with ψ, and rearrange the resulting terms using Eq. (2) and the chain rule of differentiation, yielding

$$\partial_t\rho\psi X^p+\boldsymbol{\nabla}\cdot\rho\boldsymbol{u}\psi X^p=\rho\dot{\psi}X^p.\tag{66}$$

The field ψ can change in time for four distinct reasons ($\dot{\psi}=\dot{\psi}_\mathrm{b}+\dot{\psi}_\mathrm{g}+\dot{\psi}_\mathrm{c}+\dot{\psi}_\mathrm{f}$): body sources ($\dot{\psi}_\mathrm{b}$), particle-internal interactions ($\dot{\psi}_\mathrm{g}$), particle-particle contact interactions ($\dot{\psi}_\mathrm{c}$), and fluid-particle interactions ($\dot{\psi}_\mathrm{f}$). Using Eq. (22) for $\rho\dot{\psi}_\mathrm{gcf}\equiv\rho\dot{\psi}_\mathrm{g}+\rho\dot{\psi}_\mathrm{cf}\equiv\rho\dot{\psi}_\mathrm{g}+\rho\dot{\psi}_\mathrm{c}+\rho\dot{\psi}_\mathrm{f}$ and $\underline{\rho\dot{\psi}_\mathrm{g}}_{\mathcal{V}^p}=0$ (property of rigid bodies) yields

$$\partial_t\rho\psi X^p+\boldsymbol{\nabla}\cdot\rho\boldsymbol{u}\psi X^p=\rho\dot{\psi}_\mathrm{b}X^p+\underline{\rho\dot{\psi}_\mathrm{c}}_{\mathcal{V}^p}X^p+\underline{\rho\dot{\psi}_\mathrm{f}}_{\mathcal{V}^p}X^p-\boldsymbol{\nabla}\cdot V^p\underline{\boldsymbol{r}^p\left(\rho\dot{\psi}_\mathrm{gcf}-\underline{\rho\dot{\psi}_\mathrm{cf}}_{\mathcal{V}^p}\right)\delta^p_{\mathrm{L}\boldsymbol{x}}}_{\mathcal{V}^p}.\tag{67}$$

To express $\underline{\rho\dot{\psi}_\mathrm{c}}_{\mathcal{V}^p}X^p$, we use Eq. (21) for $A=1$ and $\dot{\Psi}^p_\mathrm{c}=V^p\underline{\rho\dot{\psi}_\mathrm{c}}_{\mathcal{V}^p}$, yielding

$$\underline{\rho\dot{\psi}_\mathrm{c}}_{\mathcal{V}^p}X^p=\dot{\Psi}^p_\mathrm{c}\delta^p_{\boldsymbol{x}}-\boldsymbol{\nabla}\cdot\underline{\boldsymbol{r}^p\delta^p_{\mathrm{L}\boldsymbol{x}}}_{\mathcal{V}^p}\dot{\Psi}^p_\mathrm{c}.\tag{68}$$

We now introduce $\dot{\Psi}^{pq}_\mathrm{c}$, describing the temporal change of Ψ^p due to an interaction of the particle p with the particle q (by convention, $\dot{\Psi}^{pq}_\mathrm{c}=0$ in the absence of interactions and $\dot{\Psi}^{pp}_\mathrm{c}=0$), and note that $\dot{\Psi}^{pq}_\mathrm{c}$ is summable over q as the number of contacts of p is bounded. Then, the first term on the right-hand side of Eq. (68) can be manipulated further via [cf. 34]

$$\begin{aligned}
\sum\nolimits_p\dot{\Psi}^p_\mathrm{c}\delta^p_{\boldsymbol{x}}&=\sum\nolimits_{pq}\dot{\Psi}^{pq}_\mathrm{c}\delta^p_{\boldsymbol{x}}=\sum\nolimits_{pq}\left(\dot{\Psi}^{[pq]}_\mathrm{c}+\dot{\Psi}^{(pq)}_\mathrm{c}\right)\delta^p_{\boldsymbol{x}}=\frac{1}{2}\sum\nolimits_{pq}\dot{\Psi}^{[pq]}_\mathrm{c}\left(\delta^p_{\boldsymbol{x}}-\delta^q_{\boldsymbol{x}}\right)+\sum\nolimits_{pq}\dot{\Psi}^{(pq)}_\mathrm{c}\delta^p_{\boldsymbol{x}}\\
&=\boldsymbol{\nabla}\cdot\frac{1}{2}\sum\nolimits_{pq}\boldsymbol{r}^{pq}\dot{\Psi}^{[pq]}_\mathrm{c}\delta^{pq}_{\mathrm{L}\boldsymbol{x}}+\sum\nolimits_{pq}\dot{\Psi}^{(pq)}_\mathrm{c}\delta^p_{\boldsymbol{x}},
\end{aligned}\tag{69}$$

Balance of	ψ	$\dot{\Psi}^p_{\mathrm{c(f)}}$	$M^p\left(\dot{\psi}_{\mathrm{gcf}}-\underline{\dot{\psi}_{\mathrm{cf}}}_{\mathcal{M}^p}\right)$ for $\boldsymbol{x}\in\mathcal{V}^p$
Mass	1	0	0
Momentum	$\boldsymbol{u}$	$\boldsymbol{F}^p_{\mathrm{c(f)}}$	$M^p\dot{\boldsymbol{v}}^p_{\circlearrowleft\mathrm{gcf}}=M^p\left(\dot{\boldsymbol{\omega}}^p_{\mathrm{gcf}}\times\boldsymbol{r}^p+\boldsymbol{\omega}^p\times\boldsymbol{v}^p_{\circlearrowleft}\right)$
Angular momentum	$\boldsymbol{x}\times\boldsymbol{u}$	$\boldsymbol{x}^p\times\boldsymbol{F}^p_{\mathrm{c(f)}}+\boldsymbol{T}^p_{\mathrm{c(f)}}$	$M^p\boldsymbol{x}\times\dot{\boldsymbol{v}}^p_{\circlearrowleft\mathrm{gcf}}+\boldsymbol{r}^p\times\boldsymbol{F}^p_{\mathrm{cf}}-\boldsymbol{T}^p_{\mathrm{cf}}$
Mechanical energy	$\boldsymbol{u}^2/2$	$\boldsymbol{F}^p_{\mathrm{c(f)}}\cdot\boldsymbol{v}^p_{\uparrow}+\boldsymbol{T}^p_{\mathrm{c(f)}}\cdot\boldsymbol{\omega}^p$	$M^p\dot{\boldsymbol{v}}^p_{\circlearrowleft\mathrm{gcf}}\cdot(\boldsymbol{v}^p_{\uparrow}+\boldsymbol{v}^p_{\circlearrowleft})+\boldsymbol{F}^p_{\mathrm{cf}}\cdot\boldsymbol{v}^p_{\circlearrowleft}-\boldsymbol{T}^p_{\mathrm{cf}}\cdot\boldsymbol{\omega}^p$

TABLE III. Examples for the terms $M^p\left(\dot{\psi}_{\mathrm{gcf}}-\underline{\dot{\psi}_{\mathrm{cf}}}_{\mathcal{M}^p}\right)$, $\dot{\Psi}^p_{\mathrm{cf}}$, and $\dot{\Psi}^p_{\mathrm{c}}$, appearing in Eqs. (75)-(78). Here $\boldsymbol{F}^p=M^p\dot{\boldsymbol{v}}^p_{\uparrow}$ and $\boldsymbol{T}^p=M^p\underline{\boldsymbol{r}^p\times\dot{\boldsymbol{v}}^p_{\circlearrowleft}}_{\mathcal{M}^p}$ denote the total force and torque, respectively, applied on the particle p. Furthermore, $\boldsymbol{F}^p_{\mathrm{cf}}=\boldsymbol{F}^p_{\mathrm{c}}+\boldsymbol{F}^p_{\mathrm{f}}$ and $\boldsymbol{T}^p_{\mathrm{cf}}=\boldsymbol{T}^p_{\mathrm{c}}+\boldsymbol{T}^p_{\mathrm{f}}$, where the subscripts 'c' and 'f' refer to contributions from contact and fluid-particle interactions, respectively, while 'c(f)' means either 'c' or 'cf'. The angular acceleration $\dot{\boldsymbol{\omega}}^p_{\mathrm{gcf}}$ from particle-internal, contact, and fluid-particle interactions can be calculated, using angular momentum conservation, $\mathrm{D}_t\boldsymbol{I}^p\cdot\boldsymbol{\omega}^p=\boldsymbol{T}^p$, as $\dot{\boldsymbol{\omega}}^p_{\mathrm{gcf}}=(\boldsymbol{I}^p)^{-1}\cdot(\boldsymbol{T}^p_{\mathrm{cf}}-\boldsymbol{\omega}^p\times\boldsymbol{I}^p\cdot\boldsymbol{\omega}^p)$, with $I^p_{ij}=M^p\underline{r^p_k r^p_k\delta_{ij}-r^p_i r^p_j}_{\mathcal{M}^p}$ the moment-of-inertia tensor.

where $[pq]$ and (pq) denote the antisymmetrization and symmetrization, respectively, in the indices p and q. The antisymmetric term, associated with those contact interactions that cancel out upon summation (e.g., contact forces), describes the transport of Ψ, whereas the symmetric term describes actual gains or losses of Ψ, such as energy dissipation in particle collisions. In the case of non-sphere-symmetrical particles, the contact point $\boldsymbol{x}^{pq}_{\mathrm{c}}$ may not lie on the line connecting $\boldsymbol{x}^p$ with $\boldsymbol{x}^q$. Then, using Eq. (18), it is physically more meaningful to write [cf. 35]

$$\sum\nolimits_p\dot{\Psi}^p_{\mathrm{c}}\delta^p_{\boldsymbol{x}}=\boldsymbol{\nabla}\cdot\frac{1}{2}\sum\nolimits_{pq}\left(\boldsymbol{r}^{pq}_{\mathrm{c}}[t]\delta^{pq}_{\mathrm{cL}\boldsymbol{x}}[t]-\boldsymbol{r}^{qp}_{\mathrm{c}}[t]\delta^{qp}_{\mathrm{cL}\boldsymbol{x}}[t]\right)\dot{\Psi}^{[pq]}_{\mathrm{c}}+\sum\nolimits_{pq}\dot{\Psi}^{(pq)}_{\mathrm{c}}\delta^p_{\boldsymbol{x}}. \tag{70}$$

For sphere-symmetrical particles, the terms inside the divergences of Eqs. (69) and (70) are equivalent.

Finally, summing Eq. (67) over all particles and averaging ($\langle\cdot\rangle$), using Eqs. (68) and (70), and $\rho\dot{\psi}_{\mathrm{gcf}}-\underline{\rho\dot{\psi}_{\mathrm{cf}}}_{\mathcal{V}^p}=\rho\left(\dot{\psi}_{\mathrm{gcf}}-\underline{\dot{\psi}_{\mathrm{cf}}}_{\mathcal{M}^p}\right)+\underline{\dot{\psi}_{\mathrm{cf}}}_{\mathcal{M}^p}\left(\rho-\underline{\rho}_{\mathcal{V}^p}\right)=\rho\left(\dot{\psi}_{\mathrm{gcf}}-\underline{\dot{\psi}_{\mathrm{cf}}}_{\mathcal{M}^p}\right)+\dot{\Psi}^p_{\mathrm{cf}}\left(\rho/\underline{\rho}_{\mathcal{V}^p}-1\right)/V^p$, yields

$$\partial_t\beta_{\mathrm{s}}\langle\rho\psi\rangle^{\mathrm{s}}+\boldsymbol{\nabla}\cdot\beta_{\mathrm{s}}\langle\rho\boldsymbol{u}\psi\rangle^{\mathrm{s}}=-\boldsymbol{\nabla}\cdot(\boldsymbol{J}^{\mathbf{s}}_{\boldsymbol{\Psi}}-\boldsymbol{J}^{\mathbf{s}}_{\boldsymbol{\Psi}\mathbf{Re}})+\beta_{\mathrm{s}}\langle\rho\dot{\psi}_{\mathrm{b}}\rangle^{\mathrm{s}}+D^{\mathrm{s}}_{\Psi}+\beta_{\mathrm{s}}\langle\rho_*\dot{\psi}_{\uparrow\mathrm{f}}\rangle^{\mathrm{s}}, \tag{71}$$

$$\partial_t\beta_{\mathrm{s}}\langle\rho\rangle^{\mathrm{s}}\langle\psi\rangle^{\mathrm{s}}_{\rho}+\boldsymbol{\nabla}\cdot\beta_{\mathrm{s}}\langle\rho\rangle^{\mathrm{s}}\langle\boldsymbol{u}\rangle^{\mathrm{s}}_{\rho}\langle\psi\rangle^{\mathrm{s}}_{\rho}=-\boldsymbol{\nabla}\cdot\boldsymbol{J}^{\mathbf{s}}_{\boldsymbol{\Psi}}+\beta_{\mathrm{s}}\langle\rho\rangle^{\mathrm{s}}\langle\dot{\psi}_{\mathrm{b}}\rangle^{\mathrm{s}}_{\rho}+D^{\mathrm{s}}_{\Psi}+\beta_{\mathrm{s}}\langle\rho_*\rangle^{\mathrm{s}}\langle\dot{\psi}_{\uparrow\mathrm{f}}\rangle^{\mathrm{s}}_{\rho_*}, \tag{72}$$

where $\boldsymbol{J}^{\mathbf{s}}_{\boldsymbol{\Psi}}$ is the effective solid phase surface flux of Ψ and D^{s}_{Ψ} the effective internal solid phase source of Ψ, defined as

$$\boldsymbol{J}^{\mathbf{s}}_{\boldsymbol{\Psi}}\equiv\boldsymbol{J}^{\mathbf{s}}_{\boldsymbol{\Psi}\mathbf{Re}}+\boldsymbol{J}^{\mathbf{s}}_{\boldsymbol{\Psi}\mathbf{gr}}+\boldsymbol{J}^{\mathbf{s}}_{\boldsymbol{\Psi}\mathbf{gm}}+\boldsymbol{J}^{\mathbf{s}}_{\boldsymbol{\Psi}\mathbf{c}}, \tag{73}$$

$$\boldsymbol{J}^{\mathbf{s}}_{\boldsymbol{\Psi}\mathbf{Re}}\equiv\beta_{\mathrm{s}}\langle\rho\rangle^{\mathrm{s}}\left(\langle\boldsymbol{u}\psi\rangle^{\mathrm{s}}_{\rho}-\langle\boldsymbol{u}\rangle^{\mathrm{s}}_{\rho}\langle\psi\rangle^{\mathrm{s}}_{\rho}\right)\overset{\mathrm{R}}{=}\beta_{\mathrm{s}}\langle\rho\rangle^{\mathrm{s}}\left\langle\left(\boldsymbol{u}-\langle\boldsymbol{u}\rangle^{\mathrm{s}}_{\rho}\right)\left(\psi-\langle\psi\rangle^{\mathrm{s}}_{\rho}\right)\right\rangle^{\mathrm{s}}_{\rho}, \tag{74}$$

$$\boldsymbol{J}^{\mathbf{s}}_{\boldsymbol{\Psi}\mathbf{gr}}\equiv\left\langle\sum\nolimits_p M^p\boldsymbol{r}^p\underline{\left(\dot{\psi}_{\mathrm{gcf}}-\underline{\dot{\psi}_{\mathrm{cf}}}_{\mathcal{M}^p}\right)\delta^p_{\mathrm{L}\boldsymbol{x}}}_{\mathcal{M}^p}\right\rangle, \tag{75}$$

$$\boldsymbol{J}^{\mathbf{s}}_{\boldsymbol{\Psi}\mathbf{gm}}\equiv\left\langle\sum\nolimits_p\underline{\left(\rho/\underline{\rho}_{\mathcal{V}^p}-1\right)\boldsymbol{r}^p\delta^p_{\mathrm{L}\boldsymbol{x}}}_{\mathcal{V}^p}\dot{\Psi}^p_{\mathrm{cf}}\right\rangle, \tag{76}$$

$$\boldsymbol{J}^{\mathbf{s}}_{\boldsymbol{\Psi}\mathbf{c}}\equiv\left\langle\sum\nolimits_p\underline{\boldsymbol{r}^p\delta^p_{\mathrm{L}\boldsymbol{x}}}_{\mathcal{V}^p}\dot{\Psi}^p_{\mathrm{c}}\right\rangle-\left\langle\frac{1}{2}\sum\nolimits_{pq}\left(\boldsymbol{r}^{pq}_{\mathrm{c}}[t]\delta^{pq}_{\mathrm{cL}\boldsymbol{x}}[t]-\boldsymbol{r}^{qp}_{\mathrm{c}}[t]\delta^{qp}_{\mathrm{cL}\boldsymbol{x}}[t]\right)\dot{\Psi}^{[pq]}_{\mathrm{c}}\right\rangle, \tag{77}$$

$$D^{\mathrm{s}}_{\Psi}\equiv\left\langle\sum\nolimits_{pq}\dot{\Psi}^{(pq)}_{\mathrm{c}}\delta^p_{\boldsymbol{x}}\right\rangle. \tag{78}$$

The effective surface flux $\boldsymbol{J}^{\mathbf{s}}_{\boldsymbol{\Psi}}$ consists of four components: one from the particle fluctuation motion ($\boldsymbol{J}^{\mathbf{s}}_{\boldsymbol{\Psi}\mathbf{Re}}$), one from particle rotations ($\boldsymbol{J}^{\mathbf{s}}_{\boldsymbol{\Psi}\mathbf{gr}}$), one from mass density inhomogeneities in the particle interiors ($\boldsymbol{J}^{\mathbf{s}}_{\boldsymbol{\Psi}\mathbf{gm}}$), and one from particle-particle contact interactions ($\boldsymbol{J}^{\mathbf{s}}_{\boldsymbol{\Psi}\mathbf{c}}$). Examples for the terms $M^p\left(\dot{\psi}_{\mathrm{gcf}}-\underline{\dot{\psi}_{\mathrm{cf}}}_{\mathcal{M}^p}\right)$, $\dot{\Psi}^p_{\mathrm{cf}}$, and $\dot{\Psi}^p_{\mathrm{c}}$, appearing in Eqs. (75)-(78), are given in Table III.

C. Generic mixture balance equation

The local mixture balance equation of $\rho\psi \mathrm{d}V$ is obtained from adding Eqs. (57) and (71):

$$\partial_t\langle\rho\psi\rangle + \boldsymbol{\nabla}\cdot\langle\rho\boldsymbol{u}\psi\rangle = -\boldsymbol{\nabla}\cdot(\boldsymbol{J}^{\mathbf{m}}_{\boldsymbol{\Psi}} - \boldsymbol{J}^{\mathbf{m}}_{\boldsymbol{\Psi}\mathbf{Re}}) + \langle\rho\dot{\psi}_{\mathrm{b}}\rangle + D^{\mathrm{m}}_{\Psi}, \tag{79}$$

$$\partial_t\langle\rho\rangle\langle\psi\rangle_\rho + \boldsymbol{\nabla}\cdot\langle\rho\rangle\langle\boldsymbol{u}\rangle_\rho\langle\psi\rangle_\rho = -\boldsymbol{\nabla}\cdot\boldsymbol{J}^{\mathbf{m}}_{\boldsymbol{\Psi}} + \langle\rho\rangle\langle\dot{\psi}_{\mathrm{b}}\rangle_\rho + D^{\mathrm{m}}_{\Psi}, \tag{80}$$

where $\boldsymbol{J}^{\mathbf{m}}_{\boldsymbol{\Psi}}$ is the effective mixture surface flux of Ψ and D^{m}_{Ψ} the effective internal mixture source of Ψ, defined as

$$\boldsymbol{J}^{\mathbf{m}}_{\boldsymbol{\Psi}} \equiv \boldsymbol{J}^{\mathbf{f}}_{\boldsymbol{\Psi}} - \boldsymbol{J}^{\mathbf{f}}_{\boldsymbol{\Psi}\mathbf{Re}} + \boldsymbol{J}^{\mathbf{s}}_{\boldsymbol{\Psi}} - \boldsymbol{J}^{\mathbf{s}}_{\boldsymbol{\Psi}\mathbf{Re}} + \boldsymbol{J}^{\mathbf{m}}_{\boldsymbol{\Psi}\mathbf{Re}}, \tag{81}$$

$$\boldsymbol{J}^{\mathbf{m}}_{\boldsymbol{\Psi}\mathbf{Re}} \equiv \langle\rho\rangle\left(\langle\boldsymbol{u}\psi\rangle_\rho - \langle\boldsymbol{u}\rangle_\rho\langle\psi\rangle_\rho\right) \overset{\mathrm{R}}{=} \langle\rho\rangle\left\langle\left(\boldsymbol{u} - \langle\boldsymbol{u}\rangle_\rho\right)\left(\psi - \langle\psi\rangle_\rho\right)\right\rangle_\rho, \tag{82}$$

$$D^{\mathrm{m}}_{\Psi} \equiv \beta_{\mathrm{f}}\langle D_\Psi\rangle^{\mathrm{f}} + D^{\mathrm{s}}_{\Psi}. \tag{83}$$

D. Balance equations (largely) without particle-rotational degrees of freedom

The formal replacement $\psi \to \psi_* \equiv \rho_*\psi_\uparrow/\rho$ in the fluid phase balance Eq. (57) and solid phase balance Eq. (71), based on the definitions in Eq. (8), leads to a substantial simplification of the latter balance, since both the solid phase surface fluxes $\boldsymbol{J}^{\mathbf{s}}_{\boldsymbol{\Psi}_*\mathbf{gr}}$ and $\boldsymbol{J}^{\mathbf{s}}_{\boldsymbol{\Psi}_*\mathbf{gm}}$ vanish identically. In fact, using $\dot{\psi}_* = \rho_*\dot{\psi}_\uparrow/\rho$ (from Eqs. (2) and (6)), this replacement yields

$$\partial_t\beta_{\mathrm{f}}\langle\rho_*\psi_\uparrow\rangle^{\mathrm{f}} + \boldsymbol{\nabla}\cdot\beta_{\mathrm{f}}\langle\rho_*\boldsymbol{u}_\uparrow\psi_\uparrow\rangle^{\mathrm{f}} = -\boldsymbol{\nabla}\cdot\left(\boldsymbol{J}^{\mathbf{f}}_{\boldsymbol{\Psi}} - \boldsymbol{J}^{\mathbf{f}}_{\boldsymbol{\Psi}\mathbf{Re}}\right) + \beta_{\mathrm{f}}\langle\rho_*\dot{\psi}_{\uparrow\mathrm{b}}\rangle^{\mathrm{f}} + \beta_{\mathrm{f}}\langle D_\Psi\rangle^{\mathrm{f}} - \beta_{\mathrm{s}}\langle\rho_*\dot{\psi}_{\uparrow\mathrm{f}}\rangle^{\mathrm{s}}, \tag{84}$$

$$\partial_t\beta_{\mathrm{s}}\langle\rho_*\psi_\uparrow\rangle^{\mathrm{s}} + \boldsymbol{\nabla}\cdot\beta_{\mathrm{s}}\langle\rho_*\boldsymbol{u}\psi_\uparrow\rangle^{\mathrm{s}} = -\boldsymbol{\nabla}\cdot\boldsymbol{J}^{\mathbf{s}}_{\boldsymbol{\Psi}\mathbf{c}} + \beta_{\mathrm{s}}\langle\rho_*\dot{\psi}_{\uparrow\mathrm{b}}\rangle^{\mathrm{s}} + D^{\mathrm{s}}_{\Psi} + \beta_{\mathrm{s}}\langle\rho_*\dot{\psi}_{\uparrow\mathrm{f}}\rangle^{\mathrm{s}}. \tag{85}$$

Note that Eq. (84) is equivalent to Eq. (57) as $\rho_* = \rho$, $\psi_\uparrow = \psi$, and $\boldsymbol{u}_\uparrow = \boldsymbol{u}$ within the fluid phase ($\boldsymbol{x} \in \mathcal{V}_{\mathrm{f}}$). Furthermore, in this framework, it makes physically more sense to weigh the averages by ρ_* rather than ρ. Then, Eqs. (84) and (85) can be transformed into

$$\partial_t\beta_{\mathrm{f}}\langle\rho_*\rangle^{\mathrm{f}}\langle\psi_\uparrow\rangle^{\mathrm{f}}_{\rho_*} + \boldsymbol{\nabla}\cdot\beta_{\mathrm{s}}\langle\rho_*\rangle^{\mathrm{f}}\langle\boldsymbol{u}_\uparrow\rangle^{\mathrm{f}}_{\rho_*}\langle\psi_\uparrow\rangle^{\mathrm{f}}_{\rho_*} = -\boldsymbol{\nabla}\cdot\boldsymbol{J}^{\mathbf{f}}_{\boldsymbol{\Psi}} + \beta_{\mathrm{f}}\langle\rho_*\rangle^{\mathrm{f}}\langle\dot{\psi}_{\uparrow\mathrm{b}}\rangle^{\mathrm{f}}_{\rho_*} + \beta_{\mathrm{f}}\langle D_\Psi\rangle^{\mathrm{f}} - \beta_{\mathrm{s}}\langle\rho_*\rangle^{\mathrm{s}}\langle\dot{\psi}_{\uparrow\mathrm{f}}\rangle^{\mathrm{s}}_{\rho_*}, \tag{86}$$

$$\partial_t\beta_{\mathrm{s}}\langle\rho_*\rangle^{\mathrm{s}}\langle\psi_\uparrow\rangle^{\mathrm{s}}_{\rho_*} + \boldsymbol{\nabla}\cdot\beta_{\mathrm{s}}\langle\rho_*\rangle^{\mathrm{s}}\langle\boldsymbol{u}\rangle^{\mathrm{s}}_{\rho_*}\langle\psi_\uparrow\rangle^{\mathrm{s}}_{\rho_*} = -\boldsymbol{\nabla}\cdot\left(\boldsymbol{J}^{\mathbf{s}}_{\boldsymbol{\Psi}\mathbf{c}} + \boldsymbol{J}^{\mathbf{s}}_{\boldsymbol{\Psi}_\uparrow\mathbf{Re}}\right) + \beta_{\mathrm{s}}\langle\rho_*\rangle^{\mathrm{s}}\langle\dot{\psi}_{\uparrow\mathrm{b}}\rangle^{\mathrm{s}}_{\rho_*} + D^{\mathrm{s}}_{\Psi} + \beta_{\mathrm{s}}\langle\rho_*\rangle^{\mathrm{s}}\langle\dot{\psi}_{\uparrow\mathrm{f}}\rangle^{\mathrm{s}}_{\rho_*}, \tag{87}$$

with a particle fluctuation surface flux $\boldsymbol{J}^{\mathbf{s}}_{\boldsymbol{\Psi}_\uparrow\mathbf{Re}}$ different from $\boldsymbol{J}^{\mathbf{s}}_{\boldsymbol{\Psi}\mathbf{Re}}$:

$$\boldsymbol{J}^{\mathbf{s}}_{\boldsymbol{\Psi}_\uparrow\mathbf{Re}} \equiv \beta_{\mathrm{s}}\langle\rho_*\rangle^{\mathrm{s}}\left(\langle\boldsymbol{u}\psi_\uparrow\rangle^{\mathrm{s}}_{\rho_*} - \langle\boldsymbol{u}\rangle^{\mathrm{s}}_{\rho_*}\langle\psi_\uparrow\rangle^{\mathrm{s}}_{\rho_*}\right) \overset{\mathrm{R}}{=} \beta_{\mathrm{s}}\langle\rho_*\rangle^{\mathrm{s}}\left\langle\left(\boldsymbol{u} - \langle\boldsymbol{u}\rangle^{\mathrm{s}}_{\rho_*}\right)\left(\psi_\uparrow - \langle\psi_\uparrow\rangle^{\mathrm{s}}_{\rho_*}\right)\right\rangle^{\mathrm{s}}_{\rho_*}. \tag{88}$$

As before, Eq. (86) is equivalent to Eq. (58).

1. *Sphere-symmetrical particles*

The only remaining quantity that contains information about the particle-rotational degrees of freedom in Eq. (85) is $\boldsymbol{u}$ within the second term on its left-hand side. In the case that all particles are sphere-symmetrical, that is, when both X^p and ρ depend only on the distance $|\boldsymbol{r}^p|$ from the particle p's center of mass for all p, the rotational velocities at all points of all particles' surfaces are always perpendicular to the unit normal vector, implying $\boldsymbol{u}\cdot\boldsymbol{\nabla}X^p = \boldsymbol{v}^p_\uparrow\cdot\boldsymbol{\nabla}X^p = \boldsymbol{\nabla}\cdot\boldsymbol{v}^p_\uparrow X^p$. Then, this term simplifies to

$$\boldsymbol{\nabla}\cdot\beta_{\mathrm{s}}\langle\rho_*\boldsymbol{u}\psi_\uparrow\rangle^{\mathrm{s}} = \boldsymbol{\nabla}\cdot\beta_{\mathrm{s}}\langle\rho_*\boldsymbol{u}_\uparrow\psi_\uparrow\rangle^{\mathrm{s}}, \tag{89}$$

and $\boldsymbol{u}$ can be formally replaced by $\boldsymbol{u}_\uparrow$ in Eqs. (85)-(88). In other words, for sphere-symmetrical particles, the balance equations of $\mathrm{d}\Psi_\uparrow = \rho_*\psi_\uparrow\mathrm{d}V$ are completely devoid of the particle-rotational degrees of freedom. The physical reason why this can be achieved is that particle rotations do not alter any pointwise property within the particle interiors, such as the local particle mass density.

2. Comparison to grain phase balance equation

Another balance equation associated with particles that is devoid of the particle-rotational degrees of freedom is the grain phase balance equation. (For clarity, we avoid the term "particle phase" used in previous studies.) It is the standard particle-associated balance equation used in analytical derivations of approximate closures [10, 14, 15]. However, as we show here, it has inherent disadvantages in a mathematically exact context.

To derive the grain phase balance of $\rho_*\psi_\uparrow \mathrm{d}V$, we apply the chain rule of differentiation on the term $\partial_t \underline{\rho\psi}_{\mathcal{V}^p}\delta^p_{\boldsymbol{x}}$ using $\boldsymbol{v}^p_\uparrow = \dot{\boldsymbol{x}}^p$ and Eq. (6):

$$\partial_t \underline{\rho\psi}_{\mathcal{V}^p}[t]\delta[\boldsymbol{x}-\boldsymbol{x}^p[t]] = \underline{\rho\dot{\psi}}_{\mathcal{V}^p}[t]\delta[\boldsymbol{x}-\boldsymbol{x}^p[t]] - \boldsymbol{\nabla}\cdot\boldsymbol{v}^p_\uparrow[t]\underline{\rho\psi}_{\mathcal{V}^p}[t]\delta[\boldsymbol{x}-\boldsymbol{x}^p[t]] = \underline{\rho\dot{\psi}}_{\mathcal{V}^p}[t]\delta[\boldsymbol{x}-\boldsymbol{x}^p[t]] - \boldsymbol{\nabla}\cdot\underline{\rho\boldsymbol{u}_\uparrow\psi}_{\mathcal{V}^p}[t]\delta[\boldsymbol{x}-\boldsymbol{x}^p[t]]. \tag{90}$$

Then, multiplying by V^p, separating $\underline{\rho\dot{\psi}}_{\mathcal{V}^p} = \underline{\rho\dot{\psi}_{\mathrm{b}}}_{\mathcal{V}^p} + \underline{\rho\dot{\psi}_{\mathrm{c}}}_{\mathcal{V}^p} + \underline{\rho\dot{\psi}_{\mathrm{f}}}_{\mathcal{V}^p}$ as before, summing over all particles, and averaging ($\langle\cdot\rangle$) yields

$$\partial_t c_{\mathrm{g}}\langle\rho\psi\rangle^{\mathrm{g}} + \boldsymbol{\nabla}\cdot c_{\mathrm{g}}\langle\rho\boldsymbol{u}_\uparrow\psi\rangle^{\mathrm{g}} = -\boldsymbol{\nabla}\cdot(\boldsymbol{J}^{\mathbf{g}}_{\boldsymbol{\Psi}} - \boldsymbol{J}^{\mathbf{g}}_{\boldsymbol{\Psi}\mathbf{Re}}) + c_{\mathrm{g}}\langle\rho\dot{\psi}_{\mathrm{b}}\rangle^{\mathrm{g}} + D^{\mathrm{s}}_\Psi + c_{\mathrm{g}}\langle\rho\dot{\psi}_{\mathrm{f}}\rangle^{\mathrm{g}}, \tag{91}$$

$$\partial_t c_{\mathrm{g}}\langle\rho\rangle^{\mathrm{g}}\langle\psi\rangle^{\mathrm{g}}_\rho + \boldsymbol{\nabla}\cdot c_{\mathrm{g}}\langle\rho\rangle^{\mathrm{g}}\langle\boldsymbol{u}\rangle^{\mathrm{g}}_\rho\langle\psi\rangle^{\mathrm{g}}_\rho = -\boldsymbol{\nabla}\cdot\boldsymbol{J}^{\mathbf{g}}_{\boldsymbol{\Psi}} + c_{\mathrm{g}}\langle\rho\rangle^{\mathrm{g}}\langle\dot{\psi}_{\mathrm{b}}\rangle^{\mathrm{g}}_\rho + D^{\mathrm{s}}_\Psi + c_{\mathrm{g}}\langle\rho\rangle^{\mathrm{g}}\langle\dot{\psi}_{\mathrm{f}}\rangle^{\mathrm{g}}_\rho, \tag{92}$$

where $\boldsymbol{J}^{\mathbf{g}}_{\boldsymbol{\Psi}}$ is the effective grain phase surface flux of Ψ, defined by

$$\boldsymbol{J}^{\mathbf{g}}_{\boldsymbol{\Psi}} \equiv \boldsymbol{J}^{\mathbf{g}}_{\boldsymbol{\Psi}\mathbf{Re}} + \boldsymbol{J}^{\mathbf{g}}_{\boldsymbol{\Psi}\mathbf{c}}, \tag{93}$$

$$\boldsymbol{J}^{\mathbf{g}}_{\boldsymbol{\Psi}\mathbf{Re}} \equiv c_{\mathrm{g}}\langle\rho\rangle^{\mathrm{g}}\left(\langle\boldsymbol{u}_\uparrow\psi\rangle^{\mathrm{g}}_\rho - \langle\boldsymbol{u}\rangle^{\mathrm{g}}_\rho\langle\psi\rangle^{\mathrm{g}}_\rho\right) \overset{\mathrm{R}}{=} c_{\mathrm{g}}\langle\rho\rangle^{\mathrm{g}}\left\langle\left(\boldsymbol{u}_\uparrow - \langle\boldsymbol{u}\rangle^{\mathrm{g}}_\rho\right)\left(\psi - \langle\psi\rangle^{\mathrm{g}}_\rho\right)\right\rangle^{\mathrm{g}}_\rho, \tag{94}$$

$$\boldsymbol{J}^{\mathbf{g}}_{\boldsymbol{\Psi}\mathbf{c}} \equiv -\left\langle\frac{1}{2}\sum\nolimits_{pq}\left(\boldsymbol{r}^{pq}_{\mathrm{c}}[t]\delta^{pq}_{\mathrm{cL}\boldsymbol{x}}[t] - \boldsymbol{r}^{qp}_{\mathrm{c}}[t]\delta^{qp}_{\mathrm{cL}\boldsymbol{x}}[t]\right)\dot{\Psi}^{[pq]}_{\mathrm{c}}\right\rangle. \tag{95}$$

Note that D^{s}_Ψ, the effective internal grain phase source of Ψ, is the same as the solid phase one given by Eq. (78). It can be seen that the topology of the grain phase balance is almost the same as that of the non-rotational solid phase balance in the case of sphere-symmetrical particles. The only but important difference is the appearance of the grain concentration c_{g} rather than the solid volume fraction β_{s}. This is not only problematic because generally $c_{\mathrm{g}} + \beta_{\mathrm{f}} \neq 1$ but also because it requires substituting the fluid-solid interaction term in the fluid phase balance Eq. (84) via

$$\beta_{\mathrm{s}}\left\langle\rho_*\dot{\psi}_{\uparrow\mathrm{f}}\right\rangle^{\mathrm{s}} = c_{\mathrm{g}}\left\langle\rho\dot{\psi}_{\mathrm{f}}\right\rangle^{\mathrm{g}} + \boldsymbol{\nabla}\cdot\left\langle\sum\nolimits_p S^p\boldsymbol{r}^p\underline{\delta^p_{\mathrm{L}\boldsymbol{x}}}_{\mathcal{V}^p}\underline{\boldsymbol{n}^p\cdot\boldsymbol{J}_{\boldsymbol{\Psi}}}_{\mathcal{S}^p}\right\rangle, \tag{96}$$

which follows from Eq. (21) for $A = \underline{\rho\dot{\psi}_{\mathrm{f}}}_{\mathcal{V}^p}$, in order to make it compatible with Eq. (91). (The interaction term should cancel upon summation of the fluid phase and grain phase balance equations.) The thus emerging additional particle contribution to the effective fluid phase surface flux would eliminate the physically desirable property that the particle contribution to $\boldsymbol{J}^{\mathbf{f}}_{\boldsymbol{\Psi}}$ in Eq. (64) is a sum of fluctuation terms. In summary, in the case of sphere-symmetrical particles, the non-rotational solid phase balance is superior over the grain phase balance as a starting point for theoretical analyses or numerical studies.

3. Decomposition of solid phase balance equations into moments of grain phase balance equation

Here, we decompose the standard and non-rotational solid phase balance equations into moments of the grain phase balance equation. The analysis below essentially follows Fintzi and Pierson [18], who performed this decomposition for the standard solid phase balance equation and, in contrast to us, considered the possibility of mass transfer across the fluid-solid interface. We carry out the decomposition at the level of individual particles and sum over all particles and macroscopically average afterward. At this level, the standard and non-rotational solid phase balance equations read

$$S^p \equiv \partial_t\rho\psi X^p + \boldsymbol{\nabla}\cdot\boldsymbol{u}\rho\psi X^p - \rho\dot{\psi}X^p = 0, \tag{97}$$

$$S^p_\uparrow \equiv \partial_t\underline{\rho\psi}_{\mathcal{V}^p}X^p + \boldsymbol{\nabla}\cdot\boldsymbol{u}\underline{\rho\psi}_{\mathcal{V}^p}X^p - \underline{\rho\dot{\psi}}_{\mathcal{V}^p}X^p = 0. \tag{98}$$

Equation (97) is the same as Eq. (66), and Eq. (98) follows from the formal replacement $\psi \to \rho_*\psi_\uparrow/\rho$ in Eq. (97). Furthermore, we define the standard and non-rotational k-th moments, respectively, of the nonaveraged grain phase

balance equation as

$$\boldsymbol{G}^{p(k)} \equiv \partial_t \underline{(\boldsymbol{r}^p)^{(k)}\rho\psi}_{\mathcal{V}^p} V^p \delta^p_{\boldsymbol{x}} + \boldsymbol{\nabla}\cdot\boldsymbol{v}^p_{\uparrow}\underline{(\boldsymbol{r}^p)^{(k)}\rho\psi}_{\mathcal{V}^p} V^p\delta^p_{\boldsymbol{x}} - \left(\mathrm{D}_t\underline{(\boldsymbol{r}^p)^{(k)}\rho\psi}_{\mathcal{V}^p}\right) V^p\delta^p_{\boldsymbol{x}} = 0, \tag{99}$$

$$\boldsymbol{G}^{p(k)}_{\uparrow} \equiv \partial_t \underline{(\boldsymbol{r}^p)^{(k)}}_{\mathcal{V}^p}\underline{\rho\psi}_{\mathcal{V}^p} V^p \delta^p_{\boldsymbol{x}} + \boldsymbol{\nabla}\cdot\boldsymbol{v}^p_{\uparrow}\underline{(\boldsymbol{r}^p)^{(k)}}_{\mathcal{V}^p}\underline{\rho\psi}_{\mathcal{V}^p} V^p\delta^p_{\boldsymbol{x}} - \left(\mathrm{D}_t\underline{(\boldsymbol{r}^p)^{(k)}}_{\mathcal{V}^p}\underline{\rho\psi}_{\mathcal{V}^p}\right) V^p\delta^p_{\boldsymbol{x}} = 0, \tag{100}$$

where the equalities to zero follow from Eq. (6) used in Eq. (90) with $\underline{\rho\psi}_{\mathcal{V}^p} \to \underline{(\boldsymbol{r}^p)^{(k)}\rho\psi}_{\mathcal{V}^p}$ and $\underline{\rho\psi}_{\mathcal{V}^p} \to \underline{(\boldsymbol{r}^p)^{(k)}}_{\mathcal{V}^p}\underline{\rho\psi}_{\mathcal{V}^p}$, respectively. Now, we separate the advection term in Eq. (97) via $\boldsymbol{u}X^p = \left(\boldsymbol{v}^p_{\uparrow} + \boldsymbol{v}^p_{\circlearrowleft}\right)X^p$ and use Eqs. (19) and (25) with $A = \rho\psi$, $A = \boldsymbol{v}^p_{\circlearrowleft}\rho\psi$, or $A = \rho\dot{\psi}$ to substitute all terms of the resulting equation:

$$\begin{aligned} S^p = &\left(\partial_t + \boldsymbol{\nabla}\cdot\boldsymbol{v}^p_{\uparrow}\right)\sum_{k=0}^{\infty}\frac{(-1)^k}{k!}\boldsymbol{\nabla}^{(k)}\odot\underline{(\boldsymbol{r}^p)^{(k)}\rho\psi}_{\mathcal{V}^p}V^p\delta^p_{\boldsymbol{x}} \\ &+\sum_{k=0}^{\infty}\frac{(-1)^k}{k!}\left(\boldsymbol{\nabla}^{(k+1)}\odot\underline{\boldsymbol{v}^p_{\circlearrowleft}(\boldsymbol{r}^p)^{(k)}\rho\psi}_{\mathcal{V}^p} - \boldsymbol{\nabla}^{(k)}\odot\underline{(\boldsymbol{r}^p)^{(k)}\rho\dot{\psi}}_{\mathcal{V}^p}\right)V^p\delta^p_{\boldsymbol{x}}. \end{aligned} \tag{101}$$

The last term in Eq. (101) can be further manipulated via

$$\begin{aligned} &\sum_{k=0}^{\infty}\frac{(-1)^k}{k!}\left(\boldsymbol{\nabla}^{(k+1)}\odot\underline{\boldsymbol{v}^p_{\circlearrowleft}(\boldsymbol{r}^p)^{(k)}\rho\psi}_{\mathcal{V}^p} - \boldsymbol{\nabla}^{(k)}\odot\underline{(\boldsymbol{r}^p)^{(k)}\rho\dot{\psi}}_{\mathcal{V}^p}\right)V^p\delta^p_{\boldsymbol{x}} \\ &= -\underline{\rho\dot{\psi}}_{\mathcal{V}^p}V^p\delta^p_{\boldsymbol{x}} - \sum_{k=0}^{\infty}\frac{(-1)^{k+1}}{(k+1)!}\left((k+1)\boldsymbol{\nabla}^{(k+1)}\odot\underline{\boldsymbol{v}^p_{\circlearrowleft}(\boldsymbol{r}^p)^{(k)}\rho\psi}_{\mathcal{V}^p} + \boldsymbol{\nabla}^{(k+1)}\odot\underline{(\boldsymbol{r}^p)^{(k+1)}\rho\dot{\psi}}_{\mathcal{V}^p}\right)V^p\delta^p_{\boldsymbol{x}} \\ &= -\underline{\rho\dot{\psi}}_{\mathcal{V}^p}V^p\delta^p_{\boldsymbol{x}} - \sum_{k=0}^{\infty}\frac{(-1)^{k+1}}{(k+1)!}\boldsymbol{\nabla}^{(k+1)}\odot\left(\mathrm{D}_t\underline{(\boldsymbol{r}^p)^{(k+1)}\rho\psi}_{\mathcal{V}^p}\right)V^p\delta^p_{\boldsymbol{x}} = -\sum_{k=0}^{\infty}\frac{(-1)^k}{k!}\boldsymbol{\nabla}^{(k)}\odot\left(\mathrm{D}_t\underline{(\boldsymbol{r}^p)^{(k)}\rho\psi}_{\mathcal{V}^p}\right)V^p\delta^p_{\boldsymbol{x}}, \end{aligned} \tag{102}$$

where we used Eq. (6), $\boldsymbol{v}^p_{\circlearrowleft} = \mathrm{D}_t\boldsymbol{r}^p$, and exploited the symmetry of $\boldsymbol{\nabla}^{(k+1)}$. Insertion in Eq. (101) and exchanging the order of differentiation and a calculation for $S^p_{\uparrow}$ completely analogous to that in Eqs. (101) and (102) then yields

$$S^p = \sum_{k=0}^{\infty}\frac{(-1)^k}{k!}\boldsymbol{\nabla}^{(k)}\odot\boldsymbol{G}^{p(k)}, \qquad\qquad S^p_{\uparrow} = \sum_{k=0}^{\infty}\frac{(-1)^k}{k!}\boldsymbol{\nabla}^{(k)}\odot\boldsymbol{G}^{p(k)}_{\uparrow}. \tag{103}$$

Summing these equations over all particles and averaging ($\langle\cdot\rangle$) shows that the standard and non-rotational solid phase balance equations are equivalent to infinite sums of the standard and non-rotational moments, respectively, of the grain phase balance equation, where both the zeroth moments equations $\left\langle\sum_p G^{p(0)}\right\rangle = 0$ and $\left\langle\sum_p G^{p(0)}_{\uparrow}\right\rangle = 0$ are equivalent to Eq. (91).

IV. NUMERICAL IMPLEMENTATION FOR STEADY, BED-TANGENTIALLY HOMOGENEOUS SEDIMENT TRANSPORT

The numerical implementation of the formal expressions derived in §III is straightforward and completely avoids the Taylor expansions required in previous works. In Appendix C, we provide discretized expressions for the fields of interest associated with the mass and momentum balances for a specific example: steady, bed-tangentially homogeneous sediment transport, a particulate two-phase flow with R/L on the order of 1 to 10 [20–22]. These expressions are based on the following averaging procedure:

$$\langle A\rangle[z_n] \equiv \frac{1}{N_T L_x L_y \Delta z}\sum_{k=1}^{N_T}\left(\int_{z_n-\Delta z/2}^{z_n+\Delta z/2}\int_0^{L_y}\int_0^{L_x} A[\boldsymbol{x},t]\mathrm{d}x\mathrm{d}y\mathrm{d}z\right)_k, \tag{104}$$

which satisfies the rules in Eq. (31). Due to statistical bed-tangential homogeneity ($\partial_x = \partial_y = 0$), the averaging takes place over the entire bed-tangential domain, $x \in [0, L_x)$ and $y \in [0, L_y)$ (periodic boundary conditions), where x is in the flow direction and y in the lateral direction, at a given instant k in time and, due to the steadiness, over a

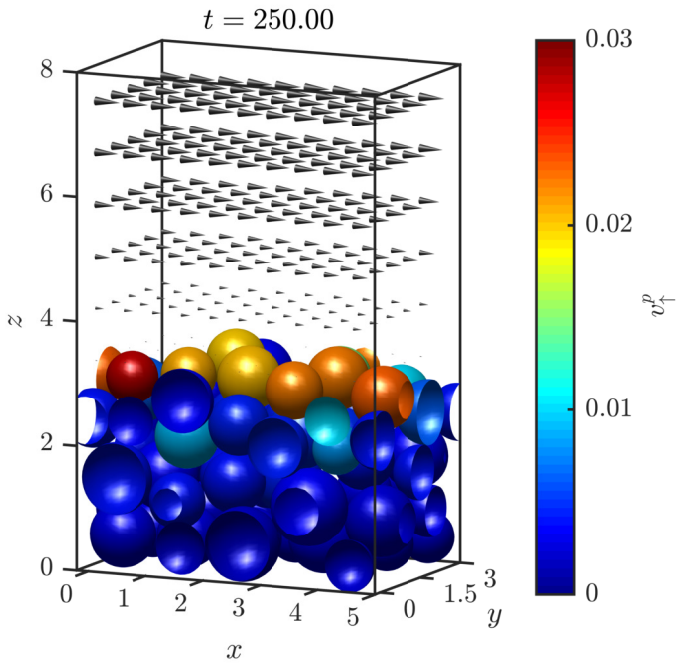

FIG. 1. Snapshot of a DNS-DEM simulation of steady, bed-tangentially homogeneous sediment transport.

sufficient number N_T of timewise well-separated instants to ensure $\partial_t \approx 0$. Furthermore, Δz is the constant extent of the intervals with centers z_n (taking the limit $\Delta z \to 0$ in the provided expressions is not forbidden) that discretize the bed-normal domain $z \in (0, H)$, with H the simulation top.

The DNS method for a flow of an incompressible Newtonian fluid (fluid density $\rho_\mathrm{f} = \mathrm{const}$) is coupled with the DEM for 50 rigid spheres of a constant density ρ_s and radius R to study a case of sediment transport, as shown in Fig. 1. The numerical model is described in detail by Biegert *et al.* [36] and Zhu *et al.* [37]. The gravitational acceleration $\boldsymbol{g}$ is driving both the liquid flow and particles down a small slope of 3°. Physical quantities are measured in natural units of ρ_f, $(\rho_\mathrm{s}/\rho_\mathrm{f} - 1)|\boldsymbol{g}|$, and $2R$. A simulation is conducted for $\rho_\mathrm{s} = 2.65$ and viscosity $\eta_\mathrm{f} = 0.36$. Since, here, we are primarily concerned with the validation of the derived formal expressions, we keep the system size small: $(L_x, L_y, H) = (5, 3, 8)$, meaning that the 50 particles form a bed of approximately three particle layers (Fig. 1). Furthermore, the simulation is averaged over $N_T = 363$ instants in time, and the discretization interval is chosen to be $\Delta z = 0.1$.

Due to $\partial_x = \partial_y = \partial_t = 0$, the fluid and solid phase momentum balances take the simple forms ($\boldsymbol{J}_\Psi = -\boldsymbol{\sigma}$)

$$\mathrm{d}_z \sigma^\mathrm{f}_{zi} = -\beta_\mathrm{f} \rho_\mathrm{f} g_i + \beta_\mathrm{s} \rho_\mathrm{s} \langle \dot{u}_{\uparrow \mathrm{f}i} \rangle^\mathrm{s}, \tag{105}$$

$$\mathrm{d}_z \sigma^\mathrm{s}_{zi} = -\beta_\mathrm{s} \rho_\mathrm{s} g_i - \beta_\mathrm{s} \rho_\mathrm{s} \langle \dot{u}_{\uparrow \mathrm{f}i} \rangle^\mathrm{s}. \tag{106}$$

In Fig. 2, we show the effective stress components σ^f_{zx}, σ^f_{zz}, σ^s_{zx}, and σ^s_{zz} calculated in three distinct manners: directly using the exact stress expressions, indirectly via integrating the exact expressions for the right-hand sides of these balances, or directly using the stress expressions approximated in the first order of R/L (all given in Appendix C). It can be seen that the exact direct and indirect calculations are equivalent to one another, except for slight discrepancies in σ^f_{zx}. The latter are owed to the fact that the employed DNS-DEM algorithm calculates fluid-particle interaction forces using a special technique based on the Immersed Boundary Method rather than by resolving the fluid traction distribution on the particle surfaces. As a consequence, for the direct calculation of $\boldsymbol{\sigma}^\mathbf{f}$, we needed to extract this distribution through an independent, less accurate interpolation algorithm, which has led to slight inconsistencies. Apart from this validation, the main takeaway of Fig. 2 is that expressions in the first order of R/L perform rather poorly for these systems. While this is a well-known fact for solid stresses in dense granular systems [38], it may come as somewhat of a surprise for the effective fluid stress $\boldsymbol{\sigma}^\mathbf{f}$. It is particularly noteworthy that the direct calculation of σ^f_{zz}, approximated in the first order of R/L, is unable to reproduce the almost perfect hydrostatic profile $\sigma^\mathrm{f}_{zz} = \rho_\mathrm{f} g_z (H - z)$ of the exact σ^f_{zz} in Fig. 2(b).

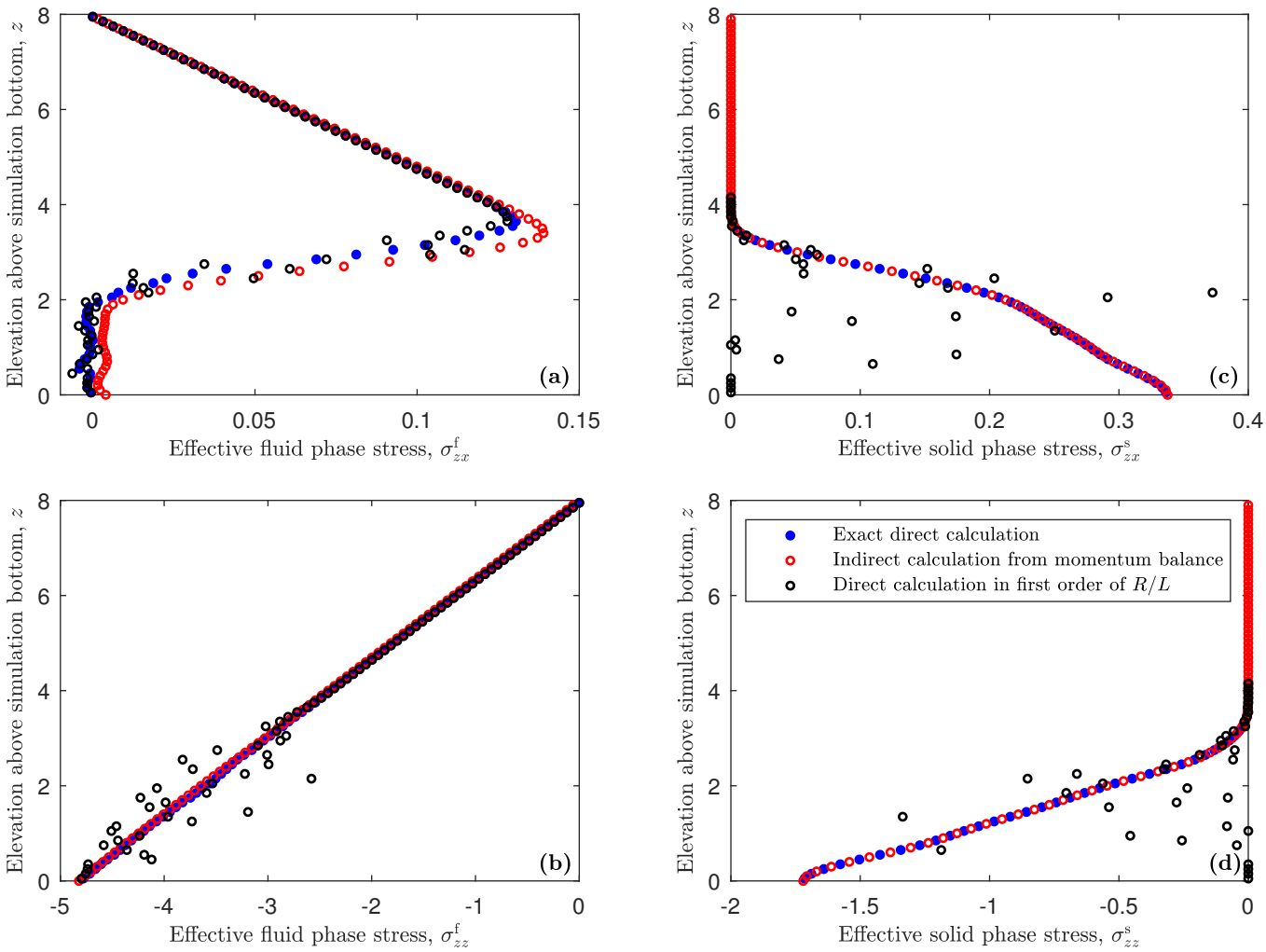

FIG. 2. Height profiles of the effective stress components (a) σ^{f}_{zx}, (b) σ^{f}_{zz}, (c) σ^{s}_{zx}, and (d) σ^{s}_{zz}. Data correspond to a DNS-DEM simulation of viscous sediment transport, calculated in three distinct manners: directly using the exact stress expressions, indirectly via integrating the exact expressions for the right-hand sides of Eq. (105) or Eq. (106), or directly using the stress expressions approximated in the first order of R/L (all given in Appendix C).

V. BUOYANCY CLOSURE

Consider a mixture of a continuous fluid and rigid, non-Brownian particles subjected to the gravitational acceleration $\boldsymbol{g}$. We average the equations of motion using an averaging procedure that satisfies (or approximately satisfies) the Reynolds rule, implying that '$\overset{\mathrm{R}}{=}$' can be replaced by the equality symbol '=' in any given expression derived in §II and §III. Then, using the expressions in §III D, the mathematically exact fluid phase and solid phase momentum balances read ($\boldsymbol{J}_{\boldsymbol{\Psi}} = -\boldsymbol{\sigma}$)

$$\partial_t \beta_{\mathrm{f}} \rho_{\mathrm{f}} \boldsymbol{u}_{\mathrm{f}} + \boldsymbol{\nabla} \cdot \beta_{\mathrm{f}} \rho_{\mathrm{f}} \boldsymbol{u}_{\mathrm{f}} \boldsymbol{u}_{\mathrm{f}} = \boldsymbol{\nabla} \cdot \boldsymbol{\sigma}^{\mathbf{f}} + \beta_{\mathrm{f}} \rho_{\mathrm{f}} \boldsymbol{g} - \boldsymbol{f}, \tag{107}$$

$$\partial_t \beta_{\mathrm{s}} \rho_{\mathrm{s}} \boldsymbol{u}_{\mathrm{s}} + \boldsymbol{\nabla} \cdot \beta_{\mathrm{s}} \rho_{\mathrm{s}} \langle \boldsymbol{u} \rangle^{\mathrm{s}}_{\rho_*} \boldsymbol{u}_{\mathrm{s}} = \boldsymbol{\nabla} \cdot \boldsymbol{\sigma}^{\mathbf{s}} + \beta_{\mathrm{s}} \rho_{\mathrm{s}} \boldsymbol{g} + \boldsymbol{f}, \tag{108}$$

where we introduced the abbreviations $\rho_{\mathrm{f,s}} \equiv \langle \rho_* \rangle^{\mathrm{f,s}}$, $\boldsymbol{u}_{\mathrm{f,s}} \equiv \langle \boldsymbol{u}_\uparrow \rangle^{\mathrm{f,s}}_{\rho_*}$, and $\boldsymbol{f} \equiv \beta_{\mathrm{s}} \rho_{\mathrm{s}} \langle \dot{\boldsymbol{u}}_{\uparrow \mathrm{f}} \rangle^{\mathrm{s}}_{\rho_*}$ to keep the notation simple. We remind the reader that $\boldsymbol{u}_\uparrow$ refers to the velocity field without the particle-rotational degrees of freedom ($\boldsymbol{u}_\uparrow = \boldsymbol{u}$ for $\boldsymbol{x} \in \mathcal{V}_{\mathrm{f}}$ and $\boldsymbol{u}_\uparrow = \boldsymbol{v}^p_\uparrow$ for $\boldsymbol{x} \in \mathcal{V}^p$). The left-hand side of Eq. (107) can be rewritten as

$$\partial_t \beta_{\mathrm{f}} \rho_{\mathrm{f}} \boldsymbol{u}_{\mathrm{f}} + \boldsymbol{\nabla} \cdot \beta_{\mathrm{f}} \rho_{\mathrm{f}} \boldsymbol{u}_{\mathrm{f}} \boldsymbol{u}_{\mathrm{f}} = \beta_{\mathrm{f}} \rho_{\mathrm{f}} (\partial_t \boldsymbol{u}_{\mathrm{f}} + \boldsymbol{u}_{\mathrm{f}} \cdot \boldsymbol{\nabla} \boldsymbol{u}_{\mathrm{f}}) + \boldsymbol{u}_{\mathrm{f}} (\partial_t \beta_{\mathrm{f}} \rho_{\mathrm{f}} + \boldsymbol{\nabla} \cdot \beta_{\mathrm{f}} \rho_{\mathrm{f}} \boldsymbol{u}_{\mathrm{f}}) = \beta_{\mathrm{f}} \rho_{\mathrm{f}} (\partial_t \boldsymbol{u}_{\mathrm{f}} + \boldsymbol{u}_{\mathrm{f}} \cdot \boldsymbol{\nabla} \boldsymbol{u}_{\mathrm{f}}) \equiv \beta_{\mathrm{f}} \rho_{\mathrm{f}} \mathrm{D}^{\mathrm{f}}_t \boldsymbol{u}_{\mathrm{f}}, \tag{109}$$

where $\mathrm{D}_t^{\mathrm{f}} \equiv \partial_t + \boldsymbol{u}_{\mathrm{f}} \cdot \boldsymbol{\nabla}$ is an effective material derivative and we used the average fluid phase mass balance, $\partial_t \beta_{\mathrm{f}} \rho_{\mathrm{f}} + \boldsymbol{\nabla} \cdot \beta_{\mathrm{f}} \rho_{\mathrm{f}} \boldsymbol{u}_{\mathrm{f}} = 0$. Performing an analogous manipulation on Eq. (108) leads to

$$\beta_{\mathrm{f}} \rho_{\mathrm{f}} \mathrm{D}_t^{\mathrm{f}} \boldsymbol{u}_{\mathrm{f}} = \boldsymbol{\nabla} \cdot \boldsymbol{\sigma}^{\mathbf{f}} + \beta_{\mathrm{f}} \rho_{\mathrm{f}} \boldsymbol{g} - \boldsymbol{f}, \tag{110}$$

$$\beta_{\mathrm{s}} \rho_{\mathrm{s}} \mathrm{D}_t^{\mathrm{s}} \boldsymbol{u}_{\mathrm{s}} = \boldsymbol{\nabla} \cdot \boldsymbol{\sigma}^{\mathbf{s}} + \beta_{\mathrm{s}} \rho_{\mathrm{s}} \boldsymbol{g} + \boldsymbol{f}, \tag{111}$$

with $\mathrm{D}_t^{\mathrm{s}} \equiv \partial_t + \langle \boldsymbol{u} \rangle_{\rho_*}^{\mathrm{s}} \cdot \boldsymbol{\nabla}$.

The expressions for the effective fluid phase ($\boldsymbol{\sigma}^{\mathbf{f}}$) and solid phase ($\boldsymbol{\sigma}^{\mathbf{s}}$) stresses in Eqs. (110) and (111), including their simplifications for spheres of a constant radius R with sphere-symmetrical interiors obtained from using Eqs. (28)-(30) with $L_{\hat{\boldsymbol{r}}^p} = R$, read (§III A, §III B, and §III D)

$$\boldsymbol{\sigma}^{\mathbf{f}} \equiv \langle \boldsymbol{\sigma} \rangle^{\mathrm{f}} + \boldsymbol{\sigma}_{\mathbf{Re}}^{\mathbf{f}} + \boldsymbol{\sigma}_{\mathbf{s}}^{\mathbf{f}} + \left[\langle \boldsymbol{\sigma} \rangle^{\mathrm{f}} \right]_{\mathrm{s}}', \tag{112}$$

$$\boldsymbol{\sigma}_{\mathbf{Re}}^{\mathbf{f}} \equiv -\beta_{\mathrm{f}} \rho_{\mathrm{f}} \left\langle (\boldsymbol{u}_\uparrow - \boldsymbol{u}_{\mathrm{f}}) (\boldsymbol{u}_\uparrow - \boldsymbol{u}_{\mathrm{f}}) \right\rangle_{\rho_*}^{\mathrm{f}}, \tag{113}$$

$$\begin{aligned} \boldsymbol{\sigma}_{\mathbf{s}}^{\mathbf{f}} &\equiv \left\langle \sum\nolimits_p S^p \left(\underline{\boldsymbol{r}^p \boldsymbol{n}^p \cdot \left(\boldsymbol{\sigma} - \langle \boldsymbol{\sigma} \rangle^{\mathrm{f}} \right) \delta_{\mathrm{L}\boldsymbol{x}}^p}_{\mathcal{S}^p} - \underline{\boldsymbol{r}^p \delta_{\mathrm{L}\boldsymbol{x}}^p}_{\mathcal{V}^p} \underline{\boldsymbol{n}^p \cdot \left(\boldsymbol{\sigma} - \langle \boldsymbol{\sigma} \rangle^{\mathrm{f}} \right)}_{\mathcal{S}^p} \right) \right\rangle \\ &\overset{\circ}{=} \left\langle \sum_p X^p \boldsymbol{r}^p \left(\frac{R^2}{|\boldsymbol{r}^p|^3} \left(\boldsymbol{n}^p \cdot \left(\boldsymbol{\sigma} - \langle \boldsymbol{\sigma} \rangle^{\mathrm{f}} \right) \right) [\boldsymbol{x}^p + R \boldsymbol{r}^p / |\boldsymbol{r}^p|] - \frac{1}{R} \left(\frac{R^3}{|\boldsymbol{r}^p|^3} - 1 \right) \underline{\boldsymbol{n}^p \cdot \left(\boldsymbol{\sigma} - \langle \boldsymbol{\sigma} \rangle^{\mathrm{f}} \right)}_{\mathcal{S}^p} \right) \right\rangle, \end{aligned} \tag{114}$$

$$\begin{aligned} \left[\langle \boldsymbol{\sigma} \rangle^{\mathrm{f}} \right]_{\mathrm{s}}' &= \left\langle \sum\nolimits_p V^p \underline{\boldsymbol{r}^p \left(\boldsymbol{\nabla} \cdot \langle \boldsymbol{\sigma} \rangle^{\mathrm{f}} - \underline{\boldsymbol{\nabla} \cdot \langle \boldsymbol{\sigma} \rangle^{\mathrm{f}}}_{\mathcal{V}^p} \right) \delta_{\mathrm{L}\boldsymbol{x}}^p}_{\mathcal{V}^p} \right\rangle \\ &\overset{\circ}{=} \left\langle \sum_p X^p \boldsymbol{r}^p \left(\int_{|\boldsymbol{r}^p|/R}^1 \frac{1}{\lambda^4} \left(\boldsymbol{\nabla} \cdot \langle \boldsymbol{\sigma} \rangle^{\mathrm{f}} \right) [\boldsymbol{x}^p + \boldsymbol{r}^p / \lambda] \, \mathrm{d}\lambda - \frac{1}{3} \left(\frac{R^3}{|\boldsymbol{r}^p|^3} - 1 \right) \underline{\boldsymbol{\nabla} \cdot \langle \boldsymbol{\sigma} \rangle^{\mathrm{f}}}_{\mathcal{V}^p} \right) \right\rangle, \end{aligned} \tag{115}$$

$$\boldsymbol{\sigma}^{\mathbf{s}} \equiv \boldsymbol{\sigma}_{\mathbf{c}}^{\mathbf{s}} + \boldsymbol{\sigma}_{\uparrow \mathbf{Re}}^{\mathbf{s}}, \tag{116}$$

$$\boldsymbol{\sigma}_{\mathbf{c}}^{\mathbf{s}} \equiv \left\langle \frac{1}{2} \sum\nolimits_{pq} \boldsymbol{r}^{pq} \boldsymbol{F}_{\mathrm{c}}^{pq} \delta_{\mathrm{L}\boldsymbol{x}}^{pq} \right\rangle - \left\langle \sum\nolimits_p \underline{\boldsymbol{r}^p \delta_{\mathrm{L}\boldsymbol{x}}^p}_{\mathcal{V}^p} \boldsymbol{F}_{\mathrm{c}}^p \right\rangle \overset{\circ}{=} \left\langle \frac{1}{2} \sum\nolimits_{pq} \boldsymbol{r}^{pq} \boldsymbol{F}_{\mathrm{c}}^{pq} \delta_{\mathrm{L}\boldsymbol{x}}^{pq} \right\rangle - \left\langle \sum\nolimits_p \frac{X^p \boldsymbol{r}^p}{4\pi R^3} \left(\frac{R^3}{|\boldsymbol{r}^p|^3} - 1 \right) \boldsymbol{F}_{\mathrm{c}}^p \right\rangle, \tag{117}$$

$$\boldsymbol{\sigma}_{\uparrow \mathbf{Re}}^{\mathbf{s}} \equiv -\beta_{\mathrm{s}} \rho_{\mathrm{s}} \left\langle \left(\boldsymbol{u} - \langle \boldsymbol{u} \rangle_{\rho_*}^{\mathrm{s}} \right) (\boldsymbol{u}_\uparrow - \boldsymbol{u}_{\mathrm{s}}) \right\rangle_{\rho_*}^{\mathrm{s}}. \tag{118}$$

Note that, for sphere-symmetrical particles, the particle-rotational contributions to $\beta_{\mathrm{s}} \rho_{\mathrm{s}} \mathrm{D}_t^{\mathrm{s}} \boldsymbol{u}_{\mathrm{s}}$ and $\boldsymbol{\nabla} \cdot \boldsymbol{\sigma}^{\mathbf{s}}$ in Eq. (111) cancel each other out, implying one can redefine both the operator $\mathrm{D}_t^{\mathrm{s}}$ and the stress $\boldsymbol{\sigma}_{\uparrow \mathbf{Re}}^{\mathbf{s}}$ through formally replacing $\boldsymbol{u} \to \boldsymbol{u}_\uparrow$, and therefore $\langle \boldsymbol{u} \rangle_{\rho_*}^{\mathrm{s}} \to \boldsymbol{u}_{\mathrm{s}}$, in their above definitions at the same time.

The stress $\langle \boldsymbol{\sigma} \rangle^{\mathrm{f}}$ in Eq. (112) describes the effect of the fluid-phase-averaged field, while $\boldsymbol{\sigma}_{\mathbf{s}}^{\mathbf{f}}$ is associated with the traction by the fluctuation stress around this field, $\boldsymbol{\sigma} - \langle \boldsymbol{\sigma} \rangle^{\mathrm{f}}$, on the particle surfaces. Furthermore, $\left[\langle \boldsymbol{\sigma} \rangle^{\mathrm{f}} \right]_{\mathrm{s}}'$, with $[\cdot]_{\mathrm{s}}'$ as defined in Eq. (46), originates from fluctuations of $\boldsymbol{\nabla} \cdot \langle \boldsymbol{\sigma} \rangle^{\mathrm{f}}$ within the particle interiors, $\boldsymbol{\sigma}_{\mathbf{c}}^{\mathbf{s}}$ in Eq. (116) from contact interactions, and the Reynolds stresses $\boldsymbol{\sigma}_{\mathbf{Re}}^{\mathbf{f}}$ and $\boldsymbol{\sigma}_{\uparrow \mathbf{Re}}^{\mathbf{s}}$ from macroscopic fluid and particle velocity fluctuations, respectively. Note that, if the fluid is incompressible and Newtonian, one can express $\langle \boldsymbol{\sigma} \rangle^{\mathrm{f}}$ as

$$\langle \boldsymbol{\sigma} \rangle^{\mathrm{f}} = -\langle P \rangle^{\mathrm{f}} \mathbf{1} + \beta_{\mathrm{f}}^{-1} \eta_{\mathrm{f}} \left(\boldsymbol{\nabla} \langle \boldsymbol{u} \rangle + (\boldsymbol{\nabla} \langle \boldsymbol{u} \rangle)^{\mathrm{T}} \right), \tag{119}$$

where P is the local, instantaneous fluid pressure, η_{f} the clear-fluid viscosity, and we used that $X^p (\partial_i u_j + \partial_j u_i) = 0$ for an individual particle p and therefore

$$\beta_{\mathrm{f}} \langle \partial_i u_j + \partial_j u_i \rangle^{\mathrm{f}} = \langle X_{\mathrm{f}} (\partial_i u_j + \partial_j u_i) \rangle = \left\langle X_{\mathrm{f}} (\partial_i u_j + \partial_j u_i) + \sum\nolimits_p X^p (\partial_i u_j + \partial_j u_i) \right\rangle = \langle \partial_i u_j + \partial_j u_i \rangle = \partial_i \langle u_j \rangle + \partial_j \langle u_i \rangle. \tag{120}$$

As a side note for readers who are interested in a comparison to previous formalisms, we compare to the fluid phase momentum balance equation [4.2] of Zhang and Prosperetti [14]. The two abstract terms appearing on its right-hand side are related to the above stresses through $\epsilon_{\mathrm{D}} \mathcal{A}[\boldsymbol{\sigma}_{\mathrm{C}}] = \boldsymbol{f} - \beta_{\mathrm{s}} \langle \boldsymbol{\sigma} \rangle^{\mathrm{f}} - \boldsymbol{\nabla} \cdot \left[\langle \boldsymbol{\sigma} \rangle^{\mathrm{f}} \right]_{\mathrm{s}}'$, which is a mathematically exact version of their equation [4.4], and $\epsilon_{\mathrm{D}} \mathcal{L}[\boldsymbol{\sigma}_{\mathrm{C}}] = \boldsymbol{\sigma}_{\mathbf{s}}^{\mathbf{f}}$. It means that the nonaveraged instantaneous, local fluid stress tensor $\boldsymbol{\sigma}$ in our Eqs. (112) and (114) plays the same role as the conditionally-averaged stress tensor $\langle \boldsymbol{\sigma}_{\mathrm{C}} \rangle_1$ in their equations [4.3] and [4.5]. Note that a comparison to their solid phase balance equation [4.12] cannot be easily done, since it mixes grain-phase-averaged quantities with the solid phase volume fraction β_{s} and already contains approximations.

Equations (110) and (111) represent (a part of) the closure problem, meaning that the fields in these equations, given by the derived mathematically exact micromechanical expressions, need to be interrelated through closures.

One of the first steps that is usually taken to this end is to decompose the fluid-solid interaction force density $\boldsymbol{f}$ into two contributions: a generalized-drag contribution ($\boldsymbol{f}^{\mathrm{D}}$, which includes drag, lift, lubrication, etc) arising from and a generalized-buoyancy contribution ($\boldsymbol{f}^{\mathrm{B}}$) independent of the relative motion between the fluid and solid phases [12],

$$\boldsymbol{f} = \boldsymbol{f}^{\mathrm{D}} + \boldsymbol{f}^{\mathrm{B}}. \tag{121}$$

This decomposition is achieved through the buoyancy closure, which relates $\boldsymbol{f}^{\mathrm{B}}$ to properties of the average fluid phase flow in a manner that is consistent with the classical buoyancy force density expected for completely stationary fluid-particle systems ($\boldsymbol{f}^{\mathrm{B}} = -\beta_{\mathrm{s}}\rho_{\mathrm{f}}\boldsymbol{g}$ if $\rho_{\mathrm{f}} = \mathrm{const}$).

It is sometimes stated that the buoyancy closure is ambiguous because any contribution not incorporated in $\boldsymbol{f}^{\mathrm{B}}$ can be incorporated in $\boldsymbol{f}^{\mathrm{D}}$ instead [12, 13]. However, this notion is fallacious, since it usually implies that force density contributions that do not arise from the relative fluid-solid motion are assigned to $\boldsymbol{f}^{\mathrm{D}}$. Only if one is aware that one has not included certain generalized-buoyancy-related terms in $\boldsymbol{f}^{\mathrm{B}}$, one is able to correct this mistake by including them in $\boldsymbol{f}^{\mathrm{D}}$ instead. However, the obvious problem is that one is usually unaware of this. In fact, although there are quite a number of distinct existing buoyancy closures, they are almost always combined with closures for $\boldsymbol{f}^{\mathrm{D}}$ that only account for relative-motion forces [e.g., 12, 13].

A. Test of existing buoyancy closures with DNS-DEM simulations of sediment transport

Here, we use the DNS-DEM simulation of steady, bed-tangentially homogeneous ($\partial_t = \partial_x = \partial_y = 0$) sediment transport described in §IV, complemented by further simulations for more turbulent conditions and larger system size, $(L_x, L_y, H) = (5, 3, 15)$, to test existing buoyancy closures. We focus on the fluid phase momentum balance in the direction normal to the sediment bed (z) and assume that the bed-normal component of the generalized-drag force density, f_z^{D}, approximately vanishes since the (actual) bed-normal drag force on descending particles tends to exactly cancel that on ascending particles on average as $u_{\mathrm{f}z} = u_{\mathrm{s}z} = 0$ [20]. This assumption implies

$$\mathrm{d}_z\sigma_{zz}^{\mathrm{f}} + \beta_{\mathrm{f}}\rho_{\mathrm{f}}g_z - f_z^{\mathrm{B}} \approx 0. \tag{122}$$

Using $\mathrm{d}_z\sigma_{zz}^{\mathrm{f}} \approx -\rho_{\mathrm{f}}g_z$ (Fig. 2(b)), it results in

$$f_z^{\mathrm{B}} \approx -\beta_{\mathrm{s}}\rho_{\mathrm{f}}g_z. \tag{123}$$

In other words, applying the assumption $f_z^{\mathrm{D}} \approx 0$ to the sediment transport data leads approximately to a stationary-like bed-normal buoyancy force density. In general, this assumption can never conclusively proven to be true, since one cannot directly measure f_z^{D} without prior knowledge of what exactly it is. However, it can be considered strong evidence in favor of a given existing buoyancy closure if its combination with this assumption led to a prediction that is consistent with the simulation data and if the same could not be said about competing existing buoyancy closures. Given that existing buoyancy closures have been derived long ago from independent physical reasoning, such a result would seem very unlikely to happen by chance. In addition, if $f_z^{\mathrm{D}} \approx 0$ was not true, it would imply that f_z^{D} just so happens to compensate the differences between f_z^{B} and $-\beta_{\mathrm{s}}\rho_{\mathrm{f}}g_z$, which would be an unreasonable coincidence in itself. One would have to explain why $f_z^{\mathrm{B}} + f_z^{\mathrm{D}}$, but not f_z^{B}, is approximately equal to an expression exactly resembling the buoyancy force density in stationary systems.

It can be directly seen that three existing buoyancy closures [11–13] reproduce Eq. (123):

$$\boldsymbol{f}^{\mathrm{B}} = -\beta_{\mathrm{s}}\rho_{\mathrm{f}}\boldsymbol{g}, \tag{124}$$

$$\boldsymbol{f}^{\mathrm{B}} = \beta_{\mathrm{s}}\rho_{\mathrm{f}}\left(\mathrm{D}_t^{\mathrm{f}}\boldsymbol{u}_{\mathrm{f}} - \boldsymbol{g}\right), \tag{125}$$

$$\boldsymbol{f}^{\mathrm{B}} = \beta_{\mathrm{s}}\rho_{\mathrm{f}}\left(\mathrm{D}_t^{\mathrm{f}}\boldsymbol{u}_{\mathrm{f}} - \boldsymbol{g} + \frac{\boldsymbol{f}^{\mathrm{D}}}{\beta_{\mathrm{f}}\rho_{\mathrm{f}}}\right) = \beta_{\mathrm{s}}\boldsymbol{\nabla}\cdot\boldsymbol{\sigma}^{\mathbf{f}}, \tag{126}$$

where the equality on the right-hand side of Eq. (126) follows from substitution into Eq. (110) using Eq. (121). However, Eq. (124) is actually not a true buoyancy closure, since, in order to be consistent, the corresponding generalized-drag force density must contain the additional term $\beta_{\mathrm{s}}\rho_{\mathrm{f}}\mathrm{D}_t^{\mathrm{f}}\langle\boldsymbol{u}_{\uparrow}\rangle^{\mathrm{f}}$ [13], which is not associated with the relative fluid-solid motion and therefore does not satisfy the earlier introduced requirements for the generalized-drag force density. Furthermore, both Eqs. (124) and (125) have essentially been falsified [30] through an experiment showing that a large 3−4 mm biomass particle of density 800 kg/m^3 can float in an air-fluidized bed of fine 170−250 μm glass particles ($\rho_{\mathrm{s}} \approx 2500$ kg/m^3) near minimum fluidization conditions [29]. In contrast, Eq. (126) predicts $\boldsymbol{f}^{\mathrm{B}} =$

$-(\beta_\mathrm{f}\rho_\mathrm{f}+\beta_\mathrm{s}\rho_\mathrm{s})\beta_\mathrm{s}\boldsymbol{g}$ for homogeneous fluidized beds, consistent with this experiment [30]. However, the associated closure relations [24]

$$\boldsymbol{f}^\mathrm{B}=-\beta_\mathrm{s}(\beta_\mathrm{f}\rho_\mathrm{f}+\beta_\mathrm{s}\rho_\mathrm{s})\boldsymbol{g}, \tag{127}$$

$$\boldsymbol{f}^\mathrm{B}=\beta_\mathrm{s}(\beta_\mathrm{f}\rho_\mathrm{f}+\beta_\mathrm{s}\rho_\mathrm{s})\left(\mathrm{D}_t^\mathrm{f}\boldsymbol{u}_\mathrm{f}-\boldsymbol{g}\right) \tag{128}$$

are inconsistent with Eq. (123), obtained from our sediment transport simulations.

From a physical perspective, Eq. (126) makes a lot of sense since it essentially states that $\boldsymbol{f}^\mathrm{B}$ opposes all non-buoyancy forces per unit fluid mass acting on the fluid, $\boldsymbol{g}$ and $-\boldsymbol{f}^\mathrm{D}/(\beta_\mathrm{f}\rho_\mathrm{f})$, relative to an observer co-accelerated with the average fluid ($\mathrm{D}_t^\mathrm{f}\boldsymbol{u}_\mathrm{f}$). However, it may not be the only existing buoyancy closure consistent with the simulation data and the fluidized-bed experiment. The alternative closures [5, 12, 25, 27, 28]

$$\boldsymbol{f}^\mathrm{B}=\beta_\mathrm{s}\boldsymbol{\nabla}\cdot\left(\boldsymbol{\sigma}^\mathbf{f}-\boldsymbol{\sigma}^\mathbf{f}_\mathbf{Re}\right), \tag{129}$$

$$\boldsymbol{f}^\mathrm{B}=\beta_\mathrm{s}\boldsymbol{\nabla}\cdot\langle\boldsymbol{\sigma}\rangle^\mathrm{f}, \tag{130}$$

$$\boldsymbol{f}^\mathrm{B}=\beta_\mathrm{s}\boldsymbol{\nabla}\mathrm{tr}\left(\boldsymbol{\sigma}^\mathbf{f}\right)/3, \tag{131}$$

$$\boldsymbol{f}^\mathrm{B}=\beta_\mathrm{s}\boldsymbol{\nabla}\mathrm{tr}\left(\boldsymbol{\sigma}^\mathbf{f}-\boldsymbol{\sigma}^\mathbf{f}_\mathbf{Re}\right)/3, \tag{132}$$

$$\boldsymbol{f}^\mathrm{B}=-\beta_\mathrm{s}\boldsymbol{\nabla}\langle P\rangle^\mathrm{f} \tag{133}$$

could also by consistent with them if the corresponding stress component, σ^f_{zz}–$\sigma^\mathrm{f}_{\mathrm{Re}zz}$, $\langle\sigma_{zz}\rangle^\mathrm{f}$, $\mathrm{tr}\left(\boldsymbol{\sigma}^\mathbf{f}\right)/3$, $\mathrm{tr}\left(\boldsymbol{\sigma}^\mathbf{f}-\boldsymbol{\sigma}^\mathbf{f}_\mathbf{Re}\right)/3$, or $-\langle P\rangle^\mathrm{f}$, is approximately equal to σ^f_{zz}. Note that Eq. (132) is included in this list because researchers in favor of Eq. (133) may have all but Reynolds normal-stress contributions in mind when referring to $\langle P\rangle^\mathrm{f}$, since there seems to be an unawareness in some communities of the existence of normal-stress contributions arising from fluid-solid interactions [e.g., 26].

Figure 3 shows that, in general, none of the above stress components approximates to σ^f_{zz}, which always exhibits an approximately hydrostatic profile across the simulated transport conditions (except for significant deviations for $\eta_\mathrm{f}=0.01$ near the bed surface, probably due to fluid lift, and slight deviations for all cases in the lower bed layers). In particular, the zz-components of the total stress associated with fluid-solid interactions, $\sigma^\mathrm{f}_{\mathrm{s}zz}+[\langle\sigma_{zz}\rangle^\mathrm{f}]'_\mathrm{s}$, and the Reynolds stress, $\sigma^\mathrm{f}_{\mathrm{Re}zz}$, which are often assumed to be negligible, turn out to substantially contribute to the overall hydrostatic behavior of σ^f_{zz}. Concerning the Reynolds stress, this is apparent from the fact that, except for the large-viscosity cases ($\eta_\mathrm{f}\gtrsim 0.05$), $\sigma^\mathrm{f}_{zz}-\sigma^\mathrm{f}_{\mathrm{Re}zz}$ slightly but notably deviates from σ^f_{zz} and the hydrostatic behavior in the central region of the flow. Note that the buoyancy closure by Drew [25], often used in geophysical settings [26], which actually reads $\boldsymbol{f}^\mathrm{B}=\langle P\rangle^\mathrm{f}\boldsymbol{\nabla}\beta_\mathrm{s}$, is included in Eq. (133), since this author neglected the extension of the particles (treating them as points), in which case $\boldsymbol{\nabla}\cdot\boldsymbol{\sigma}^\mathbf{f}=\boldsymbol{\nabla}\cdot\beta_\mathrm{f}\langle\boldsymbol{\sigma}\rangle^\mathrm{f}$ and therefore $\mathrm{d}_z\langle P\rangle^\mathrm{f}=\rho_\mathrm{f}g_z$ from Eq. (122).

In summary, only the buoyancy closure Eq. (126), which was originally proposed by Anderson and Jackson [11] and is based on the entire effective fluid stress tensor $\boldsymbol{\sigma}^\mathbf{f}$, is consistent with the simulation data. However, as we show below, Eq. (126), and all the other tested existing closures for that matter, lead to a contradiction for certain stationary fluid-particle systems.

B. Contradiction for certain stationary fluid-particle systems

When applying either of the buoyancy closures Eqs. (124)-(126) and (129)-(133) to the trivial case of completely stationary fluid and particles (e.g., one may think of a particle bed immersed in a fluid at rest), implying

$$\boldsymbol{u}_\mathrm{f}=\boldsymbol{u}_\mathrm{s}=0, \qquad \boldsymbol{f}^\mathrm{D}=0, \qquad \boldsymbol{\nabla}\cdot\langle\boldsymbol{\sigma}\rangle^\mathrm{f}=-\rho_\mathrm{f}\boldsymbol{g}, \qquad \boldsymbol{\sigma}^\mathbf{f}_\mathbf{Re}=0, \qquad \boldsymbol{\sigma}^\mathbf{f}_\mathbf{s}=0, \tag{134}$$

Eq. (110) simplifies to

$$\boldsymbol{\nabla}\cdot\left[\langle\boldsymbol{\sigma}\rangle^\mathrm{f}\right]'_\mathrm{s}=\beta_\mathrm{s}\rho_\mathrm{f}\boldsymbol{g}-\beta_\mathrm{s}\left\langle\underline{\rho_\mathrm{f}\boldsymbol{g}}_\mathcal{V}\right\rangle^\mathrm{s}=0, \tag{135}$$

where we used Eqs. (45) and (47). Although this condition is identically satisfied for a stationary fluid of constant density ρ_f, the same can no longer be said if the static fluid is allowed to have density gradients. That is, Eqs. (124)-(133) all lead to a contradiction for general scenarios and must therefore be false at a mathematically rigorous level. Physically, this is because, when taking into account density gradients, the stationary-buoyancy force density does not obey $\boldsymbol{f}^\mathrm{B}=-\beta_\mathrm{s}\rho_\mathrm{f}\boldsymbol{g}$ but instead

$$\boldsymbol{f}^\mathrm{B}=-\beta_\mathrm{s}\left\langle\underline{\rho_\mathrm{f}\boldsymbol{g}}_\mathcal{V}\right\rangle^\mathrm{s}=-\left\langle\sum\nolimits_p\frac{X^p}{V^p}\int_{\mathcal{V}^p}\rho_\mathrm{f}\boldsymbol{g}\mathrm{d}V\right\rangle. \tag{136}$$

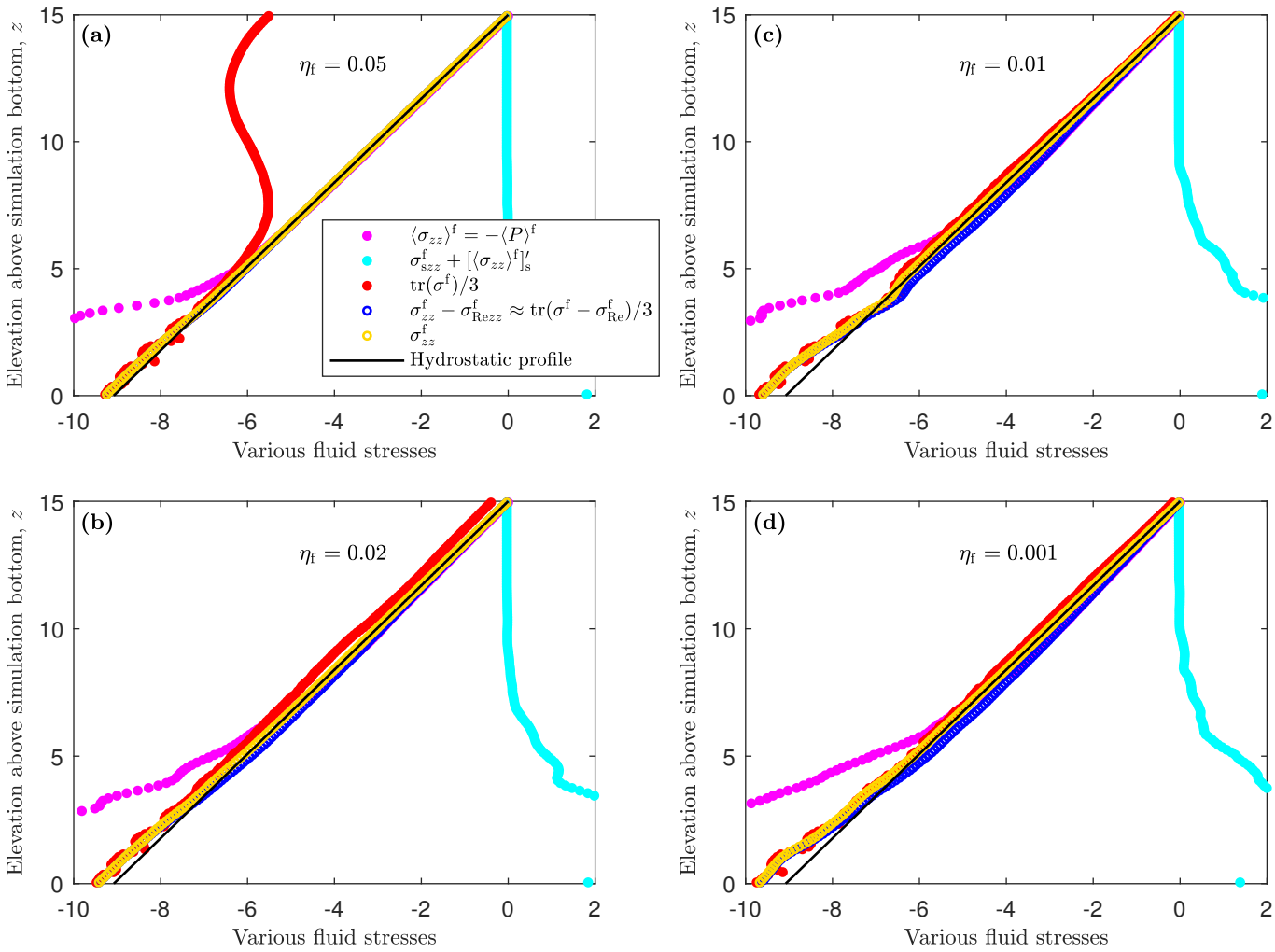

FIG. 3. Height profiles of various fluid stresses (see legend). Data correspond to DNS-DEM simulations of sediment transport for four different viscosities: (a) $\eta_f = 0.05$ (averaged over $N_T = 105$ instants of time), (b) $\eta_f = 0.02$ ($N_T = 110$), (c) $\eta_f = 0.01$ ($N_T = 48$), and (d) $\eta_f = 0.001$ ($N_T = 55$). The stresses are calculated directly using the exact stress expressions given in Appendix C. Data from simulations for larger viscosities, such as those in Fig. 2 ($\eta_f = 0.36$), are similar to the $\eta = 0.05$-case and therefore not shown. The profiles of $\langle\sigma_{zz}\rangle^f$ and $-\langle P\rangle^f$ ($\sigma^f_{zz} - \sigma^f_{Rezz}$ and $\mathrm{tr}(\sigma^f - \sigma^f_{Re})/3$) are (nearly) identical due to $u_{fz} = u_{sz} = 0$ (steady, bed-tangentially homogeneous conditions).

C. Consistent buoyancy closure

The obvious improvement of Eq. (126) that avoids the above contradiction, while remaining consistent with the simulations (because of $\rho_f = \mathrm{const}$, $\mathrm{D}^f_t = 0$, and $f^D_z \approx 0$), is

$$\boldsymbol{f}^B = \beta_s \left\langle \underline{\beta_f^{-1}\left(\boldsymbol{\nabla}\cdot\boldsymbol{\sigma}^{\mathbf{f}} - \boldsymbol{f}^B\right)_{\mathcal{V}}} \right\rangle^s = \beta_s \left\langle \underline{\rho_f \mathrm{D}^f_t \boldsymbol{u}_f - \rho_f \boldsymbol{g} + \beta_f^{-1}\boldsymbol{f}^D}_{\mathcal{V}} \right\rangle^s, \tag{137}$$

where we used Eq. (110), since it generalizes Eq. (136) in the same manner as Eq. (126) generalizes $\boldsymbol{f}^B = -\beta_s\rho_f\boldsymbol{g}$. However, Eq. (137) is an implicit definition of $\boldsymbol{f}^B$. Like for Eq. (126), it is desirable to transform it into an explicit expression that depends only on $\boldsymbol{\sigma}^{\mathbf{f}}$. For this purpose, we define

$$\boldsymbol{B} \equiv \beta_f^{-1}\left(\boldsymbol{\nabla}\cdot\boldsymbol{\sigma}^{\mathbf{f}} - \boldsymbol{f}^B\right), \tag{138}$$

which we use to transform Eq. (137) into

$$\boldsymbol{B} = \boldsymbol{\nabla}\cdot\boldsymbol{\sigma}^{\mathbf{f}} - \boldsymbol{B}', \tag{139}$$

with $\cdot'$ as defined in Eq. (45). Repeated application of this operator, using Eq. (47), then yields

$$\boldsymbol{B}' = \boldsymbol{\nabla}\cdot\left[\boldsymbol{\sigma}^{\mathbf{f}}\right]_{\mathrm{s}}' - \boldsymbol{B}'', \tag{140}$$

$$\boldsymbol{B}'' = \boldsymbol{\nabla}\cdot\left[\left[\boldsymbol{\sigma}^{\mathbf{f}}\right]_{\mathrm{s}}'\right]_{\mathrm{s}}' - \boldsymbol{B}''', \tag{141}$$

and so forth, with $[\cdot]_{\mathrm{s}}'$ as defined in Eq. (46), and therefore

$$\boldsymbol{B} = \sum_{k=0}^{\infty}(-1)^k\boldsymbol{\nabla}\cdot\left[\boldsymbol{\sigma}^{\mathbf{f}}\right]_{\mathrm{s}}^{\prime k}, \tag{142}$$

where $[\cdot]_{\mathrm{s}}^{\prime k}$ means k applications of the operator $[\cdot]_{\mathrm{s}}'$. Hence, using $\boldsymbol{f}^{\mathrm{B}} = \beta_{\mathrm{s}}\langle\underline{\boldsymbol{B}}_{\mathcal{V}}\rangle^{\mathrm{s}} = \beta_{\mathrm{s}}\boldsymbol{B} + \boldsymbol{B}'$, the two expressions below are equivalent to Eq. (137):

$$\boldsymbol{f}^{\mathrm{B}} = \beta_{\mathrm{s}}\boldsymbol{\nabla}\cdot\boldsymbol{\sigma}^{\mathbf{f}} - \beta_{\mathrm{f}}\boldsymbol{\nabla}\cdot\boldsymbol{\sigma}^{\mathbf{f}}_{\mathbf{s}'}, \tag{143}$$

$$\boldsymbol{f}^{\mathrm{B}} = \beta_{\mathrm{s}}\rho_{\mathrm{f}}\left(\mathrm{D}_t^{\mathrm{f}}\boldsymbol{u}_{\mathrm{f}} - \boldsymbol{g} + \frac{\boldsymbol{f}^{\mathrm{D}}}{\beta_{\mathrm{f}}\rho_{\mathrm{f}}}\right) - \boldsymbol{\nabla}\cdot\boldsymbol{\sigma}^{\mathbf{f}}_{\mathbf{s}'}, \tag{144}$$

where $\boldsymbol{\sigma}^{\mathbf{f}}_{\mathbf{s}'}$ is a fluid stress tensor associated with fluid-solid interactions, defined as

$$\begin{aligned}\boldsymbol{\sigma}^{\mathbf{f}}_{\mathbf{s}'} \equiv \sum_{k=1}^{\infty}(-1)^k\left[\boldsymbol{\sigma}^{\mathbf{f}}\right]_{\mathrm{s}}^{\prime k} \overset{\circ}{\simeq} &-\frac{R^2}{5}\beta_{\mathrm{s}}\boldsymbol{\nabla}\boldsymbol{\nabla}\cdot\boldsymbol{\sigma}^{\mathbf{f}} + \frac{R^4}{175}\Delta\beta_{\mathrm{s}}\boldsymbol{\nabla}\boldsymbol{\nabla}\cdot\boldsymbol{\sigma}^{\mathbf{f}} - \frac{R^4}{350}\boldsymbol{\nabla}\beta_{\mathrm{s}}\Delta\boldsymbol{\nabla}\cdot\boldsymbol{\sigma}^{\mathbf{f}} - \frac{9R^4}{350}\boldsymbol{\nabla}\cdot\beta_{\mathrm{s}}\boldsymbol{\nabla}\boldsymbol{\nabla}\boldsymbol{\nabla}\cdot\boldsymbol{\sigma}^{\mathbf{f}} \\ &+ \frac{R^4}{175}\beta_{\mathrm{s}}\boldsymbol{\nabla}\Delta\boldsymbol{\nabla}\cdot\boldsymbol{\sigma}^{\mathbf{f}} + \frac{R^4}{25}\beta_{\mathrm{s}}\boldsymbol{\nabla}\boldsymbol{\nabla}\cdot\beta_{\mathrm{s}}\boldsymbol{\nabla}\boldsymbol{\nabla}\cdot\boldsymbol{\sigma}^{\mathbf{f}} + O(R^6/L^6).\end{aligned} \tag{145}$$

The fifth-order approximation on the right-hand side, obtained using Eq. (49), includes the first and second fluctuations ($k = 1, 2$) of $\boldsymbol{\sigma}^{\mathbf{f}}_{\mathbf{s}'}$ and is applicable to the case that all particles are spheres of a constant radius R with sphere-symmetrical interiors.

The term $\beta_{\mathrm{s}}\boldsymbol{\nabla}\cdot\boldsymbol{\sigma}^{\mathbf{f}}$ in Eq. (143) may be interpreted as the standard buoyancy force density, the only non-vanishing term in the first order of R/L, while $\beta_{\mathrm{f}}\boldsymbol{\nabla}\cdot\boldsymbol{\sigma}^{\mathbf{f}}_{\mathbf{s}'}$ is a higher-order correction associated with variations of $\boldsymbol{\nabla}\cdot\boldsymbol{\sigma}^{\mathbf{f}}$ at the particle scale. Substituting Eq. (143) into Eq. (121), the momentum balances Eqs. (110) and (111) become

$$\beta_{\mathrm{f}}\rho_{\mathrm{f}}\mathrm{D}_t^{\mathrm{f}}\boldsymbol{u}_{\mathrm{f}} = \beta_{\mathrm{f}}\boldsymbol{\nabla}\cdot\left(\boldsymbol{\sigma}^{\mathbf{f}} + \boldsymbol{\sigma}^{\mathbf{f}}_{\mathbf{s}'}\right) + \beta_{\mathrm{f}}\rho_{\mathrm{f}}\boldsymbol{g} - \boldsymbol{f}^{\mathrm{D}}, \tag{146}$$

$$\beta_{\mathrm{s}}\rho_{\mathrm{s}}\mathrm{D}_t^{\mathrm{s}}\boldsymbol{u}_{\mathrm{s}} = \beta_{\mathrm{s}}\boldsymbol{\nabla}\cdot\boldsymbol{\sigma}^{\mathbf{f}} - \beta_{\mathrm{f}}\boldsymbol{\nabla}\cdot\boldsymbol{\sigma}^{\mathbf{f}}_{\mathbf{s}'} + \boldsymbol{\nabla}\cdot\boldsymbol{\sigma}^{\mathbf{s}} + \beta_{\mathrm{s}}\rho_{\mathrm{s}}\boldsymbol{g} + \boldsymbol{f}^{\mathrm{D}}. \tag{147}$$

Furthermore, using Eq. (146) in Eq. (137) and $V^p\underline{\boldsymbol{\nabla}\cdot\left(\boldsymbol{\sigma}^{\mathbf{f}} + \boldsymbol{\sigma}^{\mathbf{f}}_{\mathbf{s}'}\right)}_{\mathcal{V}^p} = S^p\underline{\boldsymbol{n}^p\cdot\left(\boldsymbol{\sigma}^{\mathbf{f}} + \boldsymbol{\sigma}^{\mathbf{f}}_{\mathbf{s}'}\right)}_{\mathcal{S}^p}$ (Gauss's theorem) yields yet another equivalent expression for $\boldsymbol{f}^{\mathrm{B}}$:

$$\boldsymbol{f}^{\mathrm{B}} = \beta_{\mathrm{s}}\left\langle\underline{\boldsymbol{\nabla}\cdot\left(\boldsymbol{\sigma}^{\mathbf{f}} + \boldsymbol{\sigma}^{\mathbf{f}}_{\mathbf{s}'}\right)}_{\mathcal{V}}\right\rangle^{\mathrm{s}} = \left\langle\sum\nolimits_p\frac{S^p}{V^p}\underline{\boldsymbol{n}^p\cdot\left(\boldsymbol{\sigma}^{\mathbf{f}} + \boldsymbol{\sigma}^{\mathbf{f}}_{\mathbf{s}'}\right)}_{\mathcal{S}^p}X^p\right\rangle. \tag{148}$$

It means that $\boldsymbol{f}^{\mathrm{B}}$ is the force density resulting from the traction by the stress $\boldsymbol{\sigma}^{\mathbf{f}} + \boldsymbol{\sigma}^{\mathbf{f}}_{\mathbf{s}'}$ on the particle surfaces, implying that $\boldsymbol{f}^{\mathrm{D}}$ results from the traction by $\boldsymbol{\sigma} - \boldsymbol{\sigma}^{\mathbf{f}} - \boldsymbol{\sigma}^{\mathbf{f}}_{\mathbf{s}'}$. Of the different equivalent expressions for $\boldsymbol{f}^{\mathrm{B}}$, Eqs. (137), (143), (144), and (148), Eq. (148) is the one most accurately extracted from our DNS-DEM simulation data. Figure 4 shows that it is consistent with these data. The significant deviations from $f_z^{\mathrm{B}} = -\beta_{\mathrm{s}}\rho_{\mathrm{f}}g_z$ observed for the cases $\eta_{\mathrm{f}} = 0.01$ and $\eta_{\mathrm{f}} = 0.001$ are probably owed to the lift force, which can be comparable to the actual drag force for elevation near the bed surface in turbulent sediment transport [39, 40].

D. Far-field stress

We remind the reader that the generalized-drag force density $\boldsymbol{f}^{\mathrm{D}}$ has been defined as the contribution to the total fluid-solid interaction force density $\boldsymbol{f}$ resulting from the relative fluid-solid motion. This definition should be equivalent (though we are unaware of a definitive proof) to defining $\boldsymbol{f}^{\mathrm{D}}$ as the force density resulting from modifications of the local stresses around the particles' surfaces relative to the distant or far-field stress due to the (typically no-slip) boundary conditions. The above analysis therefore suggests that $\boldsymbol{\sigma}^{\mathbf{f}} + \boldsymbol{\sigma}^{\mathbf{f}}_{\mathbf{s}'}$ is exactly this far-field stress. This is

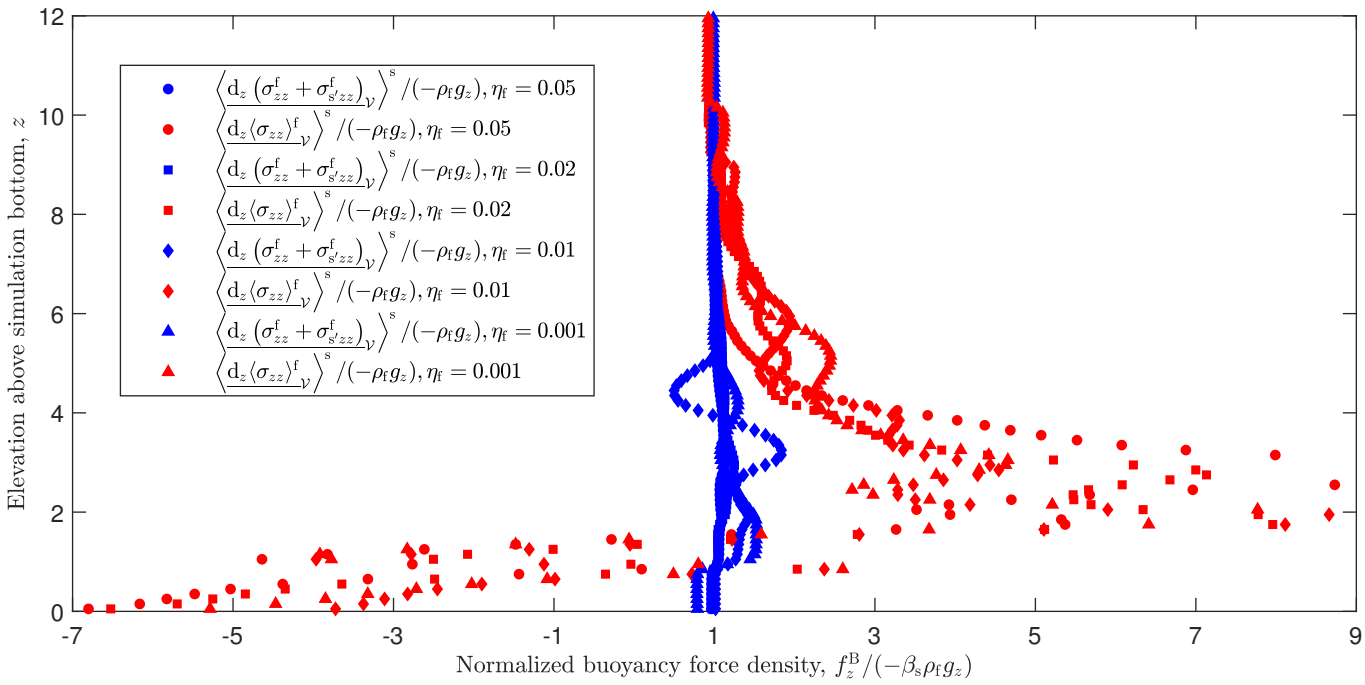

FIG. 4. Height profiles of normalized buoyancy force density, $f_z^{\mathrm{B}}/(-\beta_{\mathrm{s}}\rho_{\mathrm{f}}g_z)$, predicted by Eq. (148) or Eq. (149). Data correspond to DNS-DEM simulations of sediment transport for the same cases as in Fig. 3. The stresses are calculated directly using the exact stress expressions given in Appendix C.

an odd finding because one normally identifies the far-field stress as $\langle\boldsymbol{\sigma}\rangle^{\mathrm{f}}$ [27]. Incidentally, the buoyancy closure associated with this alternative far-field stress definition,

$$\boldsymbol{f}^{\mathrm{B}}=\beta_{\mathrm{s}}\left\langle\underline{\boldsymbol{\nabla}\cdot\langle\boldsymbol{\sigma}\rangle^{\mathrm{f}}_{\mathcal{V}}}\right\rangle^{\mathrm{s}}=\beta_{\mathrm{s}}\boldsymbol{\nabla}\cdot\langle\boldsymbol{\sigma}\rangle^{\mathrm{f}}+\boldsymbol{\nabla}\cdot\left[\langle\boldsymbol{\sigma}\rangle^{\mathrm{f}}\right]'_{\mathrm{s}}, \tag{149}$$

would also have resolved the contradiction in §V B. However, like its cousin Eq. (130), it is also completely inconsistent with the DNS-DEM simulations of sediment transport (Fig. 4). Near the bed surface, it deviates from $f_z^{\mathrm{B}}=-\beta_{\mathrm{s}}\rho_{\mathrm{f}}g_z$ by an astonishing factor of 9. This stark disagreement implies that generalized-drag force closures based on a force decomposition using Eq. (130) or Eq. (149), which is a typical starting point in theoretical studies [27, 41], cannot be relied upon, at least in systems without scale separation.

E. General far-field interactions

So far, we have limited our considerations to the momentum balances, where the buoyancy force density emerges from the traction by the far-field stress $\boldsymbol{\sigma}^{\mathbf{f}}+\boldsymbol{\sigma}^{\mathbf{f}}_{\mathbf{s}'}$ on the particle surfaces. Now, we consider generic balance equations and decompose the total fluid-solid interaction term $\beta_{\mathrm{s}}\langle\rho_*\dot{\psi}_{\uparrow\mathrm{f}}\rangle^{\mathrm{s}}$ into a buoyancy-like far-field contribution $\beta_{\mathrm{s}}\langle\rho_*\dot{\psi}^{\mathrm{B}}_{\uparrow\mathrm{f}}\rangle^{\mathrm{s}}$ and a drag-like near-field contribution $\beta_{\mathrm{s}}\langle\rho_*\dot{\psi}^{\mathrm{D}}_{\uparrow\mathrm{f}}\rangle^{\mathrm{s}}$:

$$\beta_{\mathrm{s}}\langle\rho_*\dot{\psi}_{\uparrow\mathrm{f}}\rangle^{\mathrm{s}}=\beta_{\mathrm{s}}\langle\rho_*\dot{\psi}^{\mathrm{D}}_{\uparrow\mathrm{f}}\rangle^{\mathrm{s}}+\beta_{\mathrm{s}}\langle\rho_*\dot{\psi}^{\mathrm{B}}_{\uparrow\mathrm{f}}\rangle^{\mathrm{s}}. \tag{150}$$

From an analysis completely analogous to the above, it is given by any of the following four equivalent expressions:

$$\beta_{\mathrm{s}}\langle\rho_*\dot{\psi}^{\mathrm{B}}_{\uparrow\mathrm{f}}\rangle^{\mathrm{s}}=-\beta_{\mathrm{s}}\boldsymbol{\nabla}\cdot\boldsymbol{J}^{\mathbf{f}}_{\boldsymbol{\Psi}}+\beta_{\mathrm{f}}\boldsymbol{\nabla}\cdot\boldsymbol{J}^{\mathbf{f}}_{\boldsymbol{\Psi}\mathbf{s}'}, \tag{151}$$

$$\beta_{\mathrm{s}}\langle\rho_*\dot{\psi}^{\mathrm{B}}_{\uparrow\mathrm{f}}\rangle^{\mathrm{s}}=-\beta_{\mathrm{s}}\left\langle\underline{\boldsymbol{\nabla}\cdot\left(\boldsymbol{J}^{\mathbf{f}}_{\boldsymbol{\Psi}}+\boldsymbol{J}^{\mathbf{f}}_{\boldsymbol{\Psi}\mathbf{s}'}\right)_{\mathcal{V}}}\right\rangle^{\mathrm{s}}, \tag{152}$$

$$\beta_{\mathrm{s}}\langle\rho_*\dot{\psi}^{\mathrm{B}}_{\uparrow\mathrm{f}}\rangle^{\mathrm{s}}=\beta_{\mathrm{s}}\left(\rho_{\mathrm{f}}\mathrm{D}^{\mathrm{f}}_t\langle\psi_\uparrow\rangle^{\mathrm{f}}_{\rho_*}-\rho_{\mathrm{f}}\langle\dot{\psi}_{\uparrow\mathrm{b}}\rangle^{\mathrm{f}}_{\rho_*}-\langle D_\Psi\rangle^{\mathrm{f}}+\beta_{\mathrm{f}}^{-1}\beta_{\mathrm{s}}\langle\rho_*\dot{\psi}^{\mathrm{D}}_{\uparrow\mathrm{f}}\rangle^{\mathrm{s}}\right)+\boldsymbol{\nabla}\cdot\boldsymbol{J}^{\mathbf{f}}_{\boldsymbol{\Psi}\mathbf{s}'}, \tag{153}$$

$$\beta_{\mathrm{s}}\langle\rho_*\dot{\psi}^{\mathrm{B}}_{\uparrow\mathrm{f}}\rangle^{\mathrm{s}}=\beta_{\mathrm{s}}\left\langle\underline{\rho_{\mathrm{f}}\mathrm{D}^{\mathrm{f}}_t\langle\psi_\uparrow\rangle^{\mathrm{f}}_{\rho_*}-\rho_{\mathrm{f}}\langle\dot{\psi}_{\uparrow\mathrm{b}}\rangle^{\mathrm{f}}_{\rho_*}-\langle D_\Psi\rangle^{\mathrm{f}}+\beta_{\mathrm{f}}^{-1}\beta_{\mathrm{s}}\langle\rho_*\dot{\psi}^{\mathrm{D}}_{\uparrow\mathrm{f}}\rangle^{\mathrm{s}}}_{\mathcal{V}}\right\rangle^{\mathrm{s}}. \tag{154}$$

F. Linear-stability analysis of homogeneous fluidized bed

To demonstrate that our improvement of the buoyancy closure by Anderson and Jackson [11] has not only theoretical but also practical relevance, we compare the effect of both closures on the stability of a homogeneous fluidized bed. A homogeneous fluidized bed is an idealized state where a constant fluid flow in the direction z opposite to gravity, $\boldsymbol{e_z} = -\boldsymbol{g}/|\boldsymbol{g}|$, overcompensates the weight of a particle bed settled on a surface permeable to air, causing its uniform expansion. It is characterized by an equilibrium solid volume fraction ϕ_0, equilibrium fluid phase velocity $\boldsymbol{u}_{\mathrm{f}0} = u_0\boldsymbol{e_z}$, equilibrium solid phase velocity $\boldsymbol{u}_{\mathrm{s}0} = 0$, and equilibrium value T_0 of the granular temperature $T \equiv (\langle|\boldsymbol{u}_\uparrow|^2\rangle^{\mathrm{s}} - |\boldsymbol{u}_{\mathrm{s}}|^2)/3$. These four quantities are perturbed,

$$\phi \equiv \beta_{\mathrm{s}} = \phi_0 + \phi_1, \qquad \boldsymbol{u}_{\mathrm{f}} = \boldsymbol{u}_{\mathrm{f}0} + \boldsymbol{u}_{\mathrm{f}1}, \qquad \boldsymbol{u}_{\mathrm{s}} = \boldsymbol{u}_{\mathrm{s}1}, \qquad T = T_0 + T_1, \tag{155}$$

where the perturbations ϕ_1, $\boldsymbol{u}_{\mathrm{f}1}$, $\boldsymbol{u}_{\mathrm{s}1}$, and T_1 are assumed to be sufficiently small so that a linear-stability analysis can be applied. Due to conservation of volume, $\boldsymbol{\nabla}\cdot\langle\boldsymbol{u}\rangle = 0$, the mixture velocity $\langle\boldsymbol{u}\rangle = (1-\phi)\boldsymbol{u}_{\mathrm{f}} + \phi\boldsymbol{u}_{\mathrm{s}}$ of a perturbed state is the same as that at equilibrium:

$$\langle\boldsymbol{u}\rangle = (1-\phi_0)\boldsymbol{u}_{\mathrm{f}0}. \tag{156}$$

It implies that one can express $\boldsymbol{u}_{\mathrm{f}}$ as a function of ϕ and $\boldsymbol{u}_{\mathrm{s}}$:

$$\boldsymbol{u}_{\mathrm{f}} = \frac{\langle\boldsymbol{u}\rangle - \phi\boldsymbol{u}_{\mathrm{s}}}{1-\phi} = \boldsymbol{u}_{\mathrm{f}0}\frac{1-\phi_0}{1-\phi} - \frac{\phi\boldsymbol{u}_{\mathrm{s}}}{1-\phi}. \tag{157}$$

That is, only the temporal evolutions of ϕ_1, $\boldsymbol{u}_{\mathrm{s}}$, and T_1 need to be modeled, for which the solid phase mass, momentum, and granular-temperature balances are required.

To keep the analysis simple, we consider an incompressible Newtonian fluid of constant density ρ_{f} and viscosity η_{f} and identical spheres of constant density ρ_{s} and radius R. Then, the solid mass, momentum, and granular-temperature balances can be phrased in a manner completely devoid of the particle-rotational degrees of freedom (§III D 1). Respectively, they read

$$\partial_t\phi + \boldsymbol{\nabla}\cdot\phi\boldsymbol{u}_{\mathrm{s}} = 0, \tag{158}$$

$$\rho_{\mathrm{s}}\phi\mathrm{D}_t^{\mathrm{s}}\boldsymbol{u}_{\mathrm{s}} = \boldsymbol{\nabla}\cdot\boldsymbol{\sigma}^{\mathbf{s}} + \rho_{\mathrm{s}}\phi\boldsymbol{g} + \boldsymbol{f}^{\mathrm{D}} + \boldsymbol{f}^{\mathrm{B}}, \tag{159}$$

$$\frac{3}{2}\rho_{\mathrm{s}}\phi\mathrm{D}_t^{\mathrm{s}}T = \boldsymbol{\sigma}^{\mathbf{s}} : \boldsymbol{\nabla}\boldsymbol{u}_{\mathrm{s}} - \boldsymbol{\nabla}\cdot\boldsymbol{Q} + \Gamma^{\mathrm{D}} + \Gamma^{\mathrm{B}} - \Gamma^{\mathrm{c}}, \tag{160}$$

where $\boldsymbol{Q}$ is the flux of fluctuation energy, Γ^{D} the net production rate of fluctuation energy due to near-field fluid-solid interactions, Γ^{B} a buoyancy-like production rate due to far-field interactions (based on the generalization of buoyancy discussed in §V E), and Γ^{c} the dissipation rate of fluctuation energy due to particle contacts, while the term $\boldsymbol{\sigma}^{\mathbf{s}} : \boldsymbol{\nabla}\boldsymbol{u}_{\mathrm{s}}$ describes the rate of conversion of particle mean energy into fluctuation energy. The latter emerges from subtracting the momentum balance ($\psi_\uparrow = \boldsymbol{u}_\uparrow$ in Eq. (87)) scalar multiplied with $\boldsymbol{u}_{\mathrm{s}}$ from the energy balance ($\psi_\uparrow = |\boldsymbol{u}_\uparrow|^2/2$ in Eq. (87)), yielding the fluctuation energy balance.

We largely follow the linear-stability analysis by Mandich and Cattolica [31]. These authors considered the following near-field fluid-solid interactions: fluid-solid momentum transfer ($\boldsymbol{f}^{\mathrm{D}}$) by linear-drag and virtual-mass forces and fluid-solid fluctuation energy transfer (Γ^{D}) by fluid-particle slip and viscous damping. Furthermore, they modeled $\boldsymbol{\sigma}^{\mathbf{s}}$, $\boldsymbol{Q}$, and Γ^{c} using a granular kinetic theory, modified by the presence of interstitial fluid. Here, accounting for the progress made in recent decades, we use the kinetic-theory closures proposed by Chassagne *et al.* [8], even though they are somewhat controversial [9]. In what follows, we summarize the fluid-solid interaction and kinetic-theory closures, presented in forms in which $\boldsymbol{u}_{\mathrm{f}}$ is substituted by the expression in Eq. (157).

The closures for the linear-drag and virtual-mass force densities read [31]

$$\boldsymbol{f}^{\mathrm{D}} = \beta(\langle\boldsymbol{u}\rangle - \boldsymbol{u}_{\mathrm{s}}) + \rho_{\mathrm{f}}C_\nu\phi\left(\mathrm{D}_t^{\mathrm{f}}\frac{\langle\boldsymbol{u}\rangle - \phi\boldsymbol{u}_{\mathrm{s}}}{1-\phi} - \mathrm{D}_t^{\mathrm{s}}\boldsymbol{u}_{\mathrm{s}}\right), \quad \text{with} \quad \beta = \frac{(\rho_{\mathrm{s}} - \rho_{\mathrm{f}})|\boldsymbol{g}|}{u_{\mathrm{t}}}\phi(1-\phi)^{1-n_{\mathrm{RZ}}} \quad \text{and} \quad C_\nu = \frac{1+2\phi}{2(1-\phi)}, \tag{161}$$

where C_ν is the added-mass coefficient [42, 43], u_{t} the terminal settling velocity of an individual particle in clear fluid, and n_{RZ} the Richardson-Zaki coefficient [44]. The latter two can both be expressed as a function of the Galileo number $\mathrm{Ga} \equiv 2\rho_{\mathrm{f}}R\sqrt{2(\rho_{\mathrm{s}}/\rho_{\mathrm{f}} - 1)|\boldsymbol{g}|R}/\eta_{\mathrm{f}}$ [45, 46]:

$$u_{\mathrm{t}} = \left(\sqrt{15/\mathrm{Ga} + \sqrt{10/3}} - \sqrt{15/\mathrm{Ga}}\right)^2\sqrt{2(\rho_{\mathrm{s}}/\rho_{\mathrm{f}} - 1)|\boldsymbol{g}|R}, \qquad (4.8 - n_{\mathrm{RZ}})/(n_{\mathrm{RZ}} - 2.4) = 0.043\mathrm{Ga}^{1.14}. \tag{162}$$

The closure for the sum of the temperature production rate by fluid-particle slip and temperature dissipation rate by viscous damping, Γ^{D}, is [31]

$$\Gamma^{\mathrm{D}} = (1-\phi)\left(\frac{\gamma|\langle\boldsymbol{u}\rangle - \boldsymbol{u}_{\mathrm{s}}|^2}{(1-\phi)^2\sqrt{T}} - 3\beta T\right), \quad \text{with} \quad \gamma = \frac{81\eta_{\mathrm{f}}^2\phi}{8\sqrt{\pi}\rho_{\mathrm{s}}R^3\chi}, \tag{163}$$

where χ is the radial distribution function, which we adopted from Chassagne *et al.* [8] to account for sliding friction between two contacting particles (friction coefficient μ_{c}):

$$\chi = \frac{2-\phi}{2(1-\phi)^3} + \frac{(0.58 + 3.12\tanh[\mu_{\mathrm{c}}/0.54])\phi^2}{(0.635-\phi)^{3/2}}. \tag{164}$$

Equation (163) differs from the closure by Mandich and Cattolica [31] (the term in the parentheses) in the additional the prefactor $1-\phi$, the reasons for which will be explained later.

The kinetic-theory closures read [7, 8]

$$\boldsymbol{\sigma}^{\mathbf{s}} = -P_{\mathrm{s}}\mathbf{1} + \eta_{\mathrm{s}}\left(\boldsymbol{\nabla}\boldsymbol{u}_{\mathrm{s}} + (\boldsymbol{\nabla}\boldsymbol{u}_{\mathrm{s}})^{\mathrm{T}} - \frac{2}{3}\mathbf{1}\boldsymbol{\nabla}\cdot\boldsymbol{u}_{\mathrm{s}}\right) + \zeta_{\mathrm{s}}\mathbf{1}\boldsymbol{\nabla}\cdot\boldsymbol{u}_{\mathrm{s}}, \quad \boldsymbol{Q} = -\lambda_{\mathrm{s}}\boldsymbol{\nabla}T, \quad \Gamma^{\mathrm{c}} = \frac{6\rho_{\mathrm{s}}}{\sqrt{\pi}R}\left(1-e_{\mathrm{eff}}^2\right)\phi^2\chi T^{3/2}, \tag{165}$$

where P_{s} is the solid phase pressure, η_{s} the shear viscosity, ζ_{s} the bulk viscosity, λ_{s} the conductivity, and e_{eff} an effective restitution coefficient. They are, respectively, given by [7, 8]

$$P_{\mathrm{s}} = \rho_{\mathrm{s}}\phi(1+2(1+e_{\mathrm{n}})\phi\chi)T, \qquad \eta_{\mathrm{s}} = 2\rho_{\mathrm{s}}R\sqrt{T}\left(\frac{\eta_{\mathrm{salt}}^*\eta_{\mathrm{k}}^*}{\eta_{\mathrm{salt}}^*+\eta_{\mathrm{k}}^*} + \eta_{\mathrm{c}}^* + \eta_{\mathrm{b}}^*\right), \quad \zeta_{\mathrm{s}} = \frac{10}{3}\rho_{\mathrm{s}}R\sqrt{T}\eta_{\mathrm{b}}^*, \tag{166}$$

$$\lambda_{\mathrm{s}} = 2\rho_{\mathrm{s}}R\sqrt{T}\left(\frac{\lambda_{\mathrm{salt}}^*\lambda_{\mathrm{k}}^*}{\lambda_{\mathrm{salt}}^*+\lambda_{\mathrm{k}}^*} + \lambda_{\mathrm{c}}^* + \lambda_{\mathrm{b}}^*\right), \quad e_{\mathrm{eff}} = e_{\mathrm{n}} - \frac{1}{2}\left(a_1 - a_2\frac{b_1}{b_2}\right), \tag{167}$$

with coefficients that depend, among others, on μ_{c} and the normal (e_{n}) and tangential (e_{t}) restitution coefficients, parametrizing binary particle collisions (we choose the typical values $e_{\mathrm{n}} = 0.9$, $e_{\mathrm{t}} = 0$, and $\mu_{\mathrm{c}} = 0.5$) [8]:

$$\eta_{\mathrm{salt}}^* = \frac{\rho_{\mathrm{s}}\phi^2\sqrt{T}}{10R\beta}, \quad \eta_{\mathrm{k}}^* = \frac{5\sqrt{\pi}}{96}\left(\frac{1-2/5(1+e_{\mathrm{n}})(1-3e_{\mathrm{n}})\phi\chi}{(1-1/4(1-e_{\mathrm{n}})^2-5/24(1-e_{\mathrm{n}}^2))\,\chi}\right), \quad \eta_{\mathrm{c}}^* = \frac{4}{5}(1+e_{\mathrm{n}})\phi\chi\eta_{\mathrm{k}}^*, \quad \eta_{\mathrm{b}}^* = \frac{4}{5\sqrt{\pi}}(1+e_{\mathrm{n}})\phi^2\chi, \tag{168}$$

$$\lambda_{\mathrm{salt}}^* = \frac{\rho_{\mathrm{s}}\phi^2\sqrt{T}}{5R\beta}, \quad \lambda_{\mathrm{k}}^* = \frac{225\sqrt{\pi}}{576}\left(\frac{1+3/5(1+e_{\mathrm{n}})^2(2e_{\mathrm{n}}-1)\phi\chi}{(1-7/16(1-e_{\mathrm{n}}))\,(1+e_{\mathrm{n}})\chi}\right), \quad \lambda_{\mathrm{c}}^* = \frac{6}{5}(1+e_{\mathrm{n}})\phi\chi\lambda_{\mathrm{k}}^*, \quad \lambda_{\mathrm{b}}^* = \frac{2}{\sqrt{\pi}}(1+e_{\mathrm{n}})\phi^2\chi, \tag{169}$$

$$a_1 = \mu_{\mathrm{c}}\left(\pi\left(1-\frac{2}{\pi}\arctan\mu_*\right) + \frac{2\mu_*}{1+\mu_*^2}\left(1-\frac{2\mu_{\mathrm{c}}}{\mu_*}\right)\right), \quad a_2 = \frac{5}{2}\mu_{\mathrm{c}}\left(\frac{\pi}{2}\left(1-\frac{2}{\pi}\arctan\mu_*\right) + \frac{\mu_*-\mu_*^3}{(1+\mu_*^2)^2}\right), \tag{170}$$

$$b_1 = \frac{\mu_{\mathrm{c}}^2}{1+\mu_*^2}, \quad b_2 = \frac{1}{2}\mu_{\mathrm{c}}\left(\frac{\pi}{2}\left(1-\frac{2}{\pi}\arctan\mu_*\right) + \frac{\mu_*}{1+\mu_*^2}\right), \quad \text{with} \quad \mu_* = \frac{7}{2}\mu_{\mathrm{c}}\frac{1+e_{\mathrm{n}}}{1+e_{\mathrm{t}}}. \tag{171}$$

Finally, for $\boldsymbol{f}^{\mathrm{B}}$, we employ the buoyancy closure in the form given in Eq. (137), and for Γ^{B}, its far-field generalization arising from Eq. (154), neglecting contributions associated with the change of the fluid's fluctuation energy ($\rho_{\mathrm{f}}\mathrm{D}_t^{\mathrm{f}}\langle\psi_\uparrow\rangle_{\rho_*}^{\mathrm{f}} - \langle D_\Psi\rangle^{\mathrm{f}} \approx 0$):

$$\boldsymbol{f}^{\mathrm{B}} = -\phi\rho_{\mathrm{f}}\boldsymbol{g} + \phi\left\langle\underline{\rho_{\mathrm{f}}\mathrm{D}_t^{\mathrm{f}}\boldsymbol{u}_{\mathrm{f}} + \boldsymbol{f}^{\mathrm{D}}/(1-\phi)}_{\mathcal{V}}\right\rangle^{\mathrm{s}}, \qquad \Gamma^{\mathrm{B}} = \phi\left\langle\underline{\Gamma^{\mathrm{D}}/(1-\phi)}_{\mathcal{V}}\right\rangle^{\mathrm{s}}. \tag{172}$$

The closure equations corresponding to the buoyancy formulation by Anderson and Jackson [11] are obtained from formally replacing $\langle\cdot\rangle^{\mathrm{s}} \to \cdot$ in Eq. (172). In that case, $\boldsymbol{f}^{\mathrm{D}} + \boldsymbol{f}^{\mathrm{B}}$ and $\Gamma^{\mathrm{D}} + \Gamma^{\mathrm{B}}$ are the same as their counterparts in the linear-stability analysis by Mandich and Cattolica [31], noting that these authors neglected Γ^{B}, which is why we added the prefactor $1-\phi$ to the closure of Γ^{D} in Eq. (163).

The further plan is to insert all the above closures into Eqs. (158)-(160) and linearly expand the resulting equations around the equilibrium state, indicated by the subscript '0'. This calculation is straightforward, except for the evaluation of the terms involving the operation $\langle\cdot\rangle^{\mathrm{s}}$ in Eq. (172). We exemplary demonstrate how these terms are handled by linearizing $\Gamma^{\mathrm{D}} + \Gamma^{\mathrm{B}}$ below.

We define $\tilde{\Gamma}^{\mathrm{D}} \equiv \Gamma^{\mathrm{D}}/(1-\phi)$ and use the definition of the fluctuation operator $\cdot'$, Eq. (45), and its expansion in an infinite series of spatial derivatives (applicable to identical spheres), Eq. (B14), to obtain

$$\Gamma^{\mathrm{D}} + \Gamma^{\mathrm{B}} = \Gamma^{\mathrm{D}} + \phi \left\langle \underline{\tilde{\Gamma}^{\mathrm{D}}}_{\mathcal{V}} \right\rangle^{\mathrm{s}} = \tilde{\Gamma}^{\mathrm{D}} + \left(\tilde{\Gamma}^{\mathrm{D}}\right)' = \tilde{\Gamma}^{\mathrm{D}} + \sum_{i=1}^{\infty}\sum_{j=1}^{\infty}\sum_{k=0}^{\min(i,j)} c_{ijk} R^{i+j} \Delta^{\frac{i-k}{2}} \boldsymbol{\nabla}^{(k)} \odot \phi \boldsymbol{\nabla}^{(k)} \Delta^{\frac{j-k}{2}} \tilde{\Gamma}^{\mathrm{D}}, \tag{173}$$

where c_{ijk} are the rational series coefficients derived in Appendix B. They are non-zero only when both $(i-k)$ and $(j-k)$ are even (i.e., $\Delta^{\frac{i-k}{2}}$ and $\Delta^{\frac{j-k}{2}}$ need not be well-defined when either of them or both are odd). Denoting the linear expansion of $\tilde{\Gamma}^{\mathrm{D}}$ in ϕ_1, $\boldsymbol{u}_{\mathrm{s}}$, and T_1 as

$$\tilde{\Gamma}^{\mathrm{D}} = \tilde{\Gamma}^{\mathrm{D}}_0 + \tilde{\Gamma}^{\mathrm{D}}_1 + O(2) = \tilde{\Gamma}^{\mathrm{D}}_0 + \left(\partial_\phi \tilde{\Gamma}^{\mathrm{D}}\right)_0 \phi_1 + \left(\boldsymbol{\nabla}_{\boldsymbol{u}_{\mathrm{s}}} \tilde{\Gamma}^{\mathrm{D}}\right)_0 \cdot \boldsymbol{u}_{\mathrm{s}} + \left(\partial_T \tilde{\Gamma}^{\mathrm{D}}\right)_0 T_1 + O(2), \tag{174}$$

where the subscript '1' indicates the sum of all first-order terms, Eq. (173) is linearly expanded as

$$\begin{aligned}
\Gamma^{\mathrm{D}} + \Gamma^{\mathrm{B}} &= \tilde{\Gamma}^{\mathrm{D}}_0 + \tilde{\Gamma}^{\mathrm{D}}_1 + \sum_{i=1}^{\infty}\sum_{j=1}^{\infty}\sum_{k=0}^{\min(i,j)} c_{ijk} R^{i+j} \Delta^{\frac{i-k}{2}} \boldsymbol{\nabla}^{(k)} \odot \phi_0 \boldsymbol{\nabla}^{(k)} \Delta^{\frac{j-k}{2}} \tilde{\Gamma}^{\mathrm{D}}_1 + O(2) \\
&= \tilde{\Gamma}^{\mathrm{D}}_0 + \tilde{\Gamma}^{\mathrm{D}}_1 + \phi_0 \sum_{i=1}^{\infty}\sum_{j=1}^{\infty}\sum_{k=0}^{\min(i,j)} c_{ijk} R^{i+j} \Delta^{\frac{i+j}{2}} \tilde{\Gamma}^{\mathrm{D}}_1 + O(2) = \tilde{\Gamma}^{\mathrm{D}}_0 + \tilde{\Gamma}^{\mathrm{D}}_1 + \phi_0 \sum_{n=2}^{\infty}\sum_{i=1}^{\infty}\sum_{\substack{j=1 \\ i+j=n}}^{\infty}\sum_{k=0}^{\min(i,j)} c_{ijk} R^{i+j} \Delta^{\frac{i+j}{2}} \tilde{\Gamma}^{\mathrm{D}}_1 + O(2) \\
&= \tilde{\Gamma}^{\mathrm{D}}_0 + \tilde{\Gamma}^{\mathrm{D}}_1 + \phi_0 \sum_{n=2}^{\infty} c_n R^n \Delta^{n/2} \tilde{\Gamma}^{\mathrm{D}}_1 + O(2) = \tilde{\Gamma}^{\mathrm{D}}_0 + (1-\phi_0)\tilde{\Gamma}^{\mathrm{D}}_1 + \phi_0 \sum_{n=0}^{\infty} c_n R^n \Delta^{n/2} \tilde{\Gamma}^{\mathrm{D}}_1 + O(2),
\end{aligned} \tag{175}$$

with c_n as given by Eq. (B18). Defining the differential operator

$$\mathcal{L} \equiv \sum_{n=0}^{\infty} c_n R^n \Delta^{n/2} = \sum_{n=0}^{\infty} \frac{36 \times 2^n \left(1 + (-1)^n\right)}{(n+1)!(n+3)(n+4)(n+6)} R^n \Delta^{n/2}, \tag{176}$$

where we used Eq. (B18), one can summarize the linear expansion of $\Gamma^{\mathrm{D}} + \Gamma^{\mathrm{B}}$ as

$$\Gamma^{\mathrm{D}} + \Gamma^{\mathrm{B}} = \frac{\Gamma^{\mathrm{D}}_0}{1-\phi_0} + (1 - \phi_0 + \phi_0 \mathcal{L}) \left(\frac{\Gamma^{\mathrm{D}}}{1-\phi}\right)_1 + O(2). \tag{177}$$

An analogous calculation for $\boldsymbol{f}^{\mathrm{D}} + \boldsymbol{f}^{\mathrm{B}}$ yields

$$\boldsymbol{f}^{\mathrm{D}} + \boldsymbol{f}^{\mathrm{B}} = -(\phi_0 + \phi_1)\rho_{\mathrm{f}} \boldsymbol{g} + \rho_{\mathrm{f}} \phi_0 \mathcal{L} \left(\mathrm{D}^{\mathrm{f}}_t \boldsymbol{u}_{\mathrm{f}}\right)_1 + \frac{\boldsymbol{f}^{\mathrm{D}}_0}{1-\phi_0} + (1 - \phi_0 + \phi_0 \mathcal{L}) \left(\frac{\boldsymbol{f}^{\mathrm{D}}}{1-\phi}\right)_1 + O(2). \tag{178}$$

Note that, in the case that the buoyancy formulation by Anderson and Jackson [11] is used, Eqs. (177) and (178) remain valid when formally replacing $\mathcal{L} \to 1$. Even though $\mathcal{L}$ contains an infinite number of spatial derivatives, it is possible to evaluate its effect on the stability of homogeneous fluidized beds without approximation, as we show below.

Having explained how to handle the far-field terms $\boldsymbol{f}^{\mathrm{B}}$ and Γ^{B}, we can now proceed with the linear expansion of Eqs. (158)-(160) around the equilibrium state. In this state, Eqs. (159) and (160) simplify, respectively, to

$$\rho_{\mathrm{f}} \phi_0 \boldsymbol{g} + \boldsymbol{f}^{\mathrm{D}}_0 + \boldsymbol{f}^{\mathrm{B}}_0 = 0, \tag{179}$$

$$\Gamma^{\mathrm{D}}_0 + \Gamma^{\mathrm{B}}_0 - \Gamma^{\mathrm{c}}_0 = 0. \tag{180}$$

Inserting the closures for $\boldsymbol{f}^{\mathrm{D}}$, $\boldsymbol{f}^{\mathrm{B}}$, Γ^{D}, and Γ^{B}, Eq. (179), nontrivial only in the z-direction, and Eq. (180) become

$$\beta_0 u_0 - (\rho_{\mathrm{s}} - \rho_{\mathrm{f}}) |\boldsymbol{g}| \phi_0 = 0, \tag{181}$$

$$\frac{\gamma_0 u_0^2}{\sqrt{T_0}} - 3\beta_0 T_0 - \frac{6\rho_{\mathrm{s}}}{\sqrt{\pi} R} \left(1 - e^2_{\mathrm{eff}}\right) \phi_0^2 \chi_0 T_0^{3/2} = 0, \tag{182}$$

where we used Eq. (156). These equations link u_0 to ϕ_0 and T_0 to ϕ_0 and u_0. In particular, Eq. (182) exhibits a unique, positive solution for real T_0.

Inserting all closures into Eqs. (158)-(160) and linearly expanding the resulting equations around the equilibrium state, using the above equilibrium conditions and substituting $\langle \boldsymbol{u} \rangle$ by the expression in Eq. (156), yields

$$\partial_t \phi_1 + \phi_0 \boldsymbol{\nabla} \cdot \boldsymbol{u}_\mathrm{s} = 0, \tag{183}$$

$$\begin{aligned}
&\rho_\mathrm{s}\phi_0 \partial_t \boldsymbol{u}_\mathrm{s} = (\rho_\mathrm{s} - \rho_\mathrm{f})\boldsymbol{g}\phi_1 + \beta_0 \left(1 + \frac{\phi_0}{1-\phi_0}\mathcal{L}\right)(\boldsymbol{u}_{\mathrm{f}0}\phi_1 - \boldsymbol{u}_\mathrm{s}) + (\partial_\phi \beta)_0 (1 - \phi_0 + \phi_0 \mathcal{L})\boldsymbol{u}_{\mathrm{f}0}\phi_1 \\
&+ \rho_\mathrm{f} C_{\nu 0}\phi_0 \left(1 + \frac{\phi_0}{1-\phi_0}\mathcal{L}\right)\left(\frac{\boldsymbol{u}_{\mathrm{f}0}}{1-\phi_0}\mathrm{D}_t^{\mathrm{f}0}\phi_1 - \frac{\phi_0}{1-\phi_0}\mathrm{D}_t^{\mathrm{f}0}\boldsymbol{u}_\mathrm{s} - \partial_t \boldsymbol{u}_s\right) + \rho_\mathrm{f}\phi_0 \mathcal{L}\left(\frac{\boldsymbol{u}_{\mathrm{f}0}}{1-\phi_0}\mathrm{D}_t^{\mathrm{f}0}\phi_1 - \frac{\phi_0}{1-\phi_0}\mathrm{D}_t^{\mathrm{f}0}\boldsymbol{u}_\mathrm{s}\right) \\
&- (\partial_\phi P_\mathrm{s})_0 \boldsymbol{\nabla}\phi_1 - (\partial_T P_\mathrm{s})_0 \boldsymbol{\nabla} T_1 + \eta_{\mathrm{s}0}\Delta \boldsymbol{u}_\mathrm{s} + \left(\frac{1}{3}\eta_{\mathrm{s}0} + \zeta_{\mathrm{s}0}\right)(\boldsymbol{\nabla}\boldsymbol{\nabla}\cdot\boldsymbol{u}_\mathrm{s}),
\end{aligned} \tag{184}$$

$$\begin{aligned}
&\frac{3}{2}\rho_\mathrm{s}\phi_0 \partial_t T_1 = -P_{\mathrm{s}0}\boldsymbol{\nabla}\cdot\boldsymbol{u}_\mathrm{s} + \lambda_{\mathrm{s}0}\Delta T_1 + (1 - \phi_0 + \phi_0\mathcal{L})\left(\frac{(\partial_\phi \gamma)_0 u_0^2}{\sqrt{T_0}}\phi_1 - 3(\partial_\phi\beta)_0 T_0 \phi_1 - \frac{\gamma_0 u_0^2}{2T_0^{3/2}}T_1 - 3\beta_0 T_1\right) \\
&+ 2\frac{\gamma_0}{\sqrt{T_0}}\left(1 + \frac{\phi_0}{1-\phi_0}\mathcal{L}\right)\left(u_0^2\phi_1 - \boldsymbol{u}_{\mathrm{f}0}\cdot\boldsymbol{u}_\mathrm{s}\right) - \frac{6\rho_\mathrm{s}}{\sqrt{\pi}R}\left(1 - e_\mathrm{eff}^2\right)\left(\left(\partial_\phi \phi^2 \chi\right)_0 T_0^{3/2}\phi_1 + \frac{3}{2}\phi_0^2\chi_0\sqrt{T_0}T_1\right),
\end{aligned} \tag{185}$$

where $\mathrm{D}_t^{\mathrm{f}0} \equiv \partial_t + \boldsymbol{u}_{\mathrm{f}0}\cdot\boldsymbol{\nabla}$. Fourier-transforming Eqs. (183)-(185), denoting the Fourier-transformed variables as $\hat{\phi}_1[\boldsymbol{k}, t]$, $\hat{\boldsymbol{u}}_\mathrm{s}[\boldsymbol{k}, t]$, and $\hat{T}_1[\boldsymbol{k}, t]$, where $\boldsymbol{k}$ is the wavenumber vector spanning the Fourier space, and scalar multiplying the Fourier transform of Eq. (184) by (i) $\boldsymbol{k}$ and (ii) $\boldsymbol{u}_{\mathrm{f}0}$ leads to the following system or ordinary differential equations:

$$\begin{pmatrix} 1 & 0 & 0 & 0 \\ \boldsymbol{A}\cdot\boldsymbol{k} & B & 0 & 0 \\ \boldsymbol{A}\cdot\boldsymbol{u}_{\mathrm{f}0} & 0 & B & 0 \\ 0 & 0 & 0 & \frac{3}{2}\rho_\mathrm{s}\phi_0 \end{pmatrix}\begin{pmatrix} \mathrm{d}_t\hat{\phi}_1 \\ \mathrm{d}_t\hat{\boldsymbol{u}}_\mathrm{s}\cdot\boldsymbol{k} \\ \mathrm{d}_t\hat{\boldsymbol{u}}_\mathrm{s}\cdot\boldsymbol{u}_{\mathrm{f}0} \\ \mathrm{d}_t\hat{T}_1 \end{pmatrix} + \begin{pmatrix} 0 & i\phi_0 & 0 & 0 \\ \boldsymbol{C}\cdot\boldsymbol{k} & D + \boldsymbol{E}\cdot\boldsymbol{k} & 0 & \boldsymbol{F}\cdot\boldsymbol{k} \\ \boldsymbol{C}\cdot\boldsymbol{u}_{\mathrm{f}0} & \boldsymbol{E}\cdot\boldsymbol{u}_{\mathrm{f}0} & D & \boldsymbol{F}\cdot\boldsymbol{u}_{\mathrm{f}0} \\ G & H & I & J \end{pmatrix}\begin{pmatrix} \hat{\phi}_1 \\ \hat{\boldsymbol{u}}_\mathrm{s}\cdot\boldsymbol{k} \\ \hat{\boldsymbol{u}}_\mathrm{s}\cdot\boldsymbol{u}_{\mathrm{f}0} \\ \hat{T}_1 \end{pmatrix} = 0, \tag{186}$$

with the matrix coefficients

$$\boldsymbol{A} \equiv -\rho_\mathrm{f}\left(\frac{\phi_0 f[R|\boldsymbol{k}|]}{1-\phi_0} + C_{\nu 0}\phi_0\left(\frac{1}{1-\phi_0} + \frac{\phi_0 f[R|\boldsymbol{k}|]}{(1-\phi_0)^2}\right)\right)\boldsymbol{u}_{\mathrm{f}0}, \tag{187}$$

$$B \equiv \rho_\mathrm{s}\phi_0 + \rho_\mathrm{f}\frac{\phi_0^2 f[R|\boldsymbol{k}|]}{1-\phi_0} + \rho_\mathrm{f} C_{\nu 0}\phi_0\left(\frac{1}{1-\phi_0} + \frac{\phi_0 f[R|\boldsymbol{k}|]}{(1-\phi_0)^2}\right), \tag{188}$$

$$\begin{aligned}
\boldsymbol{C} \equiv &-(\rho_\mathrm{s} - \rho_\mathrm{f})\boldsymbol{g} - \beta_0\left(1 + \frac{\phi_0 f[R|\boldsymbol{k}|]}{1-\phi_0}\right)\boldsymbol{u}_{\mathrm{f}0} - (\partial_\phi\beta)_0(1 - \phi_0 + \phi_0 f[R|\boldsymbol{k}|])\boldsymbol{u}_{\mathrm{f}0} \\
&- i\rho_\mathrm{f}\left(\frac{\phi_0 f[R|\boldsymbol{k}|]}{1-\phi_0} + C_{\nu 0}\phi_0\left(\frac{1}{1-\phi_0} + \frac{\phi_0 f[R|\boldsymbol{k}|]}{(1-\phi_0)^2}\right)\right)\boldsymbol{k}\cdot\boldsymbol{u}_{\mathrm{f}0}\boldsymbol{u}_{\mathrm{f}0} + i(\partial_\phi P_\mathrm{s})_0\boldsymbol{k},
\end{aligned} \tag{189}$$

$$D \equiv \beta_0\left(1 + \frac{\phi_0 f[R|\boldsymbol{k}|]}{1-\phi_0}\right) + i\rho_\mathrm{f}\left(\frac{\phi_0^2 f[R|\boldsymbol{k}|]}{1-\phi_0} + C_{\nu 0}\phi_0^2\left(\frac{1}{1-\phi_0} + \frac{\phi_0 f[R|\boldsymbol{k}|]}{1-\phi_0}\right)\right)\boldsymbol{k}\cdot\boldsymbol{u}_{\mathrm{f}0} + \eta_{\mathrm{s}0}|\boldsymbol{k}|^2, \tag{190}$$

$$\boldsymbol{E} \equiv \left(\frac{1}{3}\eta_{\mathrm{s}0} + \zeta_{\mathrm{s}0}\right)\boldsymbol{k}, \quad \boldsymbol{F} \equiv i(\partial_T P_\mathrm{s})_0\boldsymbol{k}, \quad H \equiv i(\partial_T P_\mathrm{s})_0 T_0, \quad I \equiv 2\frac{\gamma_0}{\sqrt{T_0}}\left(1 + \frac{\phi_0 f[R|\boldsymbol{k}|]}{1-\phi_0}\right), \tag{191}$$

$$G \equiv -2\frac{\gamma_0 u_0^2}{\sqrt{T_0}}\left(1 + \frac{\phi_0 f[R|\boldsymbol{k}|]}{1-\phi_0}\right) - \left(\frac{(\partial_\phi\gamma)_0 u_0^2}{\sqrt{T_0}} - 3(\partial_\phi\beta)_0 T_0\right)(1 - \phi_0 + \phi_0 f[R|\boldsymbol{k}|]) + \frac{6\rho_\mathrm{s}}{\sqrt{\pi}R}\left(1 - e_\mathrm{eff}^2\right)\left(\partial_\phi\phi^2\chi\right)_0 T_0^{3/2}, \tag{192}$$

$$J \equiv \lambda_{\mathrm{s}0}|\boldsymbol{k}|^2 + \left(\frac{\gamma_0 u_0^2}{2T_0^{3/2}} + 3\beta_0\right)(1 - \phi_0 + \phi_0 f[R|\boldsymbol{k}|]) + \frac{9\rho_\mathrm{s}}{\sqrt{\pi}R}\left(1 - e_\mathrm{eff}^2\right)\phi_0^2\chi_0\sqrt{T_0}, \tag{193}$$

where the function f, arising from Fourier-transforming the differential operator $\mathcal{L}$, is defined as

$$f[X] = \sum_{n=0}^{\infty} i^n c_n X^n = \frac{9\left(\sin X - X\cos X\right)^2}{X^6}. \tag{194}$$

In the limit $X \to 0$, it approaches unity, while decaying rapidly with $|X|$, reaching almost zero when $|X| \gtrsim 4$ (Fig. 5(a)). It means that periodic perturbations with nondimensionalized wavenumbers $R|\boldsymbol{k}| \gtrsim 4$ are not affected by buoyancy

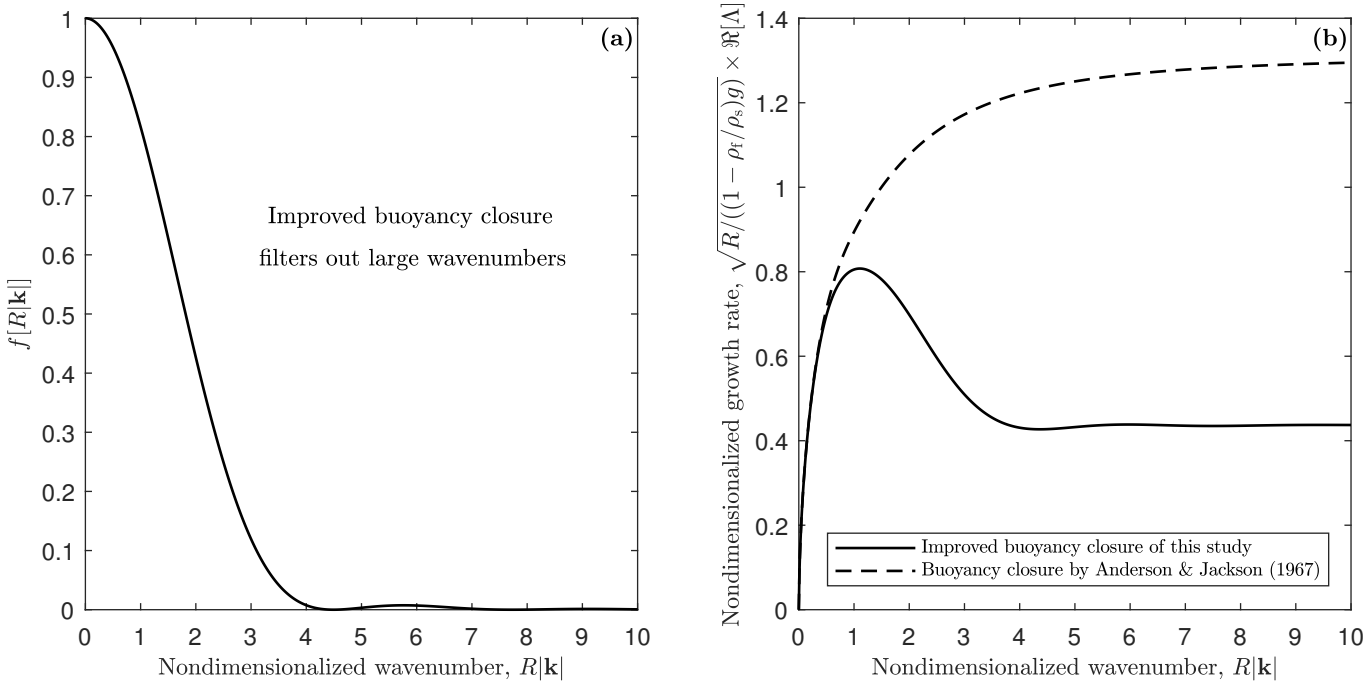

FIG. 5. (a) An exact analytical evaluation of our improved buoyancy closure within a linear-stability analysis of a homogeneous fluidized bed results in buoyancy forces and other far-field interactions being modulated by the function $f[R|\boldsymbol{k}|]$ of the nondimensionalized wavenumber $R|\boldsymbol{k}|$, given by Eq. (194), virtually filtering out contributions for $R|\boldsymbol{k}| \gtrsim 4$. (b) It causes the pattern of the growth rate $\Re[\Lambda]$ to change from a short-wavelength-dominated instability for the (unmodulated) buoyancy closure by Anderson and Jackson [11] to an intermediate-wavelength-dominated instability for its improvement. In (b), we consider an expanded bed (equilibrium volume fraction $\phi_0 = 0.5$) of particles of density $\rho_\mathrm{s} = 2500$ kg/m^3 and radius $R = 500$ μm being fluidized by air ($\rho_\mathrm{f} = 1.2$ kg/m^3, $\eta_\mathrm{f} = 1.8 \times 10^{-5}$ kg/m $\cdot$ s) in Earth's gravitational environment ($|\boldsymbol{g}| = 9.81$ m/s^2). The plots assume periodic perturbations for which $\boldsymbol{k}$ is aligned with the flow direction $\boldsymbol{e_z}$ (i.e., $\boldsymbol{k} \cdot \boldsymbol{u}_\mathrm{f0} = |\boldsymbol{k}|u_0$), since they exhibit the larges values of $\Re[\Lambda]$ all other parameters being equal.

forces and other far-field interactions. In contrast, in the case that the buoyancy formulation by Anderson and Jackson [11] is used, one should formally replace $f[R|\boldsymbol{k}|] \to 1$, implying no suppression of such interactions whatsoever. This is the key qualitative distinction between these two closures in the context of a periodically perturbed homogeneous fluidized bed.

Equation (186) can be solved through the ansatz $(\hat{\phi}_1, \hat{\boldsymbol{u}}_\mathrm{s} \cdot \boldsymbol{k}, \hat{\boldsymbol{u}}_\mathrm{s} \cdot \boldsymbol{u}_\mathrm{f0}, \hat{T}_1)[\boldsymbol{k}, t] = (\tilde{\phi}_1, \tilde{\boldsymbol{u}}_\mathrm{s} \cdot \boldsymbol{k}, \tilde{\boldsymbol{u}}_\mathrm{s} \cdot \boldsymbol{u}_\mathrm{f0}, \tilde{T}_1)[\boldsymbol{k}] \exp[\Lambda t]$. Denoting the left and right matrices in Eq. (186) as $\boldsymbol{M}_1$ and $\boldsymbol{M}_2$, respectively, the associated complex growth rate Λ is then governed by the equation

$$\det(\Lambda \boldsymbol{M}_1 + \boldsymbol{M}_2) = 0. \tag{195}$$

From its four solutions Λ_1, Λ_2, Λ_3, and Λ_4, the one with the largest real part is the actual growth rate of the perturbation, $\Re[\Lambda]$:

$$\Re[\Lambda] = \max\left[\Re[\Lambda_1], \Re[\Lambda_2], \Re[\Lambda_3], \Re[\Lambda_4]\right]. \tag{196}$$

Figure 5(b) shows that, for an exemplary homogeneous air-fluidized bed, our improvement of the buoyancy closure by Anderson and Jackson [11] can fundamentally change the bed's linear-stability pattern, from a short-wavelength-dominated to an intermediate-wavelength-dominated instability.

VI. CONCLUSIONS

We have derived balance equations for rigid particles dispersed in a continuous fluid, termed the *closure problem*, under very general circumstances (§II and §III). Our formalism applies to all standard averaging procedures and makes no assumptions about the fluid's rheology and the particles' compositions and shapes. The derived micromechanical expressions for the fields of the closure problem are mathematically exact for an arbitrarily large ratio of R/L, where

R is the particle scale and L the typical scale over which the macroscopic flow changes. We have demonstrated how to conveniently extract them without approximation from CFD-DEM simulations for a specific example: DNS-DEM simulations of steady, bed-tangentially homogeneous sediment transport (§IV and Appendix C), a dispersed flow with R/L on the order of 1 to 10 [20–22]. This achievement cannot be replicated with previous exact formalisms, since they involve Taylor expansions of infinite order in R/L, and every single additional considered order substantially increases the mathematical complexity and the required spatial resolution. Since fields of $(k+1)$-th order in R/L contain k-th spatial derivatives, finer and finer grids are required to accurately numerically extract them. For these reasons, often, only the first-order expansion has been considered. However, the first-order-approximated fields extracted from the DNS-DEM simulations are in clear disagreement with the exact ones (§IV). In particular, the first-order-approximated effective fluid phase stress is unable to reproduce the almost perfect hydrostatic behavior of the exact one. This study therefore lays the groundwork for numerically studying the rheology of dispersed two-phase flows in systems without scale separation.

Furthermore, the here presented formalism also exhibits conceptual advantages over previous mathematically exact formalisms [e.g., 19], that is, taking into account all infinite orders of their Taylor expansions in R/L. First, the balance equations and all their terms, including the fluid-solid interaction term, are phrased entirely in terms of the fluid phase (β_f) or solid phase ($\beta_\mathrm{s} = 1 - \beta_\mathrm{f}$) volume fractions rather than β_f and the grain concentration c_g based on the grain number density ($c_\mathrm{g} \neq 1 - \beta_\mathrm{f}$). It means that the resulting closure problem based on the fluid phase and solid phase balance equations contains less terms requiring closure than the closure problem in previous studies based on the fluid phase and grain phase balance equations. Second, the surface fluxes (e.g., stresses) emerging from fluid-solid interactions within the solid-phase-based (but not the grain-phase-based) framework exhibit the physically desirable property that they result from some kind of fluctuations on the particle surfaces or within their interiors, see Eqs. (64) and (112), and §III D 2. The two advantages above are somewhat weakened by the potential drawback that the solid phase balance equations, in contrast to the grain phase balance equations, contain terms associated with the particle-rotational degrees of freedom. However, for sphere-symmetrical particles, these rotational terms cancel each other out (§III D 1), since particle rotations do not alter any pointwise property within the particle interiors, such as the local particle mass density. For more general particle shapes, particle-rotational contributions remain within the advection term and solid phase Reynolds stress (§III D and §V).

Moreover, our study resolves a long-standing dispute regarding the buoyancy closure, that is, the decomposition of the fluid-solid interaction force density $\boldsymbol{f}$ into a generalized-drag force density $\boldsymbol{f}^\mathrm{D}$ (including drag, lift, lubrication, etc) resulting from the relative motion between the fluid and solid phases, and a relative-motion-independent generalized-buoyancy force density $\boldsymbol{f}^\mathrm{B}$. Although this closure is usually regarded as the most straightforward when attempting to close the closure problem [12], there have been various distinct propositions for how $\boldsymbol{f}^\mathrm{B}$ should be linked to the properties of the average fluid flow (§V). Our DNS-DEM simulations of steady, bed-tangentially homogeneous sediment transport support $\boldsymbol{f}^\mathrm{B} = \beta_\mathrm{s}\boldsymbol{\nabla}\cdot\boldsymbol{\sigma}^\mathbf{f} - \beta_\mathrm{f}\boldsymbol{\nabla}\cdot\boldsymbol{\sigma}^\mathbf{f}_\mathbf{s'}$ (see Eq. (143)), which is the closure originally proposed by Anderson and Jackson [11] improved by an additional term of order $(R/L)^2$, $-\beta_\mathrm{f}\boldsymbol{\nabla}\cdot\boldsymbol{\sigma}^\mathbf{f}_\mathbf{s'}$, that resolves a contradiction inherent in the original closure (§V B) and can fundamentally change the stability behavior of certain physical systems (e.g., homogeneous fluidized beds, see §V F). Here $\boldsymbol{\sigma}^\mathbf{f}$ refers to the effective stress tensor of the average fluid momentum balance, including contributions from the fluid-phase-averaged local, instantaneous fluid stress, from fluid-solid interactions, and from macroscopic fluid velocity fluctuations, while $\boldsymbol{\sigma}^\mathbf{f}_\mathbf{s'}$ accounts for fluctuations of $\boldsymbol{\nabla}\cdot\boldsymbol{\sigma}^\mathbf{f}$ at the particle scale. Our derived closure puts somewhat into question the numerous numerical studies, based on particle-unresolved CFD-DEM or two-fluid models, of slope-driven geophysical two-phase flows that assumed a buoyancy closure based on only the isotropic and/or non-Reynolds contributions to $\boldsymbol{\sigma}^\mathbf{f}$ or the fluid-phase-averaged fluid pressure [e.g., 5, 26, 28, 47–52]. These alternative closures falsely imply that there is nearly no buoyancy force component in the flow direction under turbulent-flow conditions [28]. Lastly, our closure can be interpreted as a generalization of Archimedes' principle from stationary to dynamic systems, as demonstrated in a companion paper [32].

ACKNOWLEDGMENTS

Z.H. acknowledges financial support from grant National Key R & D Program of China (2023YFC3008100). T.P. acknowledges financial support from grants National Natural Science Foundation of China (nos. 12350710176, 12272344). R.Z. acknowledges financial support from grant National Natural Science Foundation of China (no. 12402494). Z.H. acknowledges financial support from grant National Natural Science Foundation of China (no. 52171276).

Appendix A: Mathematical evaluation of generalized functions derived in §II B 4

Here, we evaluate terms of the form $V^p\underline{(\boldsymbol{r}^p)^{(k)}A\delta^p_{\mathrm{L}\boldsymbol{x}}}_{\mathcal{V}^p}$ and $S^p\underline{(\boldsymbol{r}^p)^{(k)}An^p_i\delta^p_{\mathrm{L}\boldsymbol{x}}}_{\mathcal{S}^p}$. To this end, we introduce the following mathematical representation of the indicator function $X^p[\boldsymbol{x}^p+\boldsymbol{r}]$:

$$X^p[\boldsymbol{x}^p+\boldsymbol{r}] = \sum_{m=1}^{N^p_{\hat{\boldsymbol{r}}}} \mathrm{sgn}\left[\hat{\boldsymbol{r}}\cdot\boldsymbol{n}^p_{\hat{\boldsymbol{r}}m}\right] H\left[L^p_{\hat{\boldsymbol{r}}m}-|\boldsymbol{r}|\right], \tag{A1}$$

where H denotes the Heaviside function. It means that, starting at $\boldsymbol{x}^p$ and going into the direction $\hat{\boldsymbol{r}}\equiv\boldsymbol{r}/|\boldsymbol{r}|$, one encounters a discrete number $N^p_{\hat{\boldsymbol{r}}}$ of transitions from particle to fluid or vice versa (if $N^p_{\hat{\boldsymbol{r}}}=0$, $X^p[\boldsymbol{x}^p+\boldsymbol{r}]=0$ by convention). The distance from $\boldsymbol{x}^p$ at each transition m shall be $L^p_{\hat{\boldsymbol{r}}m}$ and the corresponding unit normal vector $\boldsymbol{n}^p_{\hat{\boldsymbol{r}}m}$, pointing outward the particle p. That is, for a particle-to-fluid transition, $\mathrm{sgn}\left[\hat{\boldsymbol{r}}\cdot\boldsymbol{n}^p_{\hat{\boldsymbol{r}}m}\right]=1$, and for a fluid-to-particle transition, $\mathrm{sgn}\left[\hat{\boldsymbol{r}}\cdot\boldsymbol{n}^p_{\hat{\boldsymbol{r}}m}\right]=-1$. Note that, for spheres, $N^p_{\hat{\boldsymbol{r}}}=1$ and $L^p_{\hat{\boldsymbol{r}}1}=R_p$ independent of $\hat{\boldsymbol{r}}$, resulting in the well-known $X^p[\boldsymbol{x}^p+\boldsymbol{r}]=H[R_p-|\boldsymbol{r}|]$. Taking the spatial derivative of Eq. (A1) yields

$$\boldsymbol{\nabla}X^p[\boldsymbol{x}^p+\boldsymbol{r}] = -\sum_{m=1}^{N^p_{\hat{\boldsymbol{r}}}} \boldsymbol{n}^p_{\hat{\boldsymbol{r}}m}\delta\left[L^p_{\hat{\boldsymbol{r}}m}-|\boldsymbol{r}|\right]. \tag{A2}$$

Using Eqs. (A1) and (A2), the evaluations of $V^p\underline{(\boldsymbol{r}^p)^{(k)}A\delta^p_{\mathrm{L}\boldsymbol{x}}}_{\mathcal{V}^p}$ and $S^p\underline{(\boldsymbol{r}^p)^{(k)}An^p_i\delta^p_{\mathrm{L}\boldsymbol{x}}}_{\mathcal{S}^p}$ are straightforward:

$$\begin{aligned}
V^p\underline{(\boldsymbol{r}^p)^{(k)}A\delta^p_{\mathrm{L}\boldsymbol{x}}}_{\mathcal{V}^p} &= \int_{\mathcal{R}^3}\left(\boldsymbol{r}^p[\boldsymbol{y}]\right)^{(k)}\left(AX^p\right)[\boldsymbol{y}]\int_0^1\delta\left[\boldsymbol{x}-\boldsymbol{x}^p-\lambda\left(\boldsymbol{y}-\boldsymbol{x}^p\right)\right]\mathrm{d}\lambda\mathrm{d}^3y\\
\boldsymbol{y}\to\boldsymbol{x}^p+\boldsymbol{r}\Rightarrow &= \int_0^1\int_{\mathcal{R}^3}\boldsymbol{r}^{(k)}A[\boldsymbol{x}^p+\boldsymbol{r}]\sum_{m=1}^{N^p_{\hat{\boldsymbol{r}}}}\mathrm{sgn}\left[\hat{\boldsymbol{r}}\cdot\boldsymbol{n}^p_{\hat{\boldsymbol{r}}m}\right]H\left[L^p_{\hat{\boldsymbol{r}}m}-|\boldsymbol{r}|\right]\delta\left[\boldsymbol{r}^p-\lambda\boldsymbol{r}\right]\mathrm{d}^3r\mathrm{d}\lambda\\
&= \int_0^1\int_{\mathcal{R}^3}\frac{1}{\lambda^3}\boldsymbol{r}^{(k)}A[\boldsymbol{x}^p+\boldsymbol{r}]\sum_{m=1}^{N^p_{\hat{\boldsymbol{r}}}}\mathrm{sgn}\left[\hat{\boldsymbol{r}}\cdot\boldsymbol{n}^p_{\hat{\boldsymbol{r}}m}\right]H\left[L^p_{\hat{\boldsymbol{r}}m}-|\boldsymbol{r}|\right]\delta\left[\boldsymbol{r}^p/\lambda-\boldsymbol{r}\right]\mathrm{d}^3r\mathrm{d}\lambda\\
&= \left(\boldsymbol{r}^p\right)^{(k)}\sum_{m=1}^{N^p_{\hat{\boldsymbol{r}}^p}}\mathrm{sgn}\left[\hat{\boldsymbol{r}}^p\cdot\boldsymbol{n}^p_{\hat{\boldsymbol{r}}^pm}\right]\int_0^1\frac{A[\boldsymbol{x}^p+\boldsymbol{r}^p/\lambda]}{\lambda^{3+k}}H\left[L^p_{\hat{\boldsymbol{r}}^pm}-|\boldsymbol{r}^p|/\lambda\right]\mathrm{d}\lambda\\
&= \left(\boldsymbol{r}^p\right)^{(k)}\sum_{m=1}^{N^p_{\hat{\boldsymbol{r}}^p}}\mathrm{sgn}\left[\hat{\boldsymbol{r}}^p\cdot\boldsymbol{n}^p_{\hat{\boldsymbol{r}}^pm}\right]H\left[L^p_{\hat{\boldsymbol{r}}^pm}-|\boldsymbol{r}^p|\right]\int_{|\boldsymbol{r}^p|/L^p_{\hat{\boldsymbol{r}}^pm}}^1\frac{A[\boldsymbol{x}^p+\boldsymbol{r}^p/\lambda]}{\lambda^{3+k}}\mathrm{d}\lambda,
\end{aligned} \tag{A3}$$

$$\begin{aligned}
S^p\underline{(\boldsymbol{r}^p)^{(k)}An^p_i\delta^p_{\mathrm{L}\boldsymbol{x}}}_{\mathcal{S}^p} &= -\int_{\mathcal{R}^3}\left(\left(\boldsymbol{r}^p\right)^{(k)}A\partial_iX^p\right)[\boldsymbol{y}]\int_0^1\delta\left[\boldsymbol{x}-\boldsymbol{x}^p-\lambda\left(\boldsymbol{y}-\boldsymbol{x}^p\right)\right]\mathrm{d}\lambda\mathrm{d}^3y\\
\boldsymbol{y}\to\boldsymbol{x}^p+\boldsymbol{r}\Rightarrow &= \int_0^1\int_{\mathcal{R}^3}\boldsymbol{r}^{(k)}\sum_{m=1}^{N^p_{\hat{\boldsymbol{r}}}}\left(An^p_{\hat{\boldsymbol{r}}mi}\right)\left[\boldsymbol{x}^p+L^p_{\hat{\boldsymbol{r}}m}\hat{\boldsymbol{r}}\right]\delta\left[L^p_{\hat{\boldsymbol{r}}m}-|\boldsymbol{r}|\right]\delta\left[\boldsymbol{r}^p-\lambda\boldsymbol{r}\right]\mathrm{d}^3r\mathrm{d}\lambda\\
&= \int_0^1\int_{\mathcal{R}^3}\frac{1}{\lambda^3}\boldsymbol{r}^{(k)}\sum_{m=1}^{N^p_{\hat{\boldsymbol{r}}}}\left(An^p_{\hat{\boldsymbol{r}}mi}\right)\left[\boldsymbol{x}^p+L^p_{\hat{\boldsymbol{r}}m}\hat{\boldsymbol{r}}\right]\delta\left[L^p_{\hat{\boldsymbol{r}}m}-|\boldsymbol{r}|\right]\delta\left[\boldsymbol{r}^p/\lambda-\boldsymbol{r}\right]\mathrm{d}^3r\mathrm{d}\lambda\\
&= \left(\boldsymbol{r}^p\right)^{(k)}\sum_{m=1}^{N^p_{\hat{\boldsymbol{r}}^p}}\left(An^p_{\hat{\boldsymbol{r}}mi}\right)\left[\boldsymbol{x}^p+L^p_{\hat{\boldsymbol{r}}^pm}\hat{\boldsymbol{r}}^p\right]\int_0^1\frac{1}{\lambda^{3+k}}\delta\left[L^p_{\hat{\boldsymbol{r}}^pm}-|\boldsymbol{r}^p|/\lambda\right]\mathrm{d}\lambda\\
&= \left(\boldsymbol{r}^p\right)^{(k)}|\boldsymbol{r}^p|\sum_{m=1}^{N^p_{\hat{\boldsymbol{r}}^p}}\frac{1}{\left(L^p_{\hat{\boldsymbol{r}}^pm}\right)^2}\left(An^p_{\hat{\boldsymbol{r}}mi}\right)\left[\boldsymbol{x}^p+L^p_{\hat{\boldsymbol{r}}^pm}\hat{\boldsymbol{r}}^p\right]\int_0^1\frac{1}{\lambda^{3+k}}\delta\left[\lambda-|\boldsymbol{r}^p|/L^p_{\hat{\boldsymbol{r}}^pm}\right]\mathrm{d}\lambda\\
&= \frac{\left(\boldsymbol{r}^p\right)^{(k)}}{|\boldsymbol{r}^p|^{2+k}}\sum_{m=1}^{N^p_{\hat{\boldsymbol{r}}^p}}\left(L^p_{\hat{\boldsymbol{r}}^pm}\right)^{1+k}\left(An^p_{\hat{\boldsymbol{r}}mi}\right)\left[\boldsymbol{x}^p+L^p_{\hat{\boldsymbol{r}}^pm}\hat{\boldsymbol{r}}^p\right]H\left[L^p_{\hat{\boldsymbol{r}}^pm}-|\boldsymbol{r}^p|\right].
\end{aligned} \tag{A4}$$

Appendix B: Series expansion of fluctuation operator

Here, we derive a series expansion for the fluctuation $\boldsymbol{A}'$ of a macroscopically-averaged tensor field $\boldsymbol{A}$ for the case of spheres of a constant radius R with sphere-symmetrical interiors. The symbol '$\overset{\circ}{=}$' shall again indicate equalities that require the latter two properties to be true. We start the derivation with a general expression for $\underline{(r_1^p)^k}_{\mathcal{V}^p}$, with $k \geq 0$ an integer:

$$\underline{(r_1^p)^k}_{\mathcal{V}^p} \overset{\circ}{=} \frac{3}{4\pi R^3}\int_0^R\int_0^{2\pi}\int_0^{\pi}(r\cos\theta)^k r^2\sin\theta \mathrm{d}\theta\mathrm{d}\phi\mathrm{d}r = \frac{3\left(1+(-1)^k\right)(k-1)!!R^k}{2(k+3)!!}. \tag{B1}$$

Introducing the k-th power of the identity tensor $\mathbf{1}$ with respect to the tensor product, $\mathbf{1}^{(k)}$, e.g., $\left(\mathbf{1}^{(2)}\right)_{ijkl} = (\mathbf{1}\otimes\mathbf{1})_{ijkl} = \delta_{ij}\delta_{kl}+\delta_{ik}\delta_{jl}+\delta_{il}\delta_{kj}$, we can generalize Eq. (B1) to

$$\underline{(\boldsymbol{r}^p)^{(k)}}_{\mathcal{V}^p} \overset{\circ}{=} \frac{3\left(1+(-1)^k\right)R^k}{2(k+3)!!}\mathbf{1}^{(k/2)}, \tag{B2}$$

since the number of distinct permutations of Kronecker delta combinations in $\mathbf{1}^{(k/2)}$ is equal to $(k-1)!!$ if k is even. Note that, if k is odd, $\mathbf{1}^{(k/2)}$ does not need to be well-defined, since $\left(1+(-1)^k\right)=0$. Using Eq. (B2), one obtains an expression for $\underline{\boldsymbol{A}}_{\mathcal{V}^p}$ from the Taylor expansion of $\boldsymbol{A}$:

$$\boldsymbol{A}[\boldsymbol{x}] = \sum_{k=0}^{\infty}\frac{1}{k!}(\boldsymbol{r}^p[\boldsymbol{x}])^{(k)}\odot\boldsymbol{\nabla}^{(k)}\boldsymbol{A}[\boldsymbol{x}^p], \tag{B3}$$

$$\Rightarrow \underline{\boldsymbol{A}}_{\mathcal{V}^p} \overset{\circ}{=} \sum_{k=0}^{\infty}\frac{3\left(1+(-1)^k\right)(k-1)!!}{2k!(k+3)!!}R^k\Delta^{k/2}\boldsymbol{A}[\boldsymbol{x}^p] = \sum_{k=0}^{\infty}\frac{3\left(1+(-1)^k\right)}{2(k+1)!(k+3)}R^k\Delta^{k/2}\boldsymbol{A}[\boldsymbol{x}^p]. \tag{B4}$$

Note that, if k is odd, $\Delta^{k/2}$ needs not be well-defined, since $\left(1+(-1)^k\right)=0$. Furthermore, the Taylor expansion

$$\boldsymbol{\nabla}_{\boldsymbol{x}}\cdot\left(\boldsymbol{r}^p\delta^p_{\mathrm{L}\boldsymbol{x}}\right)[\boldsymbol{y}] = -\sum_{k=1}^{\infty}\frac{(-1)^k}{k!}\boldsymbol{\nabla}^{(k)}_{\boldsymbol{x}}\odot(\boldsymbol{r}^p[\boldsymbol{y}])^{(k)}\delta^p_{\boldsymbol{x}} \tag{B5}$$

follows from Eqs. (17) and (19). Together, Eqs. (B2)-(B5) allow us to express the kernel of $\boldsymbol{A}'$ in Eq. (45) as

$$\begin{aligned}
\boldsymbol{\nabla}\cdot V^p\underline{\boldsymbol{r}^p\left(\boldsymbol{A}-\underline{\boldsymbol{A}}_{\mathcal{V}^p}\right)\delta^p_{\mathrm{L}\boldsymbol{x}}}_{\mathcal{V}^p} &= -\sum_{i=1}^{\infty}\frac{(-1)^i}{i!}\boldsymbol{\nabla}^{(i)}_{\boldsymbol{x}}\odot V^p\delta^p_{\boldsymbol{x}}\underline{(\boldsymbol{r}^p)^{(i)}\left(\boldsymbol{A}-\underline{\boldsymbol{A}}_{\mathcal{V}^p}\right)}_{\mathcal{V}^p}\\
&\overset{\circ}{=} -\sum_{i=1}^{\infty}\frac{(-1)^i}{i!}\boldsymbol{\nabla}^{(i)}_{\boldsymbol{x}}\odot V^p\delta^p_{\boldsymbol{x}}\sum_{j=1}^{\infty}\left(\frac{1}{j!}\underline{(\boldsymbol{r}^p)^{(i+j)}}_{\mathcal{V}^p}\odot\boldsymbol{\nabla}^{(j)}\boldsymbol{A}[\boldsymbol{x}^p]-\underline{(\boldsymbol{r}^p)^{(i)}}_{\mathcal{V}^p}\frac{3\left(1+(-1)^j\right)}{2(j+1)!(j+3)}R^j\Delta^{j/2}\boldsymbol{A}[\boldsymbol{x}^p]\right)\\
&\overset{\circ}{=} -\sum_{i=1}^{\infty}\sum_{j=1}^{\infty}\frac{3\left((-1)^i+(-1)^j\right)}{2i!j!(i+j+3)!!}R^{i+j}\boldsymbol{\nabla}^{(i)}_{\boldsymbol{x}}\odot V^p\delta^p_{\boldsymbol{x}}\mathbf{1}^{((i+j)/2)}\odot\boldsymbol{\nabla}^{(j)}\boldsymbol{A}[\boldsymbol{x}^p]\\
&\quad+\sum_{i=1}^{\infty}\sum_{j=1}^{\infty}\frac{9\left(1+(-1)^i\right)\left(1+(-1)^j\right)}{4(i+1)!(j+1)!(i+3)(j+3)}R^{i+j}\Delta^{i/2}_{\boldsymbol{x}}V^p\delta^p_{\boldsymbol{x}}\Delta^{j/2}\boldsymbol{A}[\boldsymbol{x}^p].
\end{aligned} \tag{B6}$$

For the term $\boldsymbol{\nabla}^{(i)}_{\boldsymbol{x}}\odot\delta^p_{\boldsymbol{x}}\mathbf{1}^{((i+j)/2)}\odot\boldsymbol{\nabla}^{(j)}\boldsymbol{A}[\boldsymbol{x}^p]$, straightforward combinatorics yields

$$\boldsymbol{\nabla}^{(i)}_{\boldsymbol{x}}\odot\delta^p_{\boldsymbol{x}}\mathbf{1}^{((i+j)/2)}\odot\boldsymbol{\nabla}^{(j)}\boldsymbol{A}[\boldsymbol{x}^p] = \sum_{k=0}^{\min(i,j)}\frac{\left((-1)^i+(-1)^j\right)\left((-1)^i+(-1)^k\right)i!j!}{4\times 2^{\frac{i+j}{2}-k}k!\left(\frac{i-k}{2}\right)!\left(\frac{j-k}{2}\right)!}\Delta_{\boldsymbol{x}}^{\frac{i-k}{2}}\boldsymbol{\nabla}^{(k)}_{\boldsymbol{x}}\odot\delta^p_{\boldsymbol{x}}\boldsymbol{\nabla}^{(k)}\Delta^{\frac{j-k}{2}}\boldsymbol{A}[\boldsymbol{x}^p]. \tag{B7}$$

Note that $\min(i,j)$, the upper bound for the sum over k, can optionally be replaced by ∞, since the factorials in the denominator approach complex infinity for negative integer arguments. Insertion of Eq. (B7) into Eq. (B6) then leads to the expression

$$\boldsymbol{\nabla}\cdot V^p\underline{\boldsymbol{r}^p\left(\boldsymbol{A}-\underline{\boldsymbol{A}}_{\mathcal{V}^p}\right)\delta^p_{\mathrm{L}\boldsymbol{x}}}_{\mathcal{V}^p} \overset{\circ}{=} \sum_{i=1}^{\infty}\sum_{j=1}^{\infty}\sum_{k=0}^{\min(i,j)}(a_{ijk}+b_{ijk})R^{i+j}\Delta_{\boldsymbol{x}}^{\frac{i-k}{2}}\boldsymbol{\nabla}^{(k)}_{\boldsymbol{x}}\odot V^p\delta^p_{\boldsymbol{x}}\boldsymbol{\nabla}^{(k)}\Delta^{\frac{j-k}{2}}\boldsymbol{A}[\boldsymbol{x}^p], \tag{B8}$$

where the coefficients a_{ijk} and b_{ijk} are defined as

$$a_{ijk} \equiv -\frac{3\left((-1)^i+(-1)^j+(-1)^k+(-1)^{i+j+k}\right)}{4\times 2^{\frac{i+j}{2}-k}k!(i+j+3)!!\left(\frac{i-k}{2}\right)!\left(\frac{j-k}{2}\right)!}, \qquad b_{ijk} \equiv \begin{cases} \frac{9\left(1+(-1)^i\right)\left(1+(-1)^j\right)}{4(i+1)!(j+1)!(i+3)(j+3)} & \text{if } k=0 \\ 0 & \text{if } k\neq 0 \end{cases}. \tag{B9}$$

Using Eq. (B4), the term $R^{i+j}\Delta_{\boldsymbol{x}}^{\frac{i-k}{2}}\boldsymbol{\nabla}_{\boldsymbol{x}}^{(k)}\odot V^p\delta_{\boldsymbol{x}}^p\boldsymbol{\nabla}^{(k)}\Delta^{\frac{j-k}{2}}\boldsymbol{A}[\boldsymbol{x}^p]$ within Eq. (B8) can be manipulated via

$$\begin{aligned} R^{i+j}\Delta_{\boldsymbol{x}}^{\frac{i-k}{2}}\boldsymbol{\nabla}_{\boldsymbol{x}}^{(k)}\odot V^p\delta_{\boldsymbol{x}}^p\boldsymbol{\nabla}^{(k)}\Delta^{\frac{j-k}{2}}\boldsymbol{A}[\boldsymbol{x}^p] &\overset{\circ}{=} R^{i+j}\Delta_{\boldsymbol{x}}^{\frac{i-k}{2}}\boldsymbol{\nabla}_{\boldsymbol{x}}^{(k)}\odot V^p\delta_{\boldsymbol{x}}^p\underline{\boldsymbol{\nabla}^{(k)}\Delta^{\frac{j-k}{2}}\boldsymbol{A}}_{\mathcal{V}^p} \\ &- \sum_{m=1}^{\infty}\frac{3\left(1+(-1)^m\right)}{2(m+1)!(m+3)}R^{i+j+m}\Delta_{\boldsymbol{x}}^{\frac{i-k}{2}}\boldsymbol{\nabla}_{\boldsymbol{x}}^{(k)}\odot V^p\delta_{\boldsymbol{x}}^p\boldsymbol{\nabla}^{(k)}\Delta^{\frac{j-k+m}{2}}\boldsymbol{A}[\boldsymbol{x}^p] \end{aligned} \tag{B10}$$

and the first term on the right-hand side of the resulting expression, using Eqs. (21) and (B5), substituted through

$$\begin{aligned} &R^{i+j}\Delta_{\boldsymbol{x}}^{\frac{i-k}{2}}\boldsymbol{\nabla}_{\boldsymbol{x}}^{(k)}\odot V^p\delta_{\boldsymbol{x}}^p\underline{\boldsymbol{\nabla}^{(k)}\Delta^{\frac{j-k}{2}}\boldsymbol{A}}_{\mathcal{V}^p} \\ &= R^{i+j}\Delta^{\frac{i-k}{2}}\boldsymbol{\nabla}^{(k)}\odot X^p\boldsymbol{\nabla}^{(k)}\Delta^{\frac{j-k}{2}}\boldsymbol{A} - \sum_{m=1}^{\infty}\frac{(-1)^m}{m!}R^{i+j}\Delta_{\boldsymbol{x}}^{\frac{i-k}{2}}\boldsymbol{\nabla}_{\boldsymbol{x}}^{(k+m)}\odot V^p\delta_{\boldsymbol{x}}^p\underline{(\boldsymbol{r}^p)^{(m)}\boldsymbol{\nabla}^{(k)}\Delta^{\frac{j-k}{2}}\boldsymbol{A}}_{\mathcal{V}^p} \\ &\overset{\circ}{=} R^{i+j}\Delta^{\frac{i-k}{2}}\boldsymbol{\nabla}^{(k)}\odot X^p\boldsymbol{\nabla}^{(k)}\Delta^{\frac{j-k}{2}}\boldsymbol{A} + \sum_{m=1}^{\infty}\sum_{n=0}^{\infty}\sum_{q=0}^{\min(m,n)}a_{mnq}R^{i+j+m}\Delta_{\boldsymbol{x}}^{\frac{i-k+m-q}{2}}\boldsymbol{\nabla}_{\boldsymbol{x}}^{(k+q)}\odot V^p\delta_{\boldsymbol{x}}^p\boldsymbol{\nabla}^{(k+q)}\Delta^{\frac{j-k+n-q}{2}}\boldsymbol{A}[\boldsymbol{x}^p], \end{aligned} \tag{B11}$$

based on a calculation very similar to that in Eq. (B6). Through the manipulations in Eqs. (B10) and (B11), we have shown that the formal replacement of the term $R^{i+j}\Delta_{\boldsymbol{x}}^{\frac{i-k}{2}}\boldsymbol{\nabla}_{\boldsymbol{x}}^{(k)}\odot V^p\delta_{\boldsymbol{x}}^p\boldsymbol{\nabla}^{(k)}\Delta^{\frac{j-k}{2}}\boldsymbol{A}[\boldsymbol{x}^p]$ within Eq. (B8) by $R^{i+j}\Delta^{\frac{i-k}{2}}\boldsymbol{\nabla}^{(k)}\odot X^p\boldsymbol{\nabla}^{(k)}\Delta^{\frac{j-k}{2}}\boldsymbol{A}$ can be corrected if one alters the coefficients of order higher than R^{i+j}. This implies that iteratively applying Eqs. (B10) and (B11) to all terms $R^{i+j}\Delta_{\boldsymbol{x}}^{\frac{i-k}{2}}\boldsymbol{\nabla}_{\boldsymbol{x}}^{(k)}\odot V^p\delta_{\boldsymbol{x}}^p\boldsymbol{\nabla}^{(k)}\Delta^{\frac{j-k}{2}}\boldsymbol{A}[\boldsymbol{x}^p]$, starting with $(i,j,k)=(1,1,0)$ and looping through i, j, and k (in any order), results in

$$\boldsymbol{\nabla}\cdot V^p\underline{\boldsymbol{r}^p\left(\boldsymbol{A}-\underline{\boldsymbol{A}}_{\mathcal{V}^p}\right)\delta_{\mathrm{L}\boldsymbol{x}}^p}_{\mathcal{V}^p} \overset{\circ}{=} \sum_{i=1}^{\infty}\sum_{j=1}^{\infty}\sum_{k=0}^{\min(i,j)}c_{ijk}R^{i+j}\Delta^{\frac{i-k}{2}}\boldsymbol{\nabla}^{(k)}\odot X^p\boldsymbol{\nabla}^{(k)}\Delta^{\frac{j-k}{2}}\boldsymbol{A}, \tag{B12}$$

with updated coefficients c_{ijk}. The matrix below, where the rows and columns correspond to i and j and the entries to the k-vector, with the first element being $k=0$, shows the exact values of c_{ijk} calculated from the described procedure up to $i=j=k=4$:

$$\begin{pmatrix} [0,\frac{1}{5},0,0,0] & [0,0,0,0,0] & [0,-\frac{1}{175},0,0,0] & [0,0,0,0,0] \\ [0,0,0,0,0] & [\frac{1}{350},0,\frac{9}{350},0,0] & [0,0,0,0,0] & [-\frac{1}{7875},0,-\frac{13}{7875},0,0] \\ [0,-\frac{1}{175},0,0,0] & [0,0,0,0,0] & [0,\frac{17}{15750},0,\frac{19}{6750},0] & [0,0,0,0,0] \\ [0,0,0,0,0] & [-\frac{1}{7875},0,-\frac{13}{7875},0,0] & [0,0,0,0,0] & [\frac{107}{8085000},0,\frac{3407}{12127500},0,\frac{21059}{72765000}] \end{pmatrix}. \tag{B13}$$

Summing Eq. (B12) over all particles and averaging ($\langle\cdot\rangle$), using Eq. (45), finally yields the series expansion of $\boldsymbol{A}'$:

$$\boldsymbol{A}' \overset{\circ}{=} \sum_{i=1}^{\infty}\sum_{j=1}^{\infty}\sum_{k=0}^{\min(i,j)}c_{ijk}R^{i+j}\Delta^{\frac{i-k}{2}}\boldsymbol{\nabla}^{(k)}\odot\beta_{\mathrm{s}}\left\langle\boldsymbol{\nabla}^{(k)}\Delta^{\frac{j-k}{2}}\boldsymbol{A}\right\rangle^{\mathrm{s}} \overset{\mathrm{R}}{=} \sum_{i=1}^{\infty}\sum_{j=1}^{\infty}\sum_{k=0}^{\min(i,j)}c_{ijk}R^{i+j}\Delta^{\frac{i-k}{2}}\boldsymbol{\nabla}^{(k)}\odot\beta_{\mathrm{s}}\boldsymbol{\nabla}^{(k)}\Delta^{\frac{j-k}{2}}\boldsymbol{A}. \tag{B14}$$

For the linear-stability analysis in §V F, we require an expression for the coefficient c_n defined as

$$c_n \equiv \sum_{i=1}^{\infty}\sum_{\substack{j=1\\ i+j=n}}^{\infty}\sum_{k=0}^{\min(i,j)}c_{ijk}. \tag{B15}$$

To derive it, we first note that

$$a_{ij} \equiv \sum_{k=0}^{\min(i,j)} a_{ijk} = -\frac{3(-1)^i\left(1+(-1)^{i+j}\right)}{2i!j!(i+j+1)(i+j+3)}, \qquad b_{ij} \equiv \sum_{k=0}^{\min(i,j)} b_{ijk} = \frac{9\left(1+(-1)^i\right)\left(1+(-1)^j\right)}{4(i+1)!(j+1)!(i+3)(j+3)}. \tag{B16}$$

Then, we can calculate the associated coefficients a_n and b_n ($j = n - i$):

$$a_n \equiv \sum_{i=1}^{n-1} a_{i(n-i)} = \frac{3\left(1+(-1)^n\right)}{(n+1)!(n+3)}, \qquad b_n \equiv \sum_{i=1}^{n-1} b_{i(n-i)} = \frac{3\left(1+(-1)^n\right)(n+2)\left(12\left(2^n-2\right)-n(n+10)\right)}{(n+4)!(n+6)}. \tag{B17}$$

Now, one observes that the manipulation in Eq. (B10) involves subtracting $a_m/2$ from every term of order $i+j+m$, whereas the manipulation in Eq. (B11) involves adding $a_m + a_{m0} = a_m/2$ to each such term, implying no alteration of higher-order terms. Hence, we finally obtain

$$c_n = a_n + b_n = \frac{36 \times 2^n\left(1+(-1)^n\right)}{(n+1)!(n+3)(n+4)(n+6)}. \tag{B18}$$

Appendix C: Numerical implementation for bed-tangentially homogeneous sediment transport

Here, we describe how we numerically evaluate the derived mathematically exact expressions of the closure problem for an exemplary DNS-DEM simulation of steady, bed-tangentially homogeneous sediment transport. We consider an incompressible fluid of constant mass density ρ_f and rigid spheres of a constant mass density ρ_s. This implies

$$X_\mathrm{f}\rho \equiv X_\mathrm{f}\rho_\mathrm{f} \quad \Rightarrow \quad \langle\rho\rangle^\mathrm{f} = \rho_\mathrm{f}, \tag{C1}$$

$$X^p\rho \equiv X^p\rho_\mathrm{s} \quad \Rightarrow \quad \langle\rho\rangle^\mathrm{s} = \underline{\rho}_{\mathcal{V}^p} = \rho_\mathrm{s}, \quad \underline{A}_{\mathcal{M}^p} = \underline{A}_{\mathcal{V}^p} \tag{C2}$$

and allows us to express the indicator function of an individual particle p as

$$X^p[\boldsymbol{x},t] = H[R_p - |\boldsymbol{r}^p[\boldsymbol{x},t]|] = H[R_p - |\boldsymbol{x} - \boldsymbol{x}^p[t]|], \tag{C3}$$

where R_p is the radius of the particle p.

1. Streamwise-lateral averaging

The considered system is statistically homogeneous in the bed-tangential direction. Introducing a Cartesian coordinate system (x, y, z), with x in the flow direction, z in the bed-normal direction and oriented upwards, and y in the lateral direction, it means that statistically $\partial_x = \partial_y = 0$. Hence, we define an averaging procedure as

$$\overline{A}[z,t] = \overline{A[\boldsymbol{x},t]} \equiv \frac{1}{L_xL_y}\int_0^{L_y}\int_0^{L_x} A[x-x', y-y', z, t]\mathrm{d}x'\mathrm{d}y' = \frac{1}{L_xL_y}\int_0^{L_y}\int_0^{L_x} A[\boldsymbol{x},t]\mathrm{d}x\mathrm{d}y, \tag{C4}$$

where L_x and L_y are the length of the streamwise and lateral, respectively, simulation domain (periodic boundary conditions). This allows us to further simplify Eq. (30). Introducing polar coordinates, $\boldsymbol{r}^p = r\cos\phi\boldsymbol{e_x} + r\sin\phi\boldsymbol{e_y} + (z-z^p)\boldsymbol{e_z}$, with $\boldsymbol{e_x}$, $\boldsymbol{e_y}$, and $\boldsymbol{e_z}$ the unit vectors of the Cartesian coordinate system, we evaluate Eq. (30) for the case $k = 1$ as follows:

$$\begin{aligned}\overline{\underline{\boldsymbol{r}^p\delta^p_{\mathrm{L}\boldsymbol{x}}}_{\mathcal{V}^p}} &= \frac{H[R_p - |z-z^p|]}{4\pi R_p^3 L_xL_y}\int_0^{\sqrt{R_p^2-(z-z^p)^2}}\int_0^{2\pi}\boldsymbol{r}^p\left(\left(\frac{R_p}{\sqrt{r^2+(z-z^p)^2}}\right)^3 - 1\right)r\mathrm{d}\phi\mathrm{d}r \\ &= \frac{H[R_p - |z-z^p|]\boldsymbol{e_z}}{2R_p^3L_xL_y}\left(R_p^3\mathrm{sgn}[z-z^p] - \frac{3}{2}R_p^2(z-z^p) + \frac{1}{2}(z-z^p)^3\right).\end{aligned} \tag{C5}$$

2. Discretization and time averaging

The bed-normal simulation domain shall be discretized into grid cells numbered consecutively by n, with z_n the center of the n-th grid cell and Δz the constant grid cell thickness. Discretized and time-averaged quantities A are then calculated as

$$\langle A\rangle[z_n] = \frac{1}{N_T \Delta z} \sum_{k=1}^{N_T} \left(\int_{z_n-\Delta z/2}^{z_n+\Delta z/2} \overline{A}[z,t]\mathrm{d}z \right)_k , \tag{C6}$$

where N_T is a sufficient number of well-separated instants k in time to ensure $\partial_t \approx 0$. In the equations below, the writing of the time averaging is omitted for convenience. We now define a few quantities that will ease the later notation

$$z_{n2}^p \equiv \min\left(z_n + \Delta z/2, z^p + R_p\right), \tag{C7}$$
$$z_{n1}^p \equiv \max\left(z_n - \Delta z/2, z^p - R_p\right), \tag{C8}$$
$$l_n^p[z] \equiv \min\left(\max(z, z^p), z_n + \Delta z/2\right) - \max\left(\min(z, z^p), z_n - \Delta z/2\right). \tag{C9}$$

The former two definitions allow us to calculate

$$\int_{z_n-\Delta z/2}^{z_n+\Delta z/2} H[R_p - |z - z^p|]\overline{A}[z]\mathrm{d}z = H\left[z_{n2}^p - z_{n1}^p\right] \int_{z_{n1}^p}^{z_{n2}^p} \overline{A}[z]\mathrm{d}z, \tag{C10}$$

while the latter definition permits calculating the fraction $w_n^p[z]$ of the line connecting z with z^p that is contained within the discretization interval $[z_n - \Delta z/2, z_n + \Delta z/2)$ as

$$w_n^p[z] = \begin{cases} 0 & \text{if} \quad l_n^p[z] < 0 \\ 1 & \text{if} \quad l_n^p[z] = 0 \wedge z = z^p \\ l_n^p[z]/|z - z^p| & \text{else} \end{cases}. \tag{C11}$$

It will be used to evaluate particle surface integrals of $A\delta_{\mathrm{L}\boldsymbol{x}}^p$, since the infinitesimal volume of delta lines surrounding the delta line connecting a surface point $\boldsymbol{x}_\mathrm{S} \in \mathcal{S}^p$ of the particle p with its center $\boldsymbol{x}^p$ contributes to all discretization intervals proportionally to $w_n^p[z_\mathrm{S}]$. To ease the notation of expressions first-order-approximated in R/L, we also define

$$(w_n^p)_1 \equiv \begin{cases} 1 & \text{if} \quad z^p \in [z_n - \Delta z/2, z_n + \Delta z/2) \\ 0 & \text{else} \end{cases}. \tag{C12}$$

Using Eq. (C10), the discretized version of Eq. (C5) becomes

$$\left\langle \underline{\boldsymbol{r}^p \delta_{\mathrm{L}\boldsymbol{x}}^p}_{\mathcal{V}^p} \right\rangle [z_n] = \frac{H\left[z_{n2}^p - z_{n1}^p\right] \boldsymbol{e_z}}{2R_p^3 L_x L_y \Delta z} \left[R_p^3|z - z^p| - \frac{3}{4}R_p^2(z - z^p)^2 + \frac{1}{8}(z - z^p)^4 \right]_{z=z_{n1}^p}^{z=z_{n2}^p}. \tag{C13}$$

3. Particle quantities

With Eqs. (C10)-(C13), we finally have the toolkit to evaluate discretized average particle quantities, for example:

$$\left(\beta_\mathrm{s}\langle A\rangle^\mathrm{s}\right)[z_n] = \frac{1}{L_x L_y \Delta z} \sum\nolimits_{p:z_{n2}^p > z_{n1}^p} \int_{z_{n1}^p}^{z_{n2}^p} \int_0^{\sqrt{R_p^2-(z-z^p)^2}} \int_0^{2\pi} A[r,\phi,z] r \mathrm{d}\phi \mathrm{d}r \mathrm{d}z. \tag{C14}$$

We apply Eq. (C14) to calculate the following particle-velocity-based expressions:

$$\beta_\mathrm{s}[z_n] = \frac{\pi}{L_x L_y \Delta z} \sum\nolimits_{p:z_{n2}^p > z_{n1}^p} \left[R_p^2 z - \frac{1}{3}(z - z^p)^3 \right]_{z=z_{n1}^p}^{z=z_{n2}^p}, \tag{C15}$$

$$\left(\beta_\mathrm{s}\langle \boldsymbol{u}_\uparrow\rangle^\mathrm{s}\right)[z_n] = \frac{\pi}{L_x L_y \Delta z} \sum\nolimits_{p:z_{n2}^p > z_{n1}^p} \boldsymbol{v}_\uparrow^p \left[R_p^2 z - \frac{1}{3}(z - z^p)^3 \right]_{z=z_{n1}^p}^{z=z_{n2}^p}, \tag{C16}$$

$$\left(\beta_\mathrm{s}\langle \boldsymbol{u}_\uparrow \boldsymbol{u}_\uparrow\rangle^\mathrm{s}\right)[z_n] = \frac{\pi}{L_x L_y \Delta z} \sum\nolimits_{p:z_{n2}^p > z_{n1}^p} \boldsymbol{v}_\uparrow^p \boldsymbol{v}_\uparrow^p \left[R_p^2 z - \frac{1}{3}(z - z^p)^3 \right]_{z=z_{n1}^p}^{z=z_{n2}^p}. \tag{C17}$$

Furthermore, using $\rho_\mathrm{s} = \mathrm{const}$, Eq. (C13), and the expression above, we can evaluate the solid stress tensor contributions (using $\boldsymbol{J}_{\boldsymbol{\Psi}} = -\boldsymbol{\sigma}$ within the expressions in §III D):

$$\sigma^\mathrm{s}_{ij}[z_n] = \sigma^\mathrm{s}_{\uparrow\mathrm{Re}ij}[z_n] + \sigma^\mathrm{s}_{\mathrm{c}ij}[z_n], \tag{C18}$$

$$\sigma^\mathrm{s}_{\uparrow\mathrm{Re}ij}[z_n] = \rho_\mathrm{s}\left(\beta_\mathrm{s}\langle u_{\uparrow i}\rangle^\mathrm{s}\langle u_{\uparrow j}\rangle^\mathrm{s}\right)[z_n] - \rho_\mathrm{s}\left(\beta_\mathrm{s}\langle u_{\uparrow i}u_{\uparrow j}\rangle^\mathrm{s}\right)[z_n], \tag{C19}$$

$$\sigma^\mathrm{s}_{\mathrm{c}ij}[z_n] = -\sum\nolimits_p F^p_{\mathrm{c}j}\left\langle \underline{r^p_i \delta^p_{\mathrm{L}\boldsymbol{x}\mathcal{V}^p}}\right\rangle[z_n] + \frac{1}{2L_xL_y\Delta z}\sum\nolimits_{pq} F^{pq}_{\mathrm{c}j} r^{pq}_i w^p_n[z^q]. \tag{C20}$$

In the first order of R/L (denoted by the symbol '$\overset{1}{=}$'), the latter contribution is approximated as

$$\sigma^\mathrm{s}_{\mathrm{c}ij}[z_n] \overset{1}{=} \frac{1}{2L_xL_y\Delta z}\sum\nolimits_{pq} F^{pq}_{\mathrm{c}j} r^{pq}_i \left(w^p_n\right)_1. \tag{C21}$$

4. Fluid quantities

Fluid quantities can be calculated using

$$\begin{aligned}\left(\beta_\mathrm{f}\langle A\rangle^\mathrm{f}\right)[z_n] &= \frac{1}{L_xL_y\Delta z}\int_{(L_x\times L_y\times\Delta z)\cap\mathcal{V}_\mathrm{f}} A[\boldsymbol{x}]\mathrm{d}V \\ &= \frac{1}{L_xL_y\Delta z}\sum\nolimits_{\alpha:z_\alpha\in[z_n-\Delta z/2,z_n+\Delta z/2)} V_\alpha A_\alpha,\end{aligned} \tag{C22}$$

where the index α enumerates the grid cells of the DNS mesh grid, and V_α and $\boldsymbol{x}_\alpha = (x_\alpha, y_\alpha, z_\alpha)$ are the volume and position, respectively, of the α-th grid cell, and A_α is the value of A in that cell. Hence,

$$\beta_\mathrm{f}[z_n] = 1 - \beta_\mathrm{s}[z_n] \overset{1}{=} \frac{1}{L_xL_y\Delta z}\sum\nolimits_{\alpha:z_\alpha\in[z_n-\Delta z/2,z_n+\Delta z/2)} V_\alpha, \tag{C23}$$

$$\left(\beta_\mathrm{f}\langle \boldsymbol{u}\rangle^\mathrm{f}\right)[z_n] = \frac{1}{L_xL_y\Delta z}\sum\nolimits_{\alpha:z_\alpha\in[z_n-\Delta z/2,z_n+\Delta z/2)} V_\alpha \boldsymbol{u}_\alpha, \tag{C24}$$

$$\left(\beta_\mathrm{f}\langle u_iu_j\rangle^\mathrm{f}\right)[z_n] = \frac{1}{L_xL_y\Delta z}\sum\nolimits_{\alpha:z_\alpha\in[z_n-\Delta z/2,z_n+\Delta z/2)} V_\alpha u_{i\alpha}u_{j\alpha}, \tag{C25}$$

$$\left(\beta_\mathrm{f}\langle \sigma_{ij}\rangle^\mathrm{f}\right)[z_n] = \frac{1}{L_xL_y\Delta z}\sum\nolimits_{\alpha:z_\alpha\in[z_n-\Delta z/2,z_n+\Delta z/2)} V_\alpha \sigma_{ij\alpha}, \tag{C26}$$

$$\sigma^\mathrm{f}_{\mathrm{Re}ij}[z_n] = \rho_\mathrm{f}\left(\beta_\mathrm{f}\langle u_i\rangle^\mathrm{f}\langle u_j\rangle^\mathrm{f}\right)[z_n] - \rho_\mathrm{f}\left(\beta_\mathrm{f}\langle u_iu_j\rangle^\mathrm{f}\right)[z_n]. \tag{C27}$$

5. Fluid-solid interaction quantities

Obtaining the fluid-particle interaction force applied on the particle p from the fluid grid,

$$\boldsymbol{F}^p_\mathrm{f} = S^p\underline{\boldsymbol{n}^p\cdot\boldsymbol{\sigma}}_{\mathcal{S}^p} = \sum\nolimits_{\alpha:\boldsymbol{x}_\alpha\in\mathcal{S}^p}\boldsymbol{n}^p_\alpha\cdot\boldsymbol{\sigma}_\alpha\Delta S_\alpha, \tag{C28}$$

where ΔS_α is the area of the particle-neighboring surface of the α-th grid cell, we can calculate $\beta_\mathrm{s}\rho_\mathrm{s}\langle\dot{u}_{\uparrow\mathrm{f}i}\rangle^\mathrm{s}[z_n]$, $\sigma^{\tilde{\mathrm{f}}}_{\mathrm{s}ij}[z_n]$, $\left(\sigma^\mathrm{f}_{\mathrm{s}zi} + \left[\langle\sigma_{zi}\rangle^\mathrm{f}\right]'_\mathrm{s}\right)[z_n]$, and $\sigma^\mathrm{f}_{zi}[z_n]$, respectively, as

$$\beta_\mathrm{s}\rho_\mathrm{s}\langle\dot{u}_{\uparrow\mathrm{f}i}\rangle^\mathrm{s}[z_n] = \frac{\pi}{L_xL_y\Delta z}\sum\nolimits_{p:z^p_{n2}>z^p_{n1}}\frac{F^p_{\mathrm{f}i}}{V^p}\left[R^2_pz - \frac{1}{3}(z-z^p)^3\right]^{z=z^p_{n2}}_{z=z^p_{n1}}, \tag{C29}$$

$$\sigma^{\tilde{\mathrm{f}}}_{\mathrm{s}ij}[z_n] = \sum\nolimits_p\left(\frac{1}{L_xL_y\Delta z}\sum\nolimits_{\alpha:\boldsymbol{x}_\alpha\in\mathcal{S}^p}\sigma_{kj\alpha}n^p_{k\alpha}r^p_{i\alpha}w^p_n[z_\alpha]\Delta S_\alpha - F^p_{\mathrm{f}j}\left\langle\underline{r^p_i\delta^p_{\mathrm{L}\boldsymbol{x}\mathcal{V}^p}}\right\rangle[z_n]\right) \tag{C30}$$

$$\sigma^{\tilde{\mathrm{f}}}_{\mathrm{s}ij}[z_n] \overset{1}{=} \frac{1}{L_xL_y\Delta z}\sum\nolimits_p\sum\nolimits_{\alpha:\boldsymbol{x}_\alpha\in\mathcal{S}^p}\sigma_{kj\alpha}n^p_{k\alpha}r^p_{i\alpha}\left(w^p_n\right)_1\Delta S_\alpha, \tag{C31}$$

$$\left(\sigma^\mathrm{f}_{\mathrm{s}zi} + \left[\langle\sigma_{zi}\rangle^\mathrm{f}\right]'_\mathrm{s}\right)[z_n] = \sigma^{\tilde{\mathrm{f}}}_{\mathrm{s}zi}[z_n] - \beta_\mathrm{s}[z_n]\langle\sigma_{zi}\rangle^\mathrm{f}[z_n], \tag{C32}$$

$$\sigma^\mathrm{f}_{zi}[z_n] = \langle\sigma_{zi}\rangle^\mathrm{f}[z_n] + \sigma^\mathrm{f}_{\mathrm{Re}zi}[z_n] + \left(\sigma^\mathrm{f}_{\mathrm{s}zi} + \left[\langle\sigma_{zi}\rangle^\mathrm{f}\right]'_\mathrm{s}\right)[z_n]. \tag{C33}$$

Here the symbol '$\overset{1}{=}$' denotes again the first-order approximation in R/L, and we used again Eqs. (C10) and (C13). Note that Eq. (C32) follows from $\mathrm{d}_z\left(\sigma^{\mathrm{f}}_{\mathrm{s}zi}+\left[\langle\sigma_{zi}\rangle^{\mathrm{f}}\right]^{\prime}_{\mathrm{s}}\right)=\mathrm{d}_z\left(\sigma^{\tilde{\mathrm{f}}}_{\mathrm{s}zi}-\beta_{\mathrm{s}}\langle\sigma_{zi}\rangle^{\mathrm{f}}\right)$ (cf. Eqs. (62)-(65)) and the boundary condition that β_{s}, $\sigma^{\tilde{\mathrm{f}}}_{\mathrm{s}zi}$, and therefore $\left(\sigma^{\mathrm{f}}_{\mathrm{s}zi}+\left[\langle\sigma_{zi}\rangle^{\mathrm{f}}\right]^{\prime}_{\mathrm{s}}\right)$ all vanish at the free surface.

[1] R. Verzicco, Immersed boundary methods: Historical perspective and future outlook, Annual Review of Fluid Mechanics **55**, 129 (2023).
[2] J. Wang, Continuum theory for dense gas-solid flow: A state-of-the-art review, Chemical Engineering Science **215**, 115428 (2020).
[3] Q. Zhang, E. Deal, J. T. Perron, J. G. Venditti, S. J. Benavides, M. Rushlow, and K. Kamrin, Fluid-driven transport of round sediment particles: From discrete simulations to continuum modeling, Journal of Geophysical Research: Earth Surface **127**, e2021JF006504 (2022).
[4] R. Maurin, J. Chauchat, and P. Frey, Dense granular flow rheology in turbulent bedload transport, Journal of Fluid Mechanics **804**, 490 (2016).
[5] J. Chauchat, A comprehensive two-phase flow model for unidirectional sheet-flows, Journal of Hydraulic Research **56**, 15 (2018).
[6] A. S. Baumgarten and K. Kamrin, A general fluid-sediment mixture model and constitutive theory validated in many flow regimes, Journal of Fluid Mechanics **861**, 721 (2019).
[7] V. Garzó and J. W. Dufty, Dense fluid transport for inelastic hard spheres, Physical Review E **59**, 5895 (1999).
[8] R. Chassagne, C. Bonamy, and J. Chauchat, A frictional–collisional model for bedload transport based on kinetic theory of granular flows: discrete and continuum approaches, Journal of Fluid Mechanics **964**, A27 (2023).
[9] D. Berzi, On granular flows: From kinetic theory to inertial rheology and nonlocal constitutive models, Physical Review Fluids **9**, 034304 (2024).
[10] R. Jackson, Locally averaged equations of motion for a mixture of identical spherical particles and a Newtonian fluid, Chemical Engineering Science **52**, 2457 (1997).
[11] T. B. Anderson and R. Jackson, Fluid mechanical description of fluidized beds. Equations of motion, Industrial & Engineering Chemistry Fundamentals **6**, 527 (1967).
[12] R. Jackson, *The Dynamics of Fluidized Particles* (Cambridge University Press, New York, 2000).
[13] R. Jamshidi and L. Mazzei, CFD modeling of fluidized beds, Reference Module in Chemistry, Molecular Sciences and Chemical Engineering /10.1016/B978-0-12-409547-2.13698-4 (2018).
[14] D. Z. Zhang and A. Prosperetti, Momentum and energy equations for disperse two-phase flows and their closure for dilute suspensions, International Journal of Multiphase Flow **23**, 425 (1997).
[15] A. Prosperetti, The average stress in incompressible disperse flow, International Journal of Multiphase Flow **30**, 1011 (2004).
[16] A. Prosperetti, Ensemble averaging techniques for disperse flows, in *Particulate Flows: Processing and Rheology*, edited by D. A. Drew, D. D. Joseph, and S. L. Passman (Springer, New York, 1998) pp. 99–136.
[17] Y. A. Buyevich and I. N. Shchelchkova, Flow of dense suspensions, Progress in Aerospace Sciences **18**, 121 (1979).
[18] N. Fintzi and J. L. Pierson, Averaged equations for disperse two-phase flow with interfacial transport, https://doi.org/10.48550/arXiv.2410.10752 (2024).
[19] P. R. Nott, E. Guazzelli, and O. Pouliquen, The suspension balance model revisited, Physics of Fluids **23**, 043304 (2011).
[20] T. Pähtz and O. Durán, Universal friction law at granular solid-gas transition explains scaling of sediment transport load with excess fluid shear stress, Physical Review Fluids **3**, 104302 (2018).
[21] K. Tholen, T. Pähtz, S. Kamath, E. J. R. Parteli, and K. Kroy, Anomalous scaling of aeolian sand transport reveals coupling to bed rheology, Physical Review Letters **130**, 058204 (2023).
[22] B. Fry, L. Lacaze, T. Bonometti, P. Elyakime, and F. Charru, From discrete to continuum description of weakly inertial bedload transport, Physical Review Fluids **9**, 024304 (2024).
[23] A. G. Kidanemariam, M. Scherer, and M. Uhlmann, Open-channel flow over evolving subaqueous ripples, Journal of Fluid Mechanics **937**, A26 (2022).
[24] P. U. Foscolo and L. G. Gibilaro, Fluid dynamic stability of fluidised suspensions: the particle bed model, Chemical Engineering Science **42**, 1489 (1987).
[25] D. A. Drew, Mathematical modeling of two-phase flow, Annual Review of Fluid Mechanics **15**, 261 (1983).
[26] S. P. Pudasaini, A general two-phase debris flow model, Journal of Geophysical Research: Earth Surface **117**, F03010 (2012).
[27] D. Z. Zhang, W. B. VanderHeyden, Q. Zou, and N. T. Padial-Collins, Pressure calculations in disperse and continuous multiphase flows, International Journal of Multiphase Flow **33**, 86 (2007).
[28] R. Maurin, J. Chauchat, and P. Frey, Revisiting slope influence in turbulent bedload transport: consequences for vertical flow structure and transport rate scaling, Journal of Fluid Mechanics **839**, 135 (2018).
[29] J. Halow, K. Holsopple, B. Crawshaw, and S. Daw, Observed mixing behavior of single particles in a bubbling fluidized bed of higher-density particles, Industrial & Engineering Chemistry Research **51**, 14566 (2012).

[30] M. Rotondi, R. Di Felice, and P. Pagliai, Validation of fluid–particle interaction force relationships in binary-solid suspensions, Particuology **23**, 40 (2015).
[31] K. Mandich and R. J. Cattolica, Longitudinal and transverse disturbances in unbounded, gas-fluidized beds, Physics of Fluids **25**, 023301 (2013).
[32] Z. Rui, Y. Chen, T. Pähtz, K. Tholen, and Z. He, Dynamic archimedes' principle, jointly submitted to Physical Review Letters (2025).
[33] M. Ishii and T. Hibiki, *Thermo-Fluid Dynamics of Two-Phase Flow* (Springer, New York, 2011).
[34] M. Babic, Average balance equations for granular materials, International Journal of Engineering Science **35**, 523 (1997).
[35] T. Weinhart, A. R. Thornton, S. Luding, and O. Bokhove, From discrete particles to continuum fields near a boundary, Granular Matter **14**, 289 (2012).
[36] E. Biegert, B. Vowinckel, and E. Meiburg, A collision model for grain-resolving simulations of flows over dense, mobile, polydisperse granular sediment beds, Journal of Computational Physics **340**, 105 (2017).
[37] R. Zhu, Z. He, K. Zhao, B. Vowinckel, and E. Meiburg, Grain-resolving simulations of submerged cohesive granular collapse, Journal of Fluid Mechanics **942**, A49 (2022).
[38] I. Goldhirsch, Stress, stress asymmetry and couple stress: from discrete particles to continuous fields, Granular Matter **12**, 239 (2010).
[39] W. S. Chepil, The use of spheres to measure lift and drag on wind-eroded soil grains, Soil Science Society of America Journal **25**, 343 (1961).
[40] X. Li, S. Balachandar, H. Lee, and B. Bai, Fully resolved simulations of a stationary finite-sized particle in wall turbulence over a rough bed, Physical Review Fluids **4**, 094302 (2019).
[41] M. Wang, D. Z. Zhang, and S. Balachandar, Effect of the volume fraction gradient on the phase interaction force model for disperse two-phase flows, Physical Review Fluids **9**, 104301 (2024).
[42] H. Lamb, *Hydrodynamics*, 6th ed. (Cambridge University Press, Cambridge, UK, 1932).
[43] D. Berzi and L. Fraccarollo, Turbulence locality and granularlike fluid shear viscosity in collisional suspensions, Physical Review Letters **115**, 194501 (2015).
[44] J. F. Richardson and W. N. Zaki, Sedimentation and fluidization, Transactions of the Institution of Chemical Engineers **32**, 35 (1954).
[45] R. I. Ferguson and M. Church, A simple universal equation for grain settling velocity, Journal of Sedimentary Research **74**, 933 (2004).
[46] A. R. Khan and J. F. Richardson, Fluid-particle interactions and flow characteristics of fluidized beds and settling suspensions of spherical particles, Chemical Engineering Communications **78**, 111 (1989).
[47] B. P. Greimann, M. Muste, and F. M. Holly Jr., Two-phase formulation of suspended sediment transport, Journal of Hydraulic Research **37**, 479 (1999).
[48] T. J. Hsu, J. T. Jenkins, and P. L. U. Liu, On two-phase sediment transport: Dilute flow, Journal of Geophysical Research **208**, 3057 (2003).
[49] T. J. Hsu, J. T. Jenkins, and P. L. U. Liu, On two-phase sediment transport: sheet flow of massive particles, Proceedings of the Royal Society London Series A **460**, 2223 (2004).
[50] D. Berzi and L. Fraccarollo, Inclined, collisional sediment transport, Physics of Fluids **25**, 106601 (2013).
[51] M. Larcher and J. T. Jenkins, Saturated, collisional flows of spheres over an inclined, erodible bed between vertical sidewalls, Advances in Water Resources **72**, 15 (2012).
[52] J. T. Jenkins and M. Larcher, Dense, steady, fully developed fluid-particle flows over inclined, erodible beds, Physical Review Fluids **8**, 024303 (2023).